Daniela Mesquita Moutinho

Degree in Molecular and Cellular Biology

Human ceruloplasmin and neurotransmitters: complex stabilization and crystallization

Dissertation to obtain a
Master Degree in Molecular Genetics and Biomedicine
at Faculty of Sciences and Technology,
Universidade Nova de Lisboa

Supervisor: Isabel Bento, Ph.D., ITQB-UNL
Co-supervisor: José Paulo Sampaio, Ph.D., FCT-UNL

Júri

Presidente:	Doutora Margarida Casal Ribeiro Castro Caldas Braga
Arguente:	Doutor Colin Edward McVey
Vogal:	Doutora Isabel Maria Travassos de Almeida de Jesus Bento

FACULDADE DE CIÊNCIAS E TECNOLOGIA
UNIVERSIDADE NOVA DE LISBOA

November 2013

Daniela Mesquita Moutinho

Degree in Molecular and Cellular Biology

Human ceruloplasmin and neurotransmitters: complex stabilization and crystallization

Dissertation to obtain a
Master Degree in Molecular Genetics and Biomedicine
at Faculty of Sciences and Technology,
Universidade Nova de Lisboa

Supervisor Isabel Bento, Ph.D., ITQB-UNL
Co-supervisor: José Paulo Sampaio, Ph.D., FCT-UNL

Júri

Presidente:	Doutora Margarida Casal Ribeiro Castro Caldas Braga
Arguente:	Doutor Colin Edward McVey
Vogal:	Doutora Isabel Maria Travassos de Almeida de Jesus Bento

FACULDADE DE CIÊNCIAS E TECNOLOGIA
UNIVERSIDADE NOVA DE LISBOA

November 2013

“Human ceruloplasmin and neurotransmitters: complex stabilization and crystallization”

“Just because something doesn't do what you planned it to do doesn't mean it's useless.”

Thomas Edison

Agradecimentos

Acknowledgments

A realização deste trabalho marca o final de mais uma etapa na minha vida e só pode ocorrer devido à confiança, apoio, incentivo, dedicação e conhecimento de várias pessoas a quem não poderia deixar de expressar a minha gratidão e apreço.

A todos aqueles que me acompanharam ao longo deste ano na Unidade de Cristalografia Macromolecular do Instituto de Tecnologia Química e Biológica da Universidade Nova de Lisboa e que de alguma forma contribuíram para a realização deste trabalho e que me levam a querer prosseguir e alargar os meus horizontes nesta área.

Agradeço em especial,

A Professora Doutora Maria Arménia Carrondo por me ter recebido na Unidade de Cristalografia Macromolecular e pela sua disponibilidade.

À Doutora Isabel Bento por me ter possibilitado trabalhar num projecto que me causou grande interesse e me pode ensinar tanto e por poder fazer parte do Laboratório de Genómica Estrutural. Pela sua orientação e entusiasmo. Por todo o seu apoio e crítica.

Ao Doutor Pedro Matias e ao Doutor Tiago Bandeiras por me terem dado a possibilidade de realizar este trabalho ao mesmo tempo que trabalhei com eles e fiz parte da Unidade de Proteómica do Instituto de Biologia Experimental e Tecnológica. Por todo o seu apoio, entusiasmo, compreensão, preocupação, interesse e ajuda.

Aos meus colegas da Unidade de Proteómica do iBET e do Laboratório de Cristalografia Aplicada à Medicina e à Industria do ITQB pelo seu apoio e compreensão. À Cristiana Sousa pela cumplicidade, partilha de momentos e boa disposição! Ao Micael Freitas, Margarida Silva e Sara Silva pela sua ajuda, apoio e partilha de conhecimentos.

Aos meus colegas do Laboratório de Genómica Estrutural Ana Teresa Gonçalves, Bruno Correia, Sara Brandão e à Doutora Ana Maria Gonçalves por toda a ajuda e apoio partilhado.

Às minhas colegas e amigas do Laboratório de Biologia Estrutural Ana Rita Silva e Patrícia Borges por todos os momentos de afecto e apoio sempre que necessitei. Pelo incentivo e partilha de ideias.

A todos os meus amigos que estiveram presentes durante esta etapa e que de uma forma ou de outra me ajudaram a conseguir ultrapassá-la com sucesso.

Aos meus pais e irmã por sempre me apoiarem em todas as decisões da minha vida. Pela sua orientação, compreensão, amor e sacrifício constantes para me ajudarem no meu sucesso.

A todos, com todo o meu carinho,

Obrigada.

Abstract

Human ceruloplasmin (hCp) is the molecular linker between the copper and iron metabolism and its importance in the homeostasis of human body has been implied in some neurological diseases. This plasma cuproenzyme has ferroxidase activity, oxidizing Fe^{2+} to Fe^{3+} and incorporating it into apotransferrin. hCp also has aminoxidase activity regulating the levels of amine stress hormones in the bloodstream and brain. Thus, it is thought to have an important role in neurodegenerative diseases such as Alzheimer's or Parkinson's. To know more about the role of cerulopalsmin on the oxidation of neurotransmitters and on brain homeostasis it is essential to know which protein residues are implied in the binding and stabilization of these neurotransmitters. The primary source of structural information for protein-ligand complexes is X-ray crystallography. This is the most successful method to determine macromolecular 3D structures but has some limitations as obtaining good diffracting protein crystals.

In this study several attempts were made to achieve better hCp diffracting crystals and crystals of hcp in complex with dopamine, L-dopa, epinephrine or serotonin in order to further determine its tridimensional structure.

To improve hCp stabilization and solubility, differential scanning fluorimetry and dynamic light scattering were used in a search for a better buffer for crystallization. For hCp crystallization the vapour-diffusion technique was used in combination with several other methods. Commercial crystallization screens, crystal seeding, additives, crosslinking were the several methods used to improve crystal diffraction.

Co-crystallization of hCp with neurotransmitters was performed with no success. Soaking of hCp crystals with the neurotransmitters was performed in an attempt to get crystals of the hCp-neurotransmitter complexes. All crystals were sent for analysis at European Synchrotron Radiation Facility (ESRF) and structural data will be further processed.

Key words: ceruloplasmin, neurotransmitters, epinephrine, dopamine, L-dopa, serotonin, protein crystals, crystallization, X-ray crystallography

Resumo

A ceruloplasmina humana (hCp) é a ligação molecular entre o metabolismo do cobre e do ferro sendo de extrema importância para a homeostase corporal. Esta cuproenzima plasmática tem actividade de ferroxidase, oxidando Fe^{2+} a Fe^{3+} e incorporando-o na apotransferina. A hCp regula os níveis de hormonas na corrente sanguínea e no cérebro. Esta actividade de aminoxidase é muito importante podendo estar implicada em doenças neurodegenerativas como Alzheimer e Parkinson. Para de saber mais sobre o papel da ceruloplasmina na oxidação de neurotransmissores e na homeostase cerebral é necessário conhecer a natureza desta interacção e quais os resíduos proteicos envolvidos na ligação e estabilização destes complexos. A cristalografia de raios-X é a principal fonte de informação sobre complexos de proteína-ligandos. Apesar deste ser o método mais bem sucedido na determinação de estruturas 3D, tem algumas limitações, como a obtenção de cristais de proteína com bom poder de difracção.

Neste estudo, foram feitas várias tentativas de melhorar cristais de hCp, já previamente descritos, e de obter cristais de hCp combinados com dopamina, L-dopa, epinefrina e serotonina de forma a poder obter a sua estrutura tridimensional.

A solução tamponante onde é armazenada a proteína é muito importante para a sua estabilização e solubilidade. Para melhorar estes aspectos da hCp utilizaram-se técnicas de fluorometria de varrimento diferencial (DSF) e varrimento de luz dinâmica (DLS). Para a cristalização da hCp usou-se o método de difusão de vapor combinado com outros métodos. Usaram-se s*creens* de cristalização comerciais, semearam-se cristais, usaram-se aditivos e fez-se *crosslinking* para tentar melhorar os cristais.

A co-cristalização da ceruloplasmina com neurotransmissores não obteve sucesso e assim usaram-se cristais de hCp e mergulharam-se em neurotransmissores para tentar obter os cristais dos complexos. Todos os cristais foram enviados para análise no *European Synchrotron Radiation Facility* (ESRF) e os dados estruturais serão depois processados.

Palavras-Chave: ceruloplasmina, neurotransmissores, epinefrina, dopamina, L-dopa, serotonina, cristais de proteína, cristalização, cristalografia de raios-X

Contents

Index of Figures

Chapter 1: INTRODUCTION

Chapter 3: RESULTS

Index of Tables

Chapter 1: INTRODUCTION

Chapter 2: METHODOLOGIES

Chapter 3: RESULTS

Abbreviations

Å – Angstrom

aa – amino acid

Ab – albumin

AD – Alzhemer's disease

ADA – N-(2-Acetamido)-iminodiacetic acid

APP – amyloid precursor protein

APS – ammonium persulphate

ATOX1 – antioxidante protein 1

ATP – adenosine triphosphate

CAPS – 3-(cyclohexylamino)-1-propanesulfonic acid

Ccs – copper chaperone for SOD

cDNA – complementary desoxiribonucleic acid

CHES – 2-(cyclohexylamino)ethanesulfonic acid

CNS – central nervous system

Co – cobalt

CO – carbon monoxide

COX – cytochrome *c* oxidase

COX17 – cytochrome *c* oxidase copper chaperone

Ctr1 – Cu transporter 1

Cu – copper

Dcytb – duodenal cytochrome *b* reductase

DMT1 – divalent metal transporter 1

DNA – desoxiribonucleic acid

DLS – dynamic light scattering

DSF – differential scanning fluorometry

EPPS – 4-(2-Hydroxyethyl)-1-piperazinepropanesulfonic acid

EPR – electron paramagnetic resonance

Fe – iron

GPI – glycosylphosphatidylinositol

GTS – glutathione

HAH1 – human ATOX1 homologue

hCp – human ceruloplasmin

HFE – hemochromatosis gene

HO – heme oxygenase

IRE – iron responsive element

IREG1 – iron-regulated transporter 1 or ferroportin 1

IRP – iron regulatory protein

K – Kelvin degree

kDa – kilo Dalton

LDL – low density protein

L-dopa – 3,4-dihydroxy-L-phenylalanine

LIP – labile iron pool

MES – 2-(N-morpholino)ethane sulfonic acid

MPD – m-phenylenediamine

MNK – Menkes ATPase

MOPS – 3-(N-morpholino) propanesulfonic acid

MT – metallothioein

NADH – nicotinamide adenine dinucleotide

PAGE – polyacrylamide gel electrophoresis

PCR – polymerase chain reaction

PD – Parkinson's disease

PEG – polyethyleneglycol

PIPPS – piperazine-N,n'-Bis (3-propanesulfonic acid

SOD – superoxide dismutase

Tc – transcuprein

TCEP – tris-(2-carboxyethyl) phosphine hydrochloride

Tf – transferrin

TfR – transferrin receptor

UTR - untranslated region

WND – Wilson ATPase

SDS – sodium dodecyl sulphate

SDS-PAGE – sodium dodecyl sulphate polyacrylamide gel electrophoresis

UV – ultraviolet rays

1. INTRODUCTION

Iron (Fe) and copper (Cu) are essential nutrients and its excess or deficit cause cell function fail leading to cell death. There is a metabolic linkage between these nutrients. Copper deficiency generates cellular iron deficiency, which in humans results in diminished work capacity, reduced intellectual capacity, diminished growth, alterations in bone mineralization, and diminished immune response which can be associated to several diseases and syndromes (Fox, 2003). In humans, the molecular linker between Fe and Cu was identified as being the plasma multi-copper oxidase ceruloplasmin (hCp).

1.1. Copper and Iron Metabolism

Copper and iron belong to the sub-family of transition elements that also includes zinc, nickel, cobalt, manganese and chromium. Cu has two oxidation states, cuprous (Cu^{1+}) and cupric (Cu^{2+}). Cu^{2+} is soluble, whereas Cu^{1+} solubility is in the sub-micromolar range. In biological systems, Cu is found mainly in the Cu^{2+} form, since in the presence of oxygen or other electron acceptors Cu^{1+} is readily oxidized to Cu^{2+}. Cu oxidation is reversible as Cu^{2+} can accept an electron from strong reductants such as ascorbate and reduced glutathione (Galhardi et al., 2004).

Iron exists in two stable oxidative states, ferrous (Fe^{2+}) and ferric (Fe^{3+}). In aqueous media, as plasma, Fe^{2+} is spontaneously oxidized by molecular oxygen to Fe^{3+} to form $Fe(OH)_3$. The maximal solubility of Fe in an oxidative environment such as extracellular fluids is limited by the product solubility constant of $Fe(OH)_3$. At pH 7.0 the maximal solubility of Fe^{3+} is much lower than the maximal solubility of Fe^{2+}. Thus, because of the low solubility of Fe in the presence of oxygen, over time organisms have been forced to evolve proteins that are able to bind Fe^{3+} and keep it thermodynamically stable and, at the same time, kinetically available for biological processes. In vertebrates, Fe^{3+} binds to the plasma protein transferrin (Tf), which has two Fe^{3+} binding sites, and is delivered where needed (Aisen and Listowsky, 1980).

The essentiality of iron and copper resides in their capacity to participate in one-electron exchange reactions, but the same property that makes them essential also generates free radicals that can be deleterious to cells. Thus, a concerted regulation of cellular copper and iron levels is crucial (Arredondo and Nunez, 2005). Fe^{2+} e Cu^{1+} transform through Fenton reaction, hydrogen peroxide (H_2O_2), a weak oxidant, into hydroxyl radical ($OH^{\cdot}$), one of the most strong reactive species found in nature (Messerschmidt, 1989). This process was first described in 1894 by H.J.H. Fenton. In cellular reductive environment, Fe^{3+} or Cu^{2+} are reduced to Fe^{2+} or Cu^{1+} (Haber-Weiss reaction) generating a vicious cycle of $OH^{\cdot}$ production (figure 1.1).

Fenton reaction:	$Fe^{2+} + H_2O_2 \rightarrow Fe^{3+} + OH^- + {}^{\cdot}OH$
Haber-Weiss reaction:	$Fe^{3+} + O_2^{\cdot-} \rightarrow Fe^{2+} + O_2$
	$Fe^{3+} + H_2O \rightarrow Fe^{2+} + H^+ + {}^{\cdot}OH$
	$Fe^{3+} + H_2O_2 \rightarrow Fe^{2+} + OOH^- + H^+$

Figure 1.1 | Haber-Weiss cicle. Fenton and Hiber-Weiss reactions.

Copper is a cofactor for numerous enzymes and plays an important role in central nervous system development; low concentrations of copper may result in incomplete development, whereas excess copper maybe injurious. Copper is required for the function of over 30 proteins, some critical for the metabolism, including superoxide dismutase (SOD), ceruloplasmin (hCp) or cytochrome c oxidase (COX). SOD converts superoxide anions to hydrogen peroxide for further dismutation by catalase. Ceruloplasmin oxidizes Fe^{2+}, prior to Tf binding, and its absence does not produce marked changes in copper metabolism but leads to a gradual accumulation of Fe in liver and other tissues (Harris et al., 1995; Miyajima, 2003). Cu metabolism is altered in inflammation, infection, and cancer.

Iron is required as a cofactor for several essential biochemical activities, such as oxygen transport, energy metabolism and DNA synthesis. The biological functions of iron are based on its flexible coordination and its favorable redox potential which allows its association with proteins, oxygen binding, electron transfer and catalysis (Aisen et al., 2001). Iron is present in numerous essential proteins, such as the heme-containing proteins, electron transport chain and microsomal electron transport proteins, iron–sulfur proteins and enzymes such as ribonucleotide reductase, and tyrosine hydroxylase. Animal studies have revealed the Fe has relevant roles in neuronal and immune functions (Beard et al., 2003). A poor diet on iron leads to irreversible alterations of brain function related to insufficient myelination and defective establishment of the dopaminergic tracts (Agarwal, 2001; Beard et al., 2003). The immune response is also affected and macrophages exhibit reduced bactericidal activity (Hallquist et al., 1992).

1.1.1. Copper metabolism and homeostasis

Cooper metabolism it still not fully understood in humans. An efficient Cu absorption varies depending upon the diet. Infancy represents one of the most critical periods in life in terms of Cu requirements because rapid growth increases Cu demands, whereas diets based on milk provide low amounts of the element (Lonnerdal, 1996). 40-50% Cu is absorbed by the small intestine, and transported to liver bound to specialized proteins, to be then distributed as a cofactor in cuproproteins. Excess Cu is disposed through bile and secreted into intestine in faeces (figure 1.2).

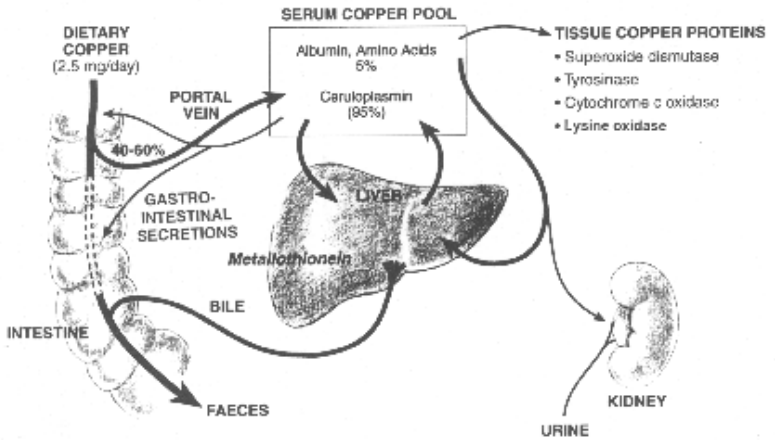

Figure 1.2 | Model of copper metabolism in humans. Ingested copper is absorbed from the gut, transported to liver bound to plasma proteins and distributed to cuproproteins. Copper is secreted into bile and excreted to the gut again in feces (personal communication by J.L. Collan to the IPCS, 1996).

Cu regulation seems to be very thigh. Body Cu levels are the result of a balance between Cu absorption and Cu excretion by the bile but although important advances have been made in the understanding of Cu excretion, the mechanisms that govern intestinal Cu absorption remain largely a mystery. In humans, Cu is absorbed primarily by the small intestine however the mechanism by which Cu enters the cells of the intestinal mucosa and crosses into the interstitial fluid and blood is not well understood. Once in blood stream, Cu binds to two proteins, albumin (Ab) and transcuprein (Tc). In hepatocytes Cu binds ceruloplasmin during its synthesis in the *trans* Golgi network.

Cell Cu homeostasis, is maintained by two homologous cation transporting P-type ATPases, Menkes (MNK) and Wilson ATPases (WND) (Bull et al., 1993; Mercer et al., 1993; Tanzi et al., 1993). They have similar structures and parallel roles in regulating the Cu status of cells and tissues and in supplying Cu to secreted cuproproteins. In most cells, MNK is responsible for excreting Cu when levels become high. In hepatocytes, this role is carried out by WND, disposing excess Cu through the bile. Both proteins supply Cu to the enzymes that are secreted by the cell by pumping the metal ion into the *trans* Golgi network, where the metal is incorporated into the apo-ceruloplasmine. The regulation of Cu efflux by the cell is achieved by copper-induced relocalization from the *trans* Golgi network to the plasma membrane in the case of MNK or to an intracellular vesicular compartment in the case of WND (figure 1.3).

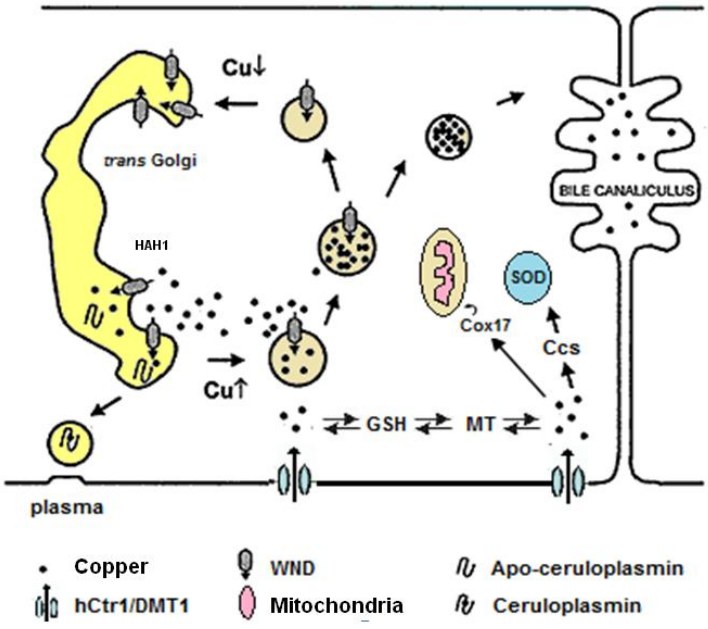

Figure 1.3 | Model of copper metabolism in hepatocytes. Copper crosses the plasma membrane through either Ctr1 (*Cu transporter 1*) or DMT1 (*Divalent Metal Transporter 1*), and is shuttled to the *trans* Golgi network by chaperone Hah1/Atox1, which delivers Cu to the WND (or MNK in enterocytes). At Cu basal levels WND is located at the *trans* Golgi network but at higher levels is distributed into vesicles in cytoplasm. As Cu is stored its intracellular concentration decays and the ATPase returns to the *trans* Golgi network and the copper in vesicles is secreted into bile. In the Golgi complex Cu is incorporated into apo-hCp which is then released into plasma. The chaperone protein, Ccs (*Copper chaperone for SOD1*) delivers Cu to cytosolic SOD, which dismutates superoxide into hydrogen peroxide. Cox17 (*cytochrome c oxidase copper chaperone*) delivers Cu to the mitochondria, where it is required for cytochrome c oxidase. Glutathione (GSH) may also be a chaperone by binding Cu^{1+} and delivering it to metallothionein (MT) and to some copper-dependent apoenzymes, such as SOD (Carroll et al., 2004). Adapted from (Arredondo and Nunez, 2005; Schaefer et al., 1999).

Ctr1 (*Cu transporter 1*), or hCtr1 in humans, promotes intestinal cells copper absorption and is also thought to facilitate the diffusion of Cu across the brush border membrane, even at low Cu concentrations (Moller et al., 2000). Another likely Cu transporter in the brush border is DMT1 (*Divalent Metal Transporter 1*), already described as a transporter of Fe^{2+}, Cd^{2+} e Mn^{2+} (Arredondo et al., 2003). Several other Cu chaperone were identified. These specialized proteins carry Cu to specific intracellular sites and enzymes, preventing the presence of free Cu ions in cell. The Cu chaperone HAH1/ATOX1 (Antioxidant protein 1 homolog) carries Cu ions to the *trans* Golgi network where deliver it to the P-type ATPase present there (WND in hepatocytes or MNK in enterocytes) (Hamza et al., 1999; Hung et al., 1998). Another chaperone is Ccs (*Copper chaperone for SOD1*) which delivers Cu to the SOD in cytoplasm. Cox17 (*cytochrome c oxidase copper chaperone*) takes Cu to the mitochondria, where it is required for cytochrome *c* oxidase. Glutathione (GTS) could also play the role of Cu chaperone delivering it to cytosolic metallothioneins (MT) or to hCtr1 in the plasma membrane, but this pathway is not fully understood and remains to be further explored.

Body copper homeostasis is the result of a balance between Cu absorption and Cu excretion by the bile (Linder and Hazegh-Azam, 1996). In the enterocytes, Cu is absorbed by Cu transporters and kept in the cytosol, binding to MTs. Cu accumulation in the hepatic or neuronal tissue results in copper intoxication and cell damage. When there is copper deficiency the iron uptake and transport within the body is affected, and iron tends to accumulate in several tissues. Thus, copper deficiency results in an anemia similar to that observed in iron deficiency.

P-type ATPases, MNK and WND are very important in Cu homeostasis and its impaired results in a severe phenotype. Wilson's disease, associated with WND ATPase impair, leads to copper accumulation in hepatic cells. Cu is not excreted into the bile nor is incorporated into hCp, causing chronic cirrhosis during childhood. Menkes' disease, associated with fail of MNK ATPase, is caused by deficient Cu absorption in the intestine leading to severe fail of several organs and tissues (muscle, kidney, lungs), bone anomalies and neuronal disorders.

Cu metabolism is also altered in inflammation, infection, and cancer, and Cu and hCp levels rise, in contrast to Fe levels, which decline in serum during infection and inflammation. Synthesis and secretion of hCp by hepatocytes is stimulated by interleukin-1 and -6 (Linder and Hazegh-Azam, 1996). Copper is essential for an efficient immune response, being necessary to the production of interleukin-2 by activated lymphocytic cells (Percival, 1998). In cancer, plasma hCp is positively correlated with disease stage and malignant tumors have concentrations of Cu that are often higher than those of their tissue of origin (Eagon et al., 1999).

1.1.2. Iron metabolism and homeostasis

Iron is an essential nutrient and its importance for the survival of animals, plants and microorganisms is well established. Accordingly to the World Health Organization estimate that about 50% of the world's 5-14 year old children are anemic, as about 50% of the world's pregnant women. The most common symptom of anemia is a general feeling of lack of energy (Beard, 2001). Fe has particularly relevant roles in neuronal and immune functions (Beard et al., 2003). The human body contains approximately 3 - 5 g of iron and from a diary diet about 15 mg of iron is ingested from which

only 1 - 2 mg is absorbed. Iron body distribution is described in figure 1.4.

A significant fraction of cellular iron is associated with proteins in the form of heme, a prosthetic group composed of protoporphyrin IX and a Fe atom. The Fe insertion into protoporphyrin IX is catalyzed by ferrochelatase in the mitochondria. Heme is then exported to the cytosol for incorporation into hemoproteins. Heme degradation is catalyzed by the microsomal heme oxygenase (HO) and the free Fe^{2+} is reutilized (Ryter and Tyrrell, 2000). This reaction also produces carbon monoxide (CO) and biliverdin, which is further converted into the antioxidant bilirubin. The most comum mammalian hemoproteins are hemoglobin and myoglobin, oxygen carriers in the erythrocytes or muscle cells, respectively. Other hemoproteins are oxygenases, peroxidases or nitric oxide synthases. Heme may also act in electron transfer reactions (such as in cytochromes *a*, *b* or *c*), as a substrate activator (in cytochrome oxidase, cytochrome P450, catalase) or as a nitric oxide sensor (in guanylate cyclase) (Papanikolaou and Pantopoulos, 2005).

The most abundant forms of non-heme iron in metaloproteins are iron-sulfer clusters, such as 2Fe-2S, 3Fe-4S or 4Fe-4S, that may be involved in electron transfer (*e.g.* the Rieske proteins in complex III of the respiratory chain), transcriptional regulation, structural stabilization or catalysis (Beinert et al., 1997). Other forms if catalytically active, protein-associated iron may include iron-oxo clusters (*e.g.* ribonuleotide reductase) or mononuclear iron centers (*e.g.* lipoxygenase and cycloxygenase).

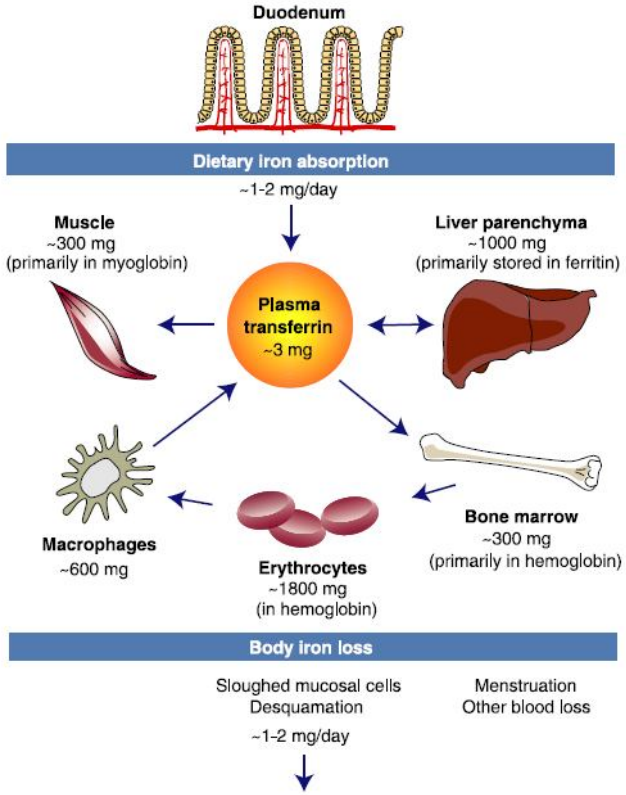

Figure 1.4 | Iron distribution in the adult human body. A healthy individual absorbs daily 1-2mg of iron from the diet, which compensates iron losses by cell desquamation in skin and the intestine. The human body contains 3-5 g of iron and the majority of body iron is used within hemoglobin in erythrocytes (60-70%). About 20-30% of body iron is stored in hepatocytes and in reticuloendothelial macrophages, as ferritin. The remain body iron is localized in myoglobin, cytochromes and iron-containing enzymes Erythropoiesis requires approximately 30 mg iron/day, which is mainly provided by macrophages iron recycling, that ingest senescent erythrocytes and release iron to transferrin (Papanikolaou and Pantopoulos, 2005).

Two thirds from absorbed iron derives from heme and the remaining fraction is inorganic. Fe absorption occurs in the apical membrane if duodenal enterocytes, but the pathway for heme uptake is not fully characterized. The mechanism for inorganic iron transport is better established. The low pH of the gastric effluent dissolves ingested inorganic iron and facilitates its enzymatic reduction to Fe^{2+} by the ferrireductase Dcytb (*Duodenal citochrome b reductase*) (McKie et al., 2001). Fe^{2+} is then transported across the membrane by DMT1 (*Divalent Metal Transporter 1*), also capable of transporting Mn^{2+}, Cu^{2+}, Co^{2+}, Zn^{2+} or Cd^{2+} (Fleming et al., 1997). In the enterocytes, heme iron is liberated by HO and follows the fate of inorganic iron, it is either stored in ferritin or transported across the membrane by ferroportin 1 (also known as IREG 1) (Donovan et al., 2000)**,** converted to Fe^{3+} by membrane ferroxidase hephaestin and transferred to plasma transferrin (Tf) (Figure 1.5). hCp shares homology with hephaestin and it may also act as a ferroxidase facilitating iron exportation from enterocytes to Tf (Hellman and Gitlin, 2002).

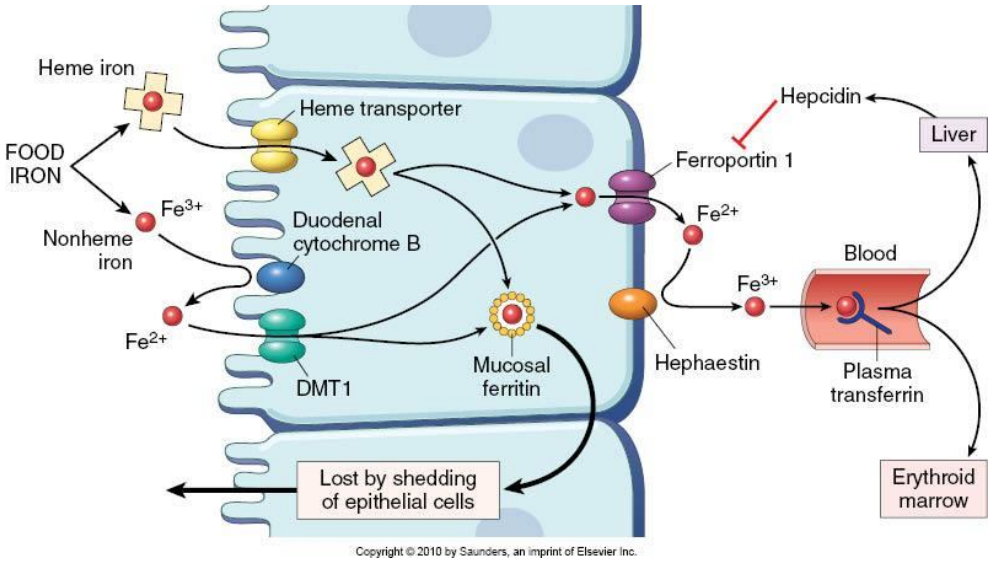

Figure 1.5 | Iron absorption in intestinal epithelium. Representation of iron uptake by enterocytes.

Cell iron homeostasis is shown in figure 1.6. When in plasma Fe-Tf binds to its specific receptor on the cell surface, TfR1 (*transferrin receptor 1*) and undergoes endocytosis being transported to the endosome (Ponka et al., 1998). Fe^{3+} is then released from Tf by acidification of the endosome to pH 5.5, reduced to Fe^{2+} by Dcytb and transported across the endosomal membrane by DMT1 to cytosol. Fe is used for incorporation into iron-containing proteins and the excess is stored into ferritin. The mechanisms of intracellular iron transport to organelles, such as mitochondria, are still not fully understood. It seems that there is a 'labile iron pool' (LIP) in the cytosol, which remains bound to chelates, such as citrate, ATP, AMP or pyrophosphate (Kakhlon and Cabantchik, 2002; Petrat et al., 2002; Wang and Pantopoulos, 2011).

Iron losses in mammals are not regulated. Thus, body iron homeostasis is regulated at the level of iron absorption by epithelial cells. Misregulation of this process leads to iron deficiency or overload. Iron absorption by enterocytes depends on body iron levels, erythropoiesis levels, hypoxia and inflammation (Papanikolaou and Pantopoulos, 2005).

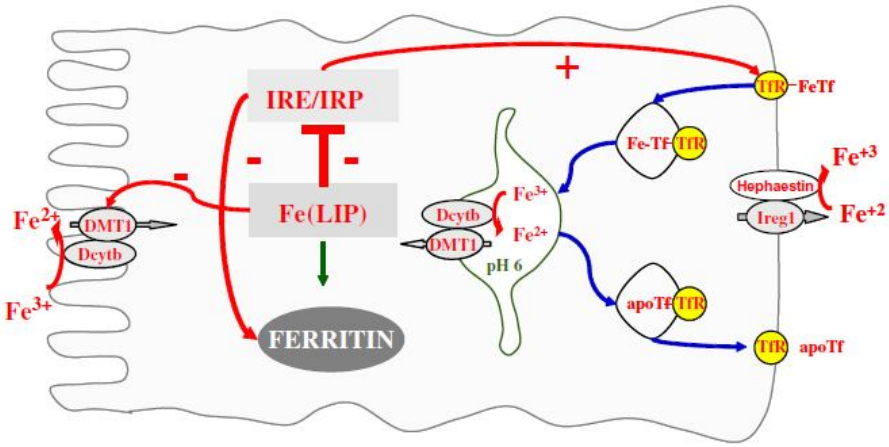

Figure 1.6 | Cellular iron metabolism model. TfR1 and ferritin are essential for the control of cellular iron homeostasis and their expression is coordinately and reciprocally controlled in response to iron levels by a mechanism involving mRNA-protein interactions (Hentze et al., 2004; Pantopoulos, 2004). TfR1 and ferritin mRNA contain 'iron responsive elements' (IRE) in their 3' or 5' UTRs. These motifs of about 30 nucleotides fold and form a loop providing a binding site for 'iron regulatory proteins' (IRP), which are activated in iron-starved cells. The IRE-IRP interactions stabilize TfR1 mRNA, which contains five IRE copies, increasing TfR1 expression levels and the iron-starved cells acquire more iron from Tf. The IRE-IRP interaction in ferritin mRNAs inhibits their translation and iron-starved cells do not express ferritin, which under these conditions is not necessary. In iron-replete cells IRPs are inactive leading to TfR1 mRNA degradation and ferritin mRNA translation. This inhibits iron uptake from transferring and storage and detoxification of excess intracellular iron (Papanikolaou and Pantopoulos, 2005; Wang and Pantopoulos, 2011).

1.2. Cooper and Iron Disorders

Copper and iron are essential metals and disorders related to these elements may be caused by misregulated transport, metabolism or homeostasis. Copper's biological, functional and structural relevance in animals and humans is related to about one dozen cuproenzymes, such as cytochrome c oxidase, superoxide dismutase, lysyl oxidase, tyrosinase, ceruloplasmin and dopamine β-monooxygenase (table 1.1). These enzymes are responsible for several important physiological reactions. These include mitochondrial transport to support oxidative phosphorylation, removal of reactive oxygen species, collagen, elastin and catecholamine biosynthesis, pigmentation, blood coagulation, amine oxidation and neuropeptide activation (Danks, 1988). Several cuproenzymes act as a ferroxidase converting ferrous to ferric iron and seem to be crucial in iron efflux and homeostasis, as is the case of hCp. Copper deficiency, caused by environmental or genetic factors, leads to altered cuproenzyme function. Genetic diseases related to copper homeostasis leading to hipocupremia include Wilson disease (WND mutations, protein responsible for copper incorporation in hCP), Menkes' disease (MNK mutations, enzyme responsible for copper absorption by enterocytes and copper incorporation into several cuproenzymes) and aceruloplaminemia (hCp mutations, cuproenzyme responsible for copper transport and with ferroxidase activity, with a role in iron homeostasis and in the oxidation of biogenic amines). Copper has an important role in neurological disturbs. When copper levels are low some alterations occur at neurotransmitters level, such as norepinephrine, serotonin or dopamine, which may explain some behavior changes and development disorders that are observed in children.

Table 1.1 | Mammal cuproenzymes.
(Adapted from (de Bie et al., 2007; Prohaska, 2011; Vashchenko and Macgillivray, 2013))

Common name	Putative function	Consequences of deficiency
Amine oxidase	Signal transduction, leukocyte adhesion	
Cytochrome c oxidase	ATP production, mitochondrial respiration	Hypothermia, muscle weakness
Dopamine-β-monoxygenase	Norepinephrine synthesis	Neurological defeats
Extracellular superoxide dismutase	Antioxidant defense	Diminished protection against oxidative stress
Lysyl oxidase	Connective tissue formation	Laxity of skin and joints
Peptidylglycine α-amidating monooxygenase	Peptide (neuropeptide) amination (maturation)	Neuroendocrine defects
Superoxide dismutase 1	Superoxide elimination	Diminished protection against oxidative stress
Tyrosinase	Pigment formation	Hypopigmentation of hair and skin
Ferroxidases:		
Ceruloplasmin	Iron/Copper mobilization; iron and amine oxidation	Decreased circulating copper levels and iron deficiency
GPI-Ceruloplasmin	Macrophage iron efflux	Neurodegeneration
Hephaestin	Intestinal iron efflux	Decreased absorption iron levels

Iron is a component of several metalloproteins having a crucial role in essential metabolic pathways. Its deficit or excess can lead to complications involving organs failure, including neurological alterations, and eventually death. Different neuropathologies are involved in iron metabolism. Iron deficit may lead to cognitive failure, learning incapability and motor deterioration (Sadrzadeh and Saffari, 2004). Brain iron accumulation has been associated with Alzheimer's disease, Parkinson disease and other neurological disorders. Iron is responsible for the oxygen reactive species formation leading to cell death, since iron excess is related to toxicity (Halliwell, 1992; Halliwell and Gutteridge, 1985). There are also some iron homeostasis alterations that are hereditary, as is the case of hemochromatosis associated with *HFE* gene and its protein, which forms a complex with TfR on cell membrane in order to lower the affinity of the receptor to Tf.

1.2.2. Wilson's disease

Wilson's disease (OMIM#277900) is an autosomal recessive disorder caused by the loss-of-function mutation in the copper transport gene *ATP7B* or *WND*. This disorder was first described in 1912 and results in toxic copper accumulation and multiple organs failure. Mutations in WND protein result in impaired excretion of copper into bile and failure to incorporate it into hCp. This leads to hepatic copper accumulation and damage, elevated levels of non-ceruloplasmin-bound copper in the plasma and copper overload in extrahepatic tissues. Copper accumulation in liver and brain result in oxidative stress, hepatic failure and hemolytic anemia (de Bie et al., 2007). Some consider that brain copper accumulation results into neurodegeneration with motor symptoms including Parkinsonism, dystonia, ataxia, chorea, convulsions and cognitive failure, eventually leading to personality and behavior changes, including aggressive behavior and irritability (Attri et al., 2006; Das and Ray, 2006; de Bie et al., 2007; Taly et al., 2007). Oral copper chelating agents are effective in restoring copper homeostasis in many patients with Wilson's disease (Taly et al., 2007).

1.2.3. Menkes' diseases

Menkes' disease (OMIM#309400) is an infantile neurogenetic disorder caused by mutations in an X-linked gene, ATP7A or MNK, first described in 1962 as a copper deficiency (Menkes et al., 1962). MNK mutations result in diminished activity and thus, weak copper intestinal absorption causing systemic body copper deficit. MNK gene is expressed in muscle, kidney, lung, brain but not in the liver. MNK plays a significant role in the development and maintenance of the central nervous system, which can be seen by the marked behavioral, neurological, and developmental abnormalities observed in Menkes' disease patients. Children born with this genetic alteration show development delay, bone anomalies, weak and disordered hair growth, neurological alterations and multiple organs failure. These symptoms reflect the lack of activity of several cuproproteins, including hCp, until death by 3 years of age, depending upon the disease severity. Nowadays, common treatment relies on an early diagnostic and regular copper salt injections (Tumer and Moller, 2010).

1.2.4. Hemochromatosis

Hemochromatosis (HFE; OMIM#235200) is an autosomal recessive disorder and the most prominent iron-related disease in which pathologic symptoms arise from an excessive uptake of dietary iron and its deposition in many organs including the brain. The gene involved in hemochromatosis is known as *HFE* and is located at chromosome 6p21.3. The function of HFE protein is to complex with the transferrin receptor on the cell membrane and to lower the affinity of the receptor for Tf (Feder et al., 1998). The homozygous mutation of the C282Y HFE is responsible for the severe type of this disorder (Feder et al., 1997). The iron deposition is observed in patients mainly after 40 years old, in the liver, heart, skin and pituitary (Connor, 2003). It is suggested that mutations in the hemochromatosis gene *HFE* that can result in increased iron accumulation in the brain might be a risk factor for AD and Parkinsonism associated with hemochromatosis (Dekker et al., 2003; Moalem et al., 2000).

1.2.5. Aceruloplasminemia

Aceruloplasminemia (OMIM#604290) is an autosomal recessive disorder caused by mutations oh hCp gene (Harris et al., 1998; Waggoner et al., 1999). Individuals with this alteration show no imunoreactive hCp in plasma (Miyajima et al., 1987). About 40 mutations on hCp gene have been identified (*frameshift*, *nonsense*, *splice site* and *missense*) in 45 different families. About half of those mutations lead to the formation of a premature stop codon originating a non-functional C-terminal truncated protein (Daimon et al., 1995a; Takahashi et al., 1996; Yazaki et al., 1998; Yoshida et al., 1995). The molecular analysis of missense mutations have shown different structure-function relationships on hCp (Kono and Miyajima, 2006). This disorder is observed in individual between 25 and 65 years old and the most common symptoms are diabetes mellitus, glucose intolerance, basal ganglia and retinal degeneration and neurodegeneration causing ataxia, dystonia, dysarthria and dementia (Harris et al., 1998; Harris et al., 1995; Logan et al., 1994; Miyajima, 2003; Morita et al., 1992; Yoshida et al., 2000). This is caused by iron accumulation in organs, including

brain, which is what distinguish aceruloplasminemia from other iron disorders, such as HFE, suggesting an important role for hCp in brain iron homeostasis.

1.3. Ceruloplasmin

Human ceruloplasmin is a 132kDa α2-globulin from human blood serum that binds six copper ions. It contains ~95% of serum copper (Harris et al., 1998) and was first described in 1944 by Holmberg (Holmberg, 1944). hCp was latter characterized in 1948 as a cuproprotein (Holmberg and Laurell, 1948; Mittal et al., 2003). In 1952, Scheinberg and Gitlin observed a decreased concentration of plasma hCp in patients with Wilson's disease (Aldred et al., 1987; Scheinberg and Gitlin, 1952). Now it is known that is not hCp concentration, but its enzymatic activity which drops as the protein is synthesized in liver predominantly in the apo-form, as there is no copper incorporation by WND.

Soon after, the hCp was described as being related to neurodegenerative processes in humans. In 1966, Friden demonstrated that hCp is a ferroxidase suggesting a role for ceruloplasmin in iron homeostasis (Osaki et al., 1966). In the 1970's indirect indications concerning possible involvement of hCp in oxidation of epinephrine and serotonin in the CNS (Barrass and Coult, 1972; Barrass et al., 1972; Barrass et al., 1973; Barrass et al., 1974) were described and the protein was detected in the brain (Linder and Moor, 1977). Later the details of its synthesis in glial cells were described (Klomp and Gitlin, 1996; Mollgard et al., 1988; Patel and David, 1997; Patel et al., 2000).

In 1984, Putnam determined the complete amino acid sequence of hCp, revealing the single-chain structure of this molecule (Takahashi et al., 1984). Isolation and characterization of hCp cDNA confirmed the amino acid sequence obtained by protein chemistry and demonstrated abundant expression of the ceruloplasmin gene in the liver (Koschinsky et al., 1986; Yang et al., 1986). hCp was identified as an essential protein in 1995 with the identification of patients with aceruloplasminemia (Harris et al., 1995).

It is thought that hCp plays an important role in the metabolism and development of nervous tissue (Friedenberg and Brighton, 1966), as its deficiency, its impaired function, or the failure of copper metabolism can lead to severe neurodegenerative diseases as Parkinson's disease, Alzheimer's disease or aceruloplasminemia (Castellani et al., 1999; Kaneko et al., 2002b; Loeffler et al., 1996).

1.3.1. Gene structure and expression

hCp gene is localized to chromosome 3q23-q24 encoded in 20 exons encompassing approximately 65kb (Daimon et al., 1995b; Koschinsky et al., 1987; Koschinsky et al., 1986). In hepatocytes, the *hCp* gene is expressed as two transcripts of 3.7 and 4.2 Kb, which arise from alternative polyadenylation sites within the 3' untranslated region (Koschinsky et al., 1986; Yang et al., 1986). Expression of these transcripts in the liver results in the 1046 amino acid protein detected in serum. hCp precursor has 1065 aa, and its first 19 residues encode for a signal peptide which is cleaved arising a 132 kDa serum protein with 6 N-glycosylation sites with 7-8% carbohydrate content (Koschinsky et al., 1986). hCp has a high homology to type-A domains of clotting factors V and VIII

(Patel and David, 1997). hCp is an acute phase reactant and the serum concentration increases during processes of inflammation, infection or trauma as a result of increased gene transcription in hepatocytes mediated by the inflammatory cytokines (Gitlin, 1988).

Serum hCp is predominantly synthesized in the liver, but extrahepatic gene expression has been described in brain, spleen, lung and testis (Aldred et al., 1987; Fleming and Gitlin, 1990; Klomp et al., 1996). In the CNS, hCp is expressed in neurons and astroglial cells, *e.g.* cerebral microvascular network involving dopaminergic neurons in *substantia nigra* (Klomp and Gitlin, 1996; Kuhlow et al., 2003; Loeffler et al., 2001). In astrocytes, and Sertoli cells, hCp is membrane anchored by glycosylphosphatidylinositol (GPI), which is caused by alternative splicing of exons 19 and 20 in *hCp* gene (Fortna et al., 1999; Mittal et al., 2003; Patel and David, 1997; Patel et al., 2000; Salzer et al., 1998). As a result, the latest 5 C-terminal aa found in serum hCp are replaced by a 30 aa stretch in GPI-hCp. This isoform seem to have an important role in iron oxidation and mobilization across blood brain barrier, which in cooperation with the iron exporter protein IREG1 provides the Fe efflux from astrocytes (Klibanoff et al., 1966; Trader and Frieden, 1966). The plasma hCp cannot cross the blood brain barrier. The insufficiency of hCp synthesis or its decreased activity in the cells of the CNS is regarded as one of the mechanisms underlying the development of a number of neurodegenerative disorders (Connor et al., 1993; Kuhlow et al., 2003; Qian and Wang, 1998; Snaedal et al., 1998; Torsdottir et al., 2001; Torsdottir et al., 1999). Both hCp isoforms are synthesized with six atoms of copper incorporated during biosynthesis in the Golgi complex (Harris, 2003; Holmberg and Laurell, 1948; Miyajima et al., 2003). Serum hCp has a half-life of 5.5 days with little or no exchange of hCp-bound copper after synthesis. Although copper has no effect on the rate of synthesis or secretion of hCp, failure to incorporate Cu during synthesis results in apo-hCp, an unstable protein with no ferroxidase activity (Kaneko et al., 2002b; Miyajima et al., 2002a; Perez-Aguilar, 2002). This apoprotein is rapidly catabolized in 5 hours (Nittis and Gitlin, 2002).

1.3.2. Metabolism

As referred, hCp is implicated in Cu and Fe metabolism. Fe is absorbed by epithelial cells in duodena and released into blood stream (Harris, 2002). hCp is involved in iron transport across the cell membrane. This protein oxidizes ferrous iron and incorporates the ferric form into apotransferrin (Kaneko et al., 2002a; Miyajima et al., 2002b). It is known that, at physiological pH, Fe^{2+} is autoxidized to Fe^{3+} with no need for a specific catalyst (Hellman et al., 2002). However, this non-enzymatic oxidation has a high probability of trigger reactions of Fenton and/or Haber-Weiss chemistry with the production of oxygen radicals. The role of hCp might be an efficient control of the level of ferrous iron oxidation without the production of hydrogen peroxide as an end product.

Cu is absorbed in duodena and transported to liver by hCtr1 and stored in hepatocytes (Miyajima, 2000a, b). Once in the cell, Cu might be *i)* stored in Cu-thioneine form, *ii)* transported by Ccs to SOD, *iii)* delivered into mitochondria by cox17 or *iv)* transported by HAH1 to WND ATPase localized in the trans-Golgi network. WND ATPase helps to Cu incorporation into hCp (Kohno et al., 2000). hCp carries about 90% of the total copper in human plasma but its synthesis is not dependent on Cu levels (*e.g*. Wilson disease). It is also thought to provide Cu^{2+} ions for other proteins. The

copper stored into hepatocytes can generate hydroxyl radicals caused by the redox cycle between Cu^{1+} e Cu^{2+} which may cause damage in DNA, proteins, lipids and cell intoxication, leading to cirrhosis. Cu can also accumulate in the brain causing neurodegeneration with hyperkinesis, dysarthria and dementia.

1.3.3. Role and function

Ceruloplasmin is a metalloenzyme belonging to the iron (II) oxygen oxidoreductase class, EC 1.16.3.1, and to the multicopper oxidases family, also known as blue oxidases.

In vitro studies showed that hCp is capable of catalyze the oxidation of different substrates:

i) Fe^{2+}, the substrate with the higher V_m and lower K_m;

ii) a group of bifunctional amines and phenols (including biogenic amines, epinephrine and serotonin (5-hydroxy-indole family) and phenothiazines) which do not depend on iron for its activity;

iii) pseudo-substrates including several reducing agents capable of reducing Fe^{3+} or partially oxidize the intermediaries in ii) (Frieden and Hsieh, 1976b).

So, hCp has ferroxidase activity, oxidizing Fe^{2+} to Fe^{3+} and incorporating it into apotransferrin (Osaki et al., 1966, 1971) and has an essential role in iron metabolism (Attieh et al., 1999; Harris et al., 1995; Lahey et al., 1952; Vulpe et al., 1999). It is also an acute phase reactant having antioxidant properties and being capable of remove H_2O_2 (Giurgea et al., 2005; Gutteridge, 1978). However, studies show that this protein can also act as a prooxidant promoting LDL (low density protein) oxidation (Mukhopadhyay et al., 1996; Mukhopadhyay et al., 1997). It is known that chloride inhibits hCp ferroxidase activity at pH 5.5, but it is thought that at neutral pH chloride might enhance the oxidase activity of hCp and this enzyme might even exhibits an important role in the oxidation of several substrates present in the serum plasma (Musci et al., 1995). A group showed that such anions as chloride or azide increase the aminoxidase activity of hCp and that this effect is observed with non iron substrates, while Fe^{2+} oxidation remains unaffected (Musci et al., 1999).

Human ceruloplasmin functions include:

a) *Ferroxidase activity, eliminating free iron in the plasma, protecting blood and lipidic membranes from peroxidative damage (antioxidant), and/or mobilize iron from cells for transporting via Tf;*
b) *Aminoxidase activity for controlling the levels of biogenic amines in the plasma, spine cord and interstitial fluids;*
c) *Copper transport for metal distribution for extra hepatic tissues.*

1.3.4. Functional mechanism

Multicopper oxidases are characterized by the presence of three types of spectroscopically distinct copper sites (Messerschmidt and Huber, 1990). These are usually referred as type I, II or III copper centers and can be characterized in the following way (Holwerda et al., 1976; Malmstrom, 1982):

a) **T*ype I***: *a single Cu^{2+} coordinated by 2 histdine residues and a cysteine residue, in which thiolate ion act as an electron donor, and a variable axial ligand, in a trigonal planar structure. Those proteins with type I copper center show high redox potentials (>250mV) and a strong absorption at 600nm, due to S→ Cu charge transfer conferring a blue color and the name 'blue oxidases'. This copper center type has a detectable EPR (electron paramagnetic resonance) spectrum (Sakurai and Kataoka, 2007; Yoshida et al., 1995).*

b) ***Type II:*** *a single Cu^{2+} coordinated by N/NO in a tetragonal square-planar configuration. EPR parameters are detectable but those ions have no specific absorption and no blue color.*

c) ***Typo III:*** *two antiferromagnetically (*i.e. *spin pairing) coupled copper ions (Cu^{2+}-Cu^{2+}), each one coordinated by 3 histidine residues. EPR parameters are not detectable but those ions absorb strongly at 330nm.*

Generally, multicopper oxidases are promiscuous with regards to their reducing substrates and are capable of performing various functions in different species. These oxidases catalyze the four-electron reduction of dioxygen to two molecules of water, with the concomitant reduction of one electron from the substrate. The type I Cu^{2+} is the primary electron acceptor. This electron cannot be passed directly to the type III center before type II Cu^{2+} is reduced, because the type III center acts as a 2 electrons cooperative acceptor. The reduction of the two type III Cu^{2+} occurs by an intramolecular transfer of the 2 electrons from type I and type II reduced centers, and then to the oxygen moiety (Malmstrom, 1982). The aa sequences responsible for the copper binding are highly conserved between the multicopper oxidases, but the substrates, number of type I copper centers and the intramolecular mechanisms for electronic transfer vary between proteins (Bento et al., 2007). As exemples of this family members there is the lacase, the ascorbate oxidase, Fet3 and hephaestin, a hCp homologue needed to the iron efflux from placenta and enterocytes (Marques et al., 2012; Vashchenko and Macgillivray, 2013).

Ceruloplasmin, the only blue copper oxidase found in humans, has 3 type I cooper centers, which conferee a intense blue color to this blue oxidase, and a type II Cu^{2+} coordinated by 2 nitrate atoms close to the 2 antiferromagnetically coupled type III Cu^{2+}. The type II and type III copper ions form a trinuclear Cu^{2+} cluster where the oxygen binds during the catalytic cycle and gets reduced to water (Miyajima et al., 1998). The hCp X-ray tridimensional structure confirmed the presence of this trinuclear cluster and the identity of the residues involved in the cooper binding and stabilization (Bento et al., 2007; Jeong and David, 2003).

1.3.5. Tridimensional structure

Ascorbate oxidase X-ray crystallography structure (D'Andrea et al., 1989; Malmstrom, 1982) and by sequence analysis allowed us to understand that hCp has a six-domain structure involving a threefold repeat and that domains 2, 4 and 6 should bind mononuclear coppers, with a possible trinuclear site between domains 1 and 6 (Messerschmidt and Huber, 1990).

Later, the overall organization of ceruloplasmin and the nature of the 6 copper binding sites was determined by X-ray crystallography at a resolution of 3.1 Å (Zaitseva et al., 1996) and more recently at 2.8 Å (Bento et al., 2007) (figure 1.7 and table 1.2). The six cupredoxin-like domains are arranged in triangular array and each of them comprises a β-barrel. Cupredoxins are single domain β-barrel proteins that bind a mononuclear type I copper redox site and are involved in inter-molecular electron transfer reactions (figure 1.8) (Roberts et al., 2002). A β-barrel is a large beta-sheet that twists and coils to form a closed structure in which the first strand is hydrogen bonded to the last. β-strands in β-barrels are typically arranged in an antiparallel way.

hCp has five disulphide bridges located in domains 1–5 and serve to anchor the last strand of each domain. The C-terminal strand in domain 6 is not anchored to domain 6 through a disulphide bridge. Ceruloplasmin is readily cleaved into three fragments with molecular weights of 67, 50 and 19 kDa respectively. The 19-kDa fragment corresponds almost exactly to domain 6 (Takahashi et al., 1983; Zaitseva et al., 1996). hCp shows heterogeneity with respect to its carbohydrate moieties, but has at least 3 glycan chains ending in sialic acid (Bento et al., 2007; Endo et al., 1982).

Figure 1.7 | A view of the human ceruloplasmin X-ray crystallography structure. Domains 1, 2, 3, 4, 5 and 6 in green, red, yellow, purple, orange and pink, respectively, and the locations of the metal binding sites for Cu^{2+} as blue spheres and O_2 as light-blue spheres. The figures were prepared with the *PyMOL* program (http://www.pymol.org) using the Research Collaboratory for Structural Bioinformatics Protein Data Base protein code 2J5W (Bento et al., 2007).

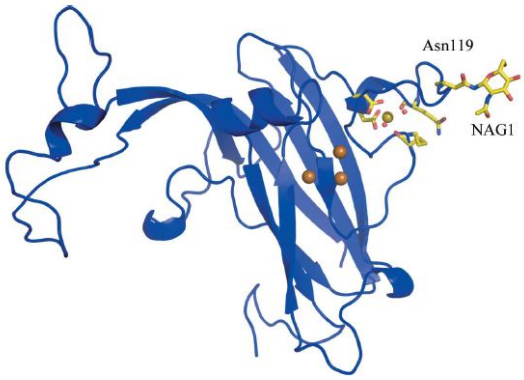

Figure 1.8 | hCp cupredoxin-like domain 1. The trinuclear copper cluster (Cu^{2+} as orange spheres) and the glucan chain at N119 residue are shown (Bento et al., 2007)*.*

1.3.5.1. Copper binding sites

As expected, three copper atoms bind in domains 2, 4 and 6 as mononuclear centers, and the remaining 3 form a trinuclear cluster between domains 1 and 6 (figure 1.9). The disposition if the trinuclear cluster and the nearest mononuclear copper, that in domain 6 is closely similar to that found in the subunit of ascorbate oxidase (Messerschmidt et al., 1989), might support the hCp oxidase function.

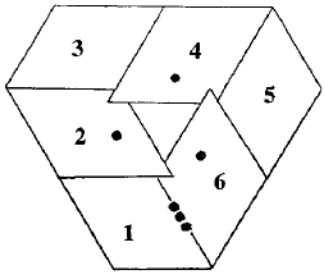

Figure 1.9 | Schematic diagram of hCp structure. Domains 1-6 and (●) copper centers (Zaitseva et al., 1996).

1.3.5.1.1. Mononuclear type I copper centres

One type I site is in the C-terminal domain (domain 6) coupled to the trinuclear cluster via a CysHis pathway and the other 2 type I Cu sites are found in domains 4 and 2 (Zaitseva et al., 1996). The type I Cu sites in domains 4 and 6 are both redox-active, and both have a divalent metal ion binding (M^{2+}) site adjacent to them and a trivalent metal ion biding site (M^{3+}) located above this and closer to surface (Lindley et al., 1997). This suggested that both may be involved in the ferroxidase activity of hCp and was latter supported by structural data (Bento et al., 2007). It seems that only the type I copper in domain 6 at a distance of 12–13 Å from the trinuclear cluster is absolutely necessary for hCp catalytic action (Messerschmidt et al., 1992). The distances between the copper ions is around 18 Å which is well within the range of effective electron transfer (figure 1.10) (Lindley et al., 1997; Patel et al., 2000) and it is possible that the copper ions in domains 2 and 4 could provide a slower route of electron transfer, allowing the oxidation of more than one substrate molecule at a

time. This could accomplish a more effective transfer of four electrons to the dioxygen molecule from the reducing substrate. The exact role of copper ion in domain 2 is yet not known. The type I Cu site in domain 2 differs from the others in lacking an axial methionine being replaced by an aliphatic leucine residue (Bento et al., 2007; Salzer et al., 1998). Metal soaking or organic substrate-soaking experiments showed no reducing substrates binding to domain 2 (Bento et al., 2007). Some studies showed that the type I copper in domain 2 remains permanently reduced, at least in part due to a high reduction potential, and since this site cannot be oxidized it is not catalytically relevant and is likely a vestige of gene duplication (Patel and David, 1997; Patel et al., 2000).

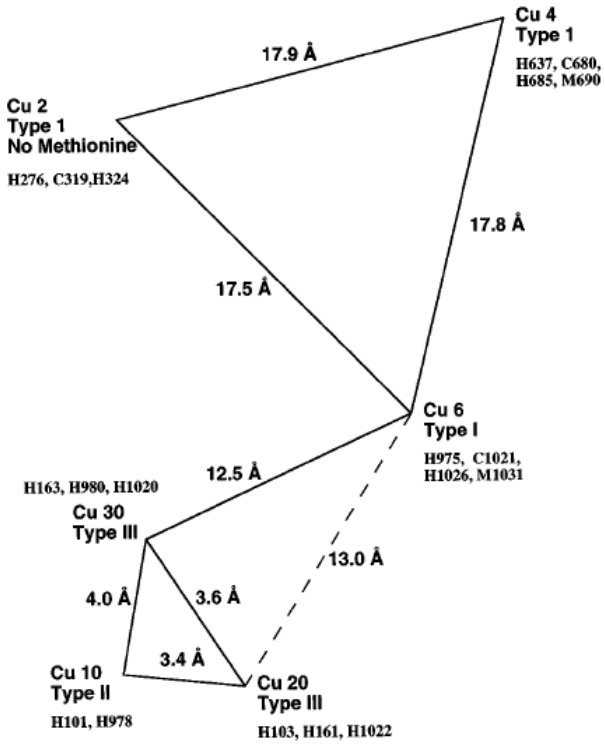

Figure 1.10 | Copper centers in hCp. Separation of the copper atoms in the trinuclear centre, the distance of this cluster from the nearest mononuclear copper in domain 6, and the separation between the mononuclear copper atoms. Copper binding histidine residues are represented in the diagram (Zaitseva et al., 1996).

1.3.5.1.2. Trinuclear copper centre

The trinuclear copper center has a type II and two type III copper cations with a dioxygen moiety bound (figure 1.11). The acidic residue E1032 may be necessary for the initial protonation of the dioxygen molecule. The type II copper seems to have two configurations, one linked to an oxygen moiety and the other to a water moiety, with a hydrogen bond formed with the hydroxyl group of Y107, in either case.

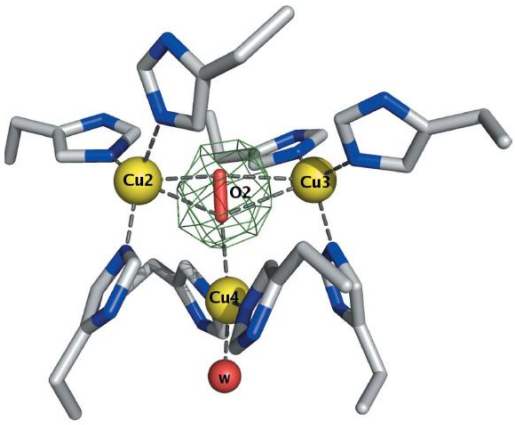

Figure 1.11 | Trinuclear copper centre. Located between domains 1 and 6 with a water molecule attached to the type II copper and a diatomic species, assumed to be dioxygen, placed within the type III cluster (Bento et al., 2007).

1.3.5.2. Iron binding sites

Structural data indicates that the iron-binding sites seem to be in domains 4 and 6 of the hCp structure, which seems to be consistent with earlier biochemical data suggesting two iron-binding sites in the enzyme (Frieden and Hsieh, 1976a). The access to these sites is limited to relatively small substrates by three large protuberances at the top of the hCp molecule (Bento et al., 2007). It is not yet fully understood and there is no published structural data but, both Fe^{2+} and Fe^{3+} seem to bind to sites near the outside of the protein. The Fe^{2+} releases an electron to the nearest mononuclear copper and then translocate to the other site with E597 and E935 in domains 4 and 6, respectively, playing key roles in the translocation process (figure 1.12). At this site the ferric iron would be available for collection, for example, by serum transferrin (Bento et al., 2007).

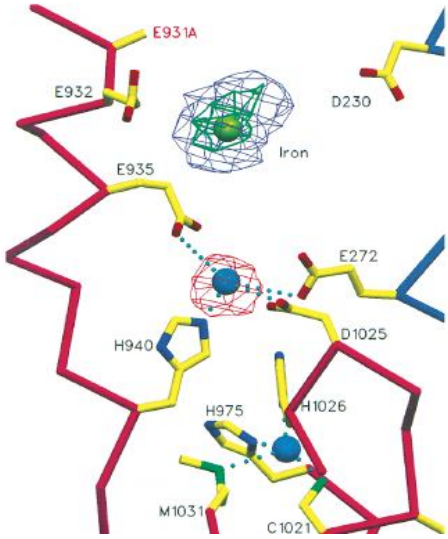

Figure 1.12 | Cation binding to ceruloplasmin by Fe^{2+}. The *red* electron density is negative indicating loss of the labile Cu^{2+} cations. The *blue* density is positive indicating acquisition of cations at the holding sites (Lindley et al., 1997).

Table 1.2 | hCp sequence features (Bento et al., 2007; Lindley et al., 1997; Zaitseva et al., 1996).

Feature	Positions (bp)	Length (bp)	Description
Molecule processing			
Signal peptide	1 – 19	19	(Takahashi et al., 1984)
Ceruloplasmin chain	20 - 1065	1046	
Domains			
1	20 – 211	191	
2	212 – 359	147	
3	360 – 572	212	
4	573 – 722	149	
5	723 – 903	180	
6	904 – 1065	161	
Sites			
Metal binding	H120	1	Type 2 Copper 1 – Domain 1
Metal binding	H122	1	Type 3 Copper 2 – Domain 1
Metal binding	H180	1	Type 3 Copper 2 – Domain 1
Metal binding	H182	1	Type 3 Copper 3 – Domain 1
Metal binding	H295	1	Type 1 Copper 4 – Domain 2
Metal binding	C338	1	Type 1 Copper 4 – Domain 2
Metal binding	H343	1	Type 1 Copper 4 – Domain 2
Metal binding	H656	1	Type 1 Copper 5 – Domain 4
Metal binding	C699	1	Type 1 Copper 5 – Domain 4
Metal binding	H704	1	Type 1 Copper 5 – Domain 4
Metal binding	M709	1	Type 1 Copper 5 – Domain 4
Metal binding	H994	1	Type 1 Copper 6 – Domain 6
Metal binding	H997	1	Type 2 Copper 1 – Domain 6
Metal binding	H999	1	Type 3 Copper 3 – Domain 6
Metal binding	H1039	1	Type 3 Copper 3 – Domain 6
Metal binding	M1040	1	Type 1 Copper 6 – Domain 6
Metal binding	H1041	1	Type 3 Copper 2 – Domain 6
Metal binding	H1045	1	Type 1 Copper 6 – Domain 6
Metal binding	M1050	1	Type 1 Copper 6 – Domain 6
Amino acid modifications			
Glycosylation	138	1	N-linked
Glycosylation	358	1	N-linked
Glycosylation	397	1	N-linked
Glycosylation	588	1	N-linked
Glycosylation	762	1	N-linked
Glycosylation	926	1	N-linked
Disulfide bond	174 ↔ 200		
Disulfide bond	276 ↔ 357		
Disulfide bond	534 ↔ 560		
Disulfide bond	637 ↔ 718		
Disulfide bond	874 ↔ 900		

1.4. Ceruloplasmin and neurodegeneration

Both GPI-anchored and secreted hCp enable IREG 1 to conduct the efflux of iron from cells of the CNS (Jeong and David, 2003). All these notions tend to indicate the important role of Cp in iron metabolism and this concept has been strengthened by some recent findings, including the one described for severe disorders of iron metabolism in aceruloplasminemia. It has been suggested that hCp catalyzed oxidation of biogenic amines, such as epinephrine, norepinephrine and serotonin, may be of importance in regulating the level of these stress hormones in the bloodstream and eventually in those areas of the brain where they act as neurotransmitters. Thus, hCp by its effect on the lifetime of biogenic amines in the bloodstream could play an important role in the regulation of brain chemistry necessary for mental function. It is also important to understand if hCp is able to enhance the oxidation of 6-hydroxydopamine (Medda et al., 1996), an intermediate product on the way to the formation of dopamine-melanin (Chapman et al., 1970). Oxidation of 6-hydroxydopamine by hCp does not result in H_2O_2 production. It seems likely that Cp might be the enzyme that controls or participates in controlling catecholamine oxidation in the brain and that its deficiency in cerebral structures underlies Parkinson's disease and perhaps other neurodegenerative syndromes (Floris et al., 2000). Enhanced oxidation of dopamine by hCp has been invoked to explain the lower dopamine levels found in Parkinson's disease.

1.4.1. Ceruloplasmin and Alzheimer's and Parkinson's diseases

Alzheimer disease (AD; OMIM#104300) is the most common disease associated to degenerative dementia with gradual deterioration of memory, behaviour, cognition and ability to perform simple tasks, due to cortical neurons death in the brain. Brain high metal levels, such as copper or iron, have been associated with AD (Altamura and Muckenthaler, 2009; Lovell et al., 1998; Roos et al., 2006). Amyloid precursor protein (APP) is a glycosylated protein of unknown biological function that is uniformly found in the membranes of cells in the body, but predominantly in the brain. Once in the CNS, this protein is cleaved into several peptides that might possible have some protecting effect on the integrity of synaptic structures. Most of these cleavage products are soluble and never accumulate. However, in AD there is a less soluble but more abundant variant, the β-amyloid peptide which aggregates forming plates that are found in the dysfunctional brain regions (Zerbinatti et al., 2004). Increased levels of copper, iron, zinc or aluminum accumulates in the plates. The β-amyloid peptide has copper and iron binding domains which interact with the peptide leading to its aggregation and oxidative stress in AD (Desai and Kaler, 2008; Dingwall, 2007; Ha et al., 2007; Sadrzadeh and Saffari, 2004; Taylor et al., 2002). The iron content in the AD brain is normally not increased and the abnormal iron accumulation must be evidence of a dysfunctional status of iron in the brain. This may indicate a dysfunctional ferritin increasing the oxidative stress and an important role of hCp in protecting the CNS from iron-mediated free radical injury (Patel et al., 2002). However, the hCp concentration was found normal in AD patients but its activity was lowered and the free copper in plasma was increased. This indicates failing in incorporating copper into hCp. Moreover, low amount of copper in AD brains may result in defective synthesis of hCp and other copper enzymes (Johannesson et al., 2012).

Parkinson's disease (PD; OMIM#168600) is a common progressive neurodegenerative motor pathology first described by James Parkinson in 1817. It is characterized by shaking, rigidity, slowness of movement, difficulty with walking and loss of equilibrium. Later, thinking and behavioral problems may arise, with dementia commonly occurring in the advanced stages of the disease (Gaggelli et al., 2006). This phenotype is associated dopaminergic neurons death in the substantia nigra and accumulation of Lewy bodies associated with mutations in α-synnuclein, a protein which is expressed in CNS with uncertain function (Rasia et al., 2005). This protein binds iron and copper and aggregates leading to the production of ROS and cell death at substantia nigra which causes motor dysfunction (Rasia et al., 2005; Sadrzadeh and Saffari, 2004). In PD patients there is loss of ferritin and iron is increased in the brain and hCp activity is lowered (Jin et al., 2011). It is possible that hCp variants may be associated with iron accumulation in the substantia nigra in PD patients. The oxidative activity of hCp is involved in the oxidation of catecholamines, as dopamine and epinephrine, in neurons. The resulting product is neuromelanin which binds iron keeping the levels of Fe^{2+} low in the midbrain. In PD the dying neurons release neuromelanin with is digested by microglia and the iron is released increasing the oxidative stress. hCp might have an important role in protecting neurons and preventing tissue damage and PD progression (Kristinsson et al., 2012). On the other hand enhanced oxidation of dopamine by hCp has been claimed to explain the lower dopamine levels found in Parkinson's disease.

1.4.2. Ceruloplasmin and neurotransmitters

As described before, biogenic amines oxidation by hCp seems to have an important role in hormones and neurotransmitters levels regulation in brain and bloodstream. hCp can use as substrates epinephrine, norepinephrine, dopamine, dopa and serotonin (figure 1.13). Zaitsev and colleagues showed that these substrates seem to bind at the same place in the hCp molecule, in domain 6, 9.7 Å distant from the type I copper site (Zaitsev et al., 1999). Apparently, residue D1025 is one of the ligands which bind the labile copper together with H940, E935 and E272. It is proposed that the amine binds to any labile copper, an electron is transferred to the domain 6 copper causing oxidation of the substrate, and eventual reduction of oxygen at the trinuclear copper site.

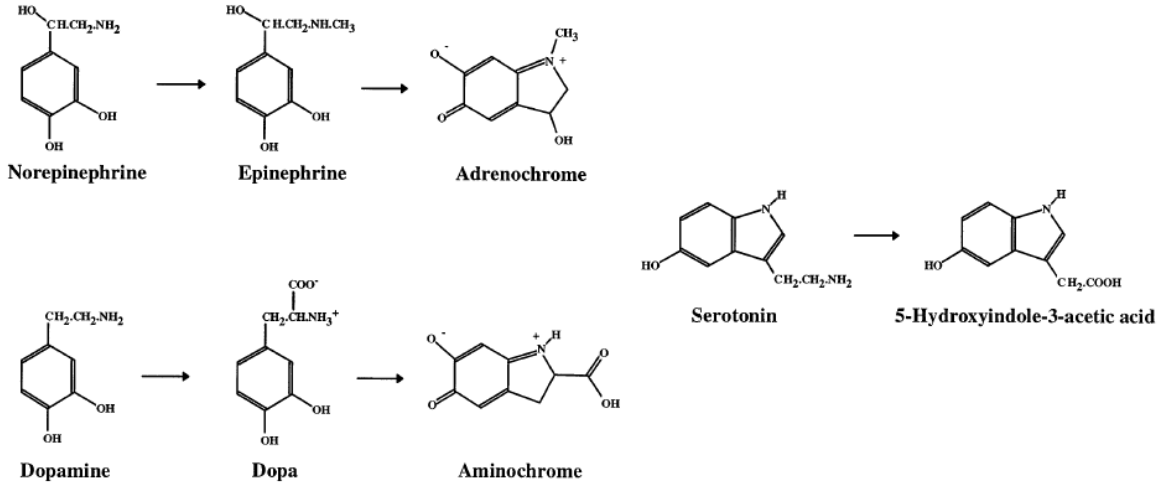

Figure 1.13 | Oxidation reactions and products of biogenic amines (Zaitsev et al., 1999).

1.5. X-ray crystallography

The aim of X-ray crystallography is to obtain a three dimensional molecular structure from a crystal. A purified sample at high concentration is crystallized and then the crystals are exposed to an X-ray beam. The resulting diffraction patterns are then processed, initially to yield information about the crystal packing symmetry and the size of the repeating unit that forms the crystal. This is obtained from the pattern of the diffraction spots. The intensities of the spots can be used to determine the "structure factors" from which a map of the electron density can be calculated. Several methods can be used to improve the quality of the map until it is of sufficient clarity to permit the building of the molecular structure using the protein sequence. The resulting structure is then refined to fit the map more accurately and to adopt a thermodynamically favored conformation.

The x-rays were first discovered in 1895 by Wilhelm Roentgen and in 1912, Max von Laue, Walter Friedrich and Paul Knipping showed that X-rays are diffracted by crystals forming a pattern (Eckert, 2012). In 1914, William Henry Bragg and is son William Lawrence Bragg analyzed a crystal structure by means of X-rays, showing that the scattering of X-rays could be represented as a reflection by successive planes of atoms within a crystal, which can be used to determine relative positions of atoms within a crystal, and so the molecular structure (Bragg's law).

X-ray crystallography is the most powerful method to obtain a macromolecular structure. Structural crystallography is based on the scattering of X-rays by the electrons in the molecules of the analyzed sample. The interference of the scattered waves can be constructive or destructive and is called diffraction. For diffraction to be observed, the wavelength (λ) of radiation must be about equal to the distances between the atoms (0 – 5Å; 1Å = 0.1 nm) which corresponds to the X-rays wavelength. The pattern of diffracted X-rays is useful to obtain the orientation of atoms in space. This pattern can only be achieved if there is repetition of the sample macromolecule in order to amplify and enhance the scattering of the X-radiation. This is why crystals are needed. A crystal is a solid with regular 3D ordering. The regular repeat and high similarity of the structural motifs forming the individual unit cell allows the enhancement of the scattering of X-radiation in selected direction and extinguish completely in others (figure 1.14).

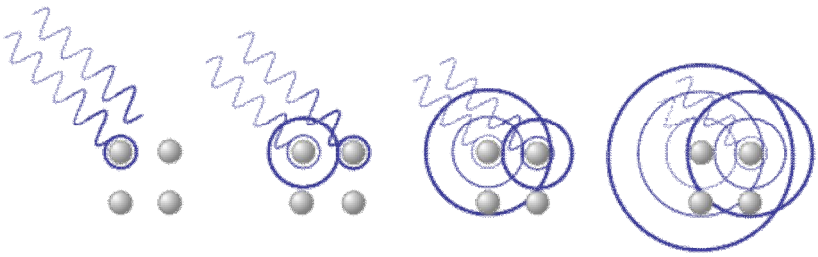

Figure 1.14 | How X-rays interact with the atoms in a crystal (from wikimedia).

1.5.1. Protein crystallization

For protein crystallography, protein crystals are needed and for that a purified sample at high concentration must be available for crystallization. One of the limiting steps of protein crystallography is the growth of good quality protein crystals. The principle of crystallization is to take a solu-

tion of the sample at high concentration and induce it to come out of solution in an ordered way to form a crystal (Gernert et al., 1988). However, if it happens too fast precipitation will occur. Unfortunately, some proteins are apparently not crystallizable. Some variables must be taken in account when trying to crystallize a protein: the precipitant, its concentration, the buffer, its pH, the temperature, the protein concentration, the inclusion of additives and the crystallization technique. The interaction of multiple variables and resulting solubility with respect to crystallization outcomes are represented using a phase diagram (figure 1.15). The two dimensional space diagram is a representation of the phase of a protein regarding its concentrations and the crystallizing agent that can be the pH, the buffer, the temperature, etc. The diagram can be divided into zones defined as undersaturated, saturated, metastable, labile, and precipitation. Undersaturated solutions will remain in a liquid phase. Saturation is a solution state where a crystal, if present, would remain in equilibrium with the surrounding solution. If a crystal is in a clear metastable solution (supersaturated), the protein would add to the surface of the growing crystal until the solution reached saturation. The two zones most relevant to crystallization are the metastable and labile zones. The labile zone is highly supersaturated and the protein undergoes spontaneous, homogeneous nucleation. Once the nuclei form, the level of supersaturation can decrease to the metastable zone that will not produce additional crystal nuclei but will support crystal growth. The precipitation zone, which is too supersaturated to support ordered aggregation, results in amorphous precipitate (Luft et al., 2011).

Initially, the experiments start based on a trial and error procedure and based on the solubility diagram proceed until crystals appear. For this there are commercially available crystal screens which cover as wide a range as possible of the variables like the precipitant, buffer, pH and salt. These screens can be set upped using the different crystallization techniques, being the most common the sitting drop vapour diffusion, hanging drop vapour diffusion and microbatch (figure 1.16). Also several techniques can be used to improve crystal size and quality, as seeding, alteration of protein concentration, or precipitant concentration, addition of additives or even alteration of the temperature. It is also important to verify if the crystals are protein crystals and not salt crystals, this can be performed by SDS-PAGE analysis, staining, UV exposure or X-ray diffraction exposure.

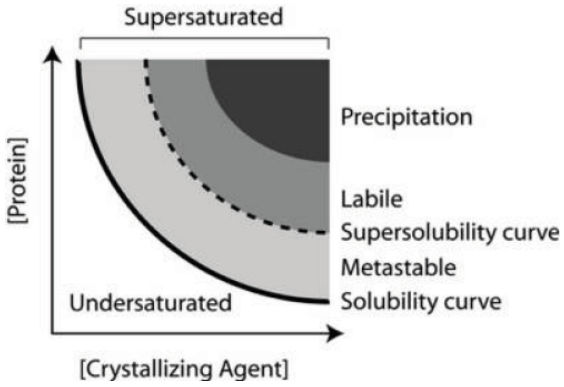

Figure 1.15 | Schematic illustration of a typical crystallization phase diagram (Luft et al., 2011).

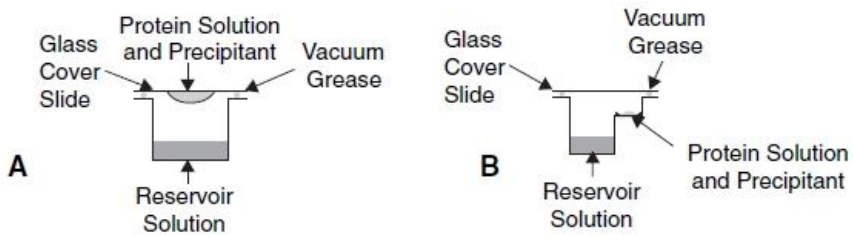

Figure 1.16 | Vapour-diffusion crystallization methods. *A*, hanging drop; B, sitting drop.

1.5.2. X-ray diffraction analysis

The X-rays can be generated from accelerating electron in a synchrotron storage ring, where a single X-ray wavelength is selected by absorption of unwanted wavelengths (monochromation), or from electrons striking a copper anode in a diffractometer, where one predominant wavelength is produced. The X-rays must be focused into a beam where the crystal will be mounted in. The crystals can be mounted in a capillary tube at room temperature, or mounted frozen in a small loop in a stream of liquid nitrogen at 100 K (Hope, 1990). The distance from the crystal to the detector is calculated and adjusted to allow for collection of diffracted spots, usually up to a maximum of 1.5–3.0 Å resolution. The first diffraction image from a crystal showing the diffraction map (figure 1.17) gives us visually already some information by detecting well ordered spots. Spots beyond 3 Å are rather required, since a carbon–carbon bond is approximately 1.5 Å but a resolution of close to 3 Å is sufficient to be able to detect the amino acid side chains in the electron density map (Smyth and Martin, 2000). It is necessary that the diffraction has sufficient resolution to make structure determination to near atomic detail possible. Then the unit cell dimensions, the crystals system and the space group must be determined. The unit cell is the smallest repeating unit that makes up the crystal. Its dimensions are given as three lengths: a, b, and c; and three angles: α, β, and γ (which are usually omitted if 90°). The shape of the unit cell determines the crystal system (table 1.2). The space group is provided by the symmetry of the diffraction pattern, allowing the packing of the molecules into the crystal lattice to be determined.

Table 1.3 | Crystal systems. Adapted from (Smyth and Martin, 2000).

Crystal system	*Axes*	*Interaxial angles*
Triclinic	$a \neq b \neq c$	$\alpha \neq \beta \neq \gamma \neq 90°$
Monoclinic	$a \neq b \neq c$	$\alpha = \gamma = 90° \neq \beta$
Orthorhombic	$a \neq b \neq c$	$\alpha = \beta = \gamma = 90°$
Tetragonal	$a = b \neq c$	$\alpha = \beta = \gamma = 90°$
Trigonal	$a = b \neq c$	$\alpha = \beta = 90°; \gamma = 120°$
Hexagonal	$a = b \neq c$	$\alpha = \beta = 90°; \gamma = 120°$
Cubic	$a = b = c$	$\alpha = \beta = \gamma = 90°$

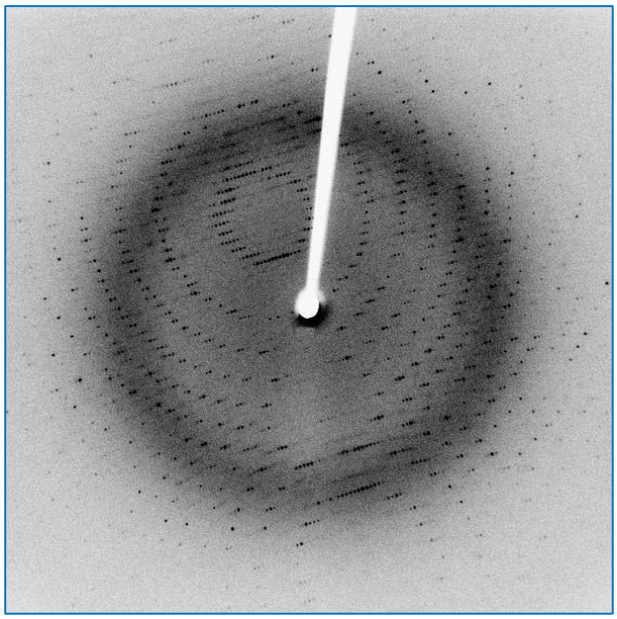

Figure 1.17 | An X-ray diffraction pattern of a crystallized enzyme. The pattern of spots (*reflections*), formed from the constructive interference of X-rays passing through a crystals, and the relative strength of each spot (*intensities*) can be used to determine the structure of the enzyme (from wikipedia).

1.5.3. The phase problem

To calculate electron densities from a diffraction experiment is necessary to know the indices of a reflection, the intensity of the reflections and the phase angles of the reflection. The first two can be determined directly from the experiment. So, the intensity of a diffracted spot is a function of the amplitude of the reflection and the phase angle between the diffracted waves. The indices of a reflection are determined by the symmetry of the crystal and the intensities can be measured by detection devices. The phase angles cannot be determined directly. From the amplitude and the phase the structure factor can be determined and the arrangement of the atoms in the unit cell can be calculated. The most frequently used methods are multiple isomorphous replacement and molecular replacement. Once amplitudes and phases are determined the structure factors can be calculate and the resulting electron density map will form the 3D map into which the protein structure will be built.

1.5.3.1. Multiple Isomorphous replacement

This method is used when no closely related structure is available and requires a data sets from the native protein crystal and another from the protein crystals with attached heavy atoms (Watenpaugh, 1985). The protein crystals can be soaked in a solution of mercury, platinum, gold to incorporate a few atoms into the protein molecule without altering to much either the conformation of the protein or the unit cell dimensions. When compared the differences between the data sets results from the heavy atoms and their positions in the protein molecules can be determined. Refinement of the heavy atom parameters is achieved and can be used to start the determination of the protein phase angles, which together with the amplitudes can be used to calculate the structure factors, used in the refinement procedure.

1.5.3.2. Molecular replacement

This method is used when a very closely related protein structure is available either if there is close homology of the amino acid sequence or if two structures are expected to be similar (Rossmann, 1990). It involves the crystallographic calculation in reverse, structure factors from the known coordinate file and then using the phases from the known model structure and applying it to the new data set to calculate the new structure factor. Before the phases can be applied, the structural model must be placed into the unit cell in exactly the same position and orientation as the new protein molecule. The phases from the model structure factors may then be applied and with the new amplitudes a new set of structure factors can be calculated and refined.

1.6. Objective

The aim of this present work is to achieve human ceruloplasmin good diffracting crystals in order to solve its tri-dimensional structure at a higher resolution than what is already published. A higher resolution structure allows us to unveil some protein residues previously not detected because of lower resolution data. Also a higher resolution can unveil copper and iron labile binding sites. Thus, several methods will be applied to obtain better stabilized and soluble ceruloplasmin, more prone to crystallize.

In this study is also essential to obtain crystals of human ceruloplasmin in combination with epinephrine, serotonin, dopamine and/or L-dopa. As ceruloplasmin has an important aminoxidase activity, being responsible for the regulation of hormones in blood and brain and for the brain homeostasis, it is important to understand in what way this protein can be involved in some neurodegenerative disorders, as Alzheimer's or Parkinson's diseases. The main objective of this study is the crystallization improvement of ceruloplasmin with these neurotransmitters for further crystallographic analysis. The determination of the tri-dimensional structure of these complexes will unveil and confirm which protein residues are involved in its binding and stabilization.

As there is a thigh relationship between protein structure and function it is thought that these structural data can help us understand better what is the role of ceruloplasmin in the human brain homeostasis and in some neuronal disorders.

2. METHODOLOGIES

2.1. Materials

In tables 2.1 to 2.3 described all the reagents, solutions, kits, crystallization screens and equipments used in the present study.

Table 2.1 | Reagents and manufacturers

Manufacturers	*Reagents*
Bio-rad	30% acrylamide/bis solution, Biorad protein assay
Carl Roth GmbH	dipotassium hydrogen phosphate, glycine, hepes, potassium chloride, sodium acetate, sodium citrate tribasic dihydrate,
Hampton Research	Izit crystal dye
Invitrogen	Simply Blue Safe Stain
Merck	Ammonium acetate, ammonium sulfate, bis tris, bromophenol blue, calcium chloride, cobalt (II) chloride hexahydrate, copper (II) sulfate pentahydrate, ethanol, ethylene glycol, glutaraldehyde, 25% aqueous solution, imidazole, iron (III) chloride hexahydrate, isopropanol, magnesium chloride hexahydrate, m-phenylenediamine (MPD), polyethyleneglycol (PEG) 400, PEG 4000, PEG 6000, PEG 20000, sodium chloride, sodium formate
Omnilabor	Glycerol, tris-base
Sigma-Aldrich	2-(cyclohexylamino)ethanesulfonic acid (CHES), 2-(N-morpholino)ethane sulfonic acid (MES), 3-(cyclohexylamino)-1-propanesulfonic acid (CAPS), 3-(N-morpholino) propanesulfonic acid (MOPS), 3,4-Dihydroxy-L-phenylalanine (L-dopa), cacodylic acid sodium salt, cadmium chloride hemi(pentahydrate), dopamine hydrochloride, epinephrine hydrochloride, D + glucose, magnesium acetate tetrahydrate, N,N-Bis(2-hydroxyethyl) glycine, *N*,*N*,*N*′,*N*′-tetramethyl ethylene diamine (TEMED), PEG 300, PEG monomethyl ether 550, PEG1000, PEG3350, PEG 5000, PEG 8000, persulfate ammonium (PSA), potassium phosphate monobasic, Serotonin hydrochloride powder, sodium iodide, sypro orange protein stain, tris-(2-carboxyethyl) phosphine hydrochloride (TCEP)

Table 2.2 | Kits, crystallization screens and manufacturers

Manufacturers	*Kits and crystallization screens*
Hampton Research	Additive screen, Index HT, Natrix HT, SaltRx HT
Jena Bioscience	JBS Solubility Kit
Molecular Dimensions	MIDAS HT-96, Pact Premier HT-96, Structure I+II HT-96, Stura Footprint HT-96
Quiagen	AmSO4 Suite, Nextal MPD Suite, PEGs Suite
Sigma-Aldrich	Gel filtration kit for proteins molecular weights 29-700 kDa

Table 2.3 | Equipments, materials and manufacturers

Manufacturers	*Equipments and materials*
700 Series	Nitrogen Gas Cryosteam Cooler
Biorad	iQ5 Real Time PCR, microseals adhesive seals, multiplate low-profile 96-well unskirted PCR plates
Bruker Corporation	X8 Proteum diffractometer AXS system
Douglas Instruments	Oryx-8 crystallization robot
GE Healthcare	AKTA Prime system, superdex 200 10/300 GL gel filtration column (24mL)
Genomic Solutions	Nanorobot Cartesian Microsys
Hampton Research	Cryschem plate (24 well sitting drop plate), VDX plate (24 well hanging drop plate)
Jena Bioscience	MRC 2-well crystallization plate (96 wells)
Leica	MZ16 microscope
Malvern Instruments	Zetasizer Nano Series
Merck Millipore	Amicon Ultra-15 Centrifugal Filter Units MWCO 100 kDa
Molecular Dimensions	Cryoloops and vials
Rigaku	Desktop Minstrel HT UV imaging system
Thermo scientific	NanoDrop 1000 Spectrophotometer

2.2. Methods

2.2.1. Human ceruloplasmin purification and quantification

hCp from human sera was previously obtained using the Broman & Kjellin method based on a chromatographic purification in presence of inhibitors of proteolysis using a anion exchange column followed by a gel filtration column and finally a hydroxyapatite column as described (Moshkov et al., 1979). Before crystallization a final purification step must be performed to eliminate degradation peptides and aggregates. A calibrated superdex 200 10/300 GL gel filtration column was used in a AKTA prime system at 277 K. The protein was loaded at a concentration of about 100 mg/mL at a flow rate of 0.5 mL/min after equilibration with three column volumes of 0.1 M sodium acetate buffer with 0.1 M NaCl, as previously described (Bento et al., 2007). Elution was monitored online at 280 nm and 1 mL fractions of the relevant peaks were collected and analyzed by native basic poly-acrylamide gel electrophoresis. The samples were mixed with free SDS and β-mercaptoethanol loading buffer and immediately loaded in a SDS-free 10% bis-acrylamide gel and analyzed using the Simply Blue Safe Stain. The peaks of interest were recovered for concentration using an Amicon Ultra-15 MCWO 100 kDa and further protein content determination by the Bradford method (Bradford, 1976) using the Bio-rad protein assay reagent and bovine serum albumin as a standard and confirmed using a NanoDrop 1000 Spectrophotometer reading UV at 280 nm.

2.2.2. Differential scanning fluorimetry (Thermofluor)

2.2.2.1. Addition of $CuSO_4$, $FeCl_3$ or $CoCl_2$

To verify if the presence of $CuSO_4$, $FeCl_3$ or $CoCl_2$ stabilizes hCp and could be helpful in this protein crystallization, a thermofluor assay was performed. For each metal a separated assay was made in triplicate. Sypro orange protein stain 5000x was used as a fluorescent dye and diluted to 50x in 25mM hepes pH 7.5 buffer. A mix containing 6.60 μL sypro orange protein stain 50x (for 5x/well), 0.33 μL of 25 mg/mL hCp (for a final 2.5 μL/well), 0.66 μL of 1M $CuSO_4$, $FeCl_3$ or $CoCl_2$ (for a final 10 mM/well) and 58.41 μL of 0.1 M NaOAc and 0.1 M NaCl buffer, to a final volume of 66 μL was performed. Another mix was equally performed but with 3.30 μL of 1M $CuSO_4$, $FeCl_3$ or $CoCl_2$ (for a final 50 mM/well). As a control a mix was performed with no metals added and disturbed also by 3 wells in the plate. All mixes were distributed by 3 wells (20 μL each) in the low-profile 96-well unskirted PCR plates and sealed using adhesive microseals. The plate was incubated in the dark for 5 min and then placed in a iQ5 Real Time PCR. The experiment was run for excitation at 465 nm and emission at 590 nm and from 20ºC to 90ºC with 10 seconds cycles

2.2.2.2. Optimum solubility screening

2.2.2.2.1. Buffer screen

To verify if there is any buffer were hCp is more stable than in 0.1 M NaOAc and 0.1 M NaCl, a thermofluor using the JBS solubility kit was used. This kit is composed by a set of 24 buffers from pH 3 to 10 and in combination with 150 mM NaCl, 150 mM KCl or 500 mM KCl (Table 2.4). Two mixes were prepared, the first without $CuSO_4$ and the second with $CuSO_4$. In the first mix, 56.16 μL of 5.5 mg/mL hCp (for a final 2.5 μL/well) were added to190.9 μL of 25mM hepes pH 7.5 buffer and 2.5 μL sypro orange 5000x (for a final 5x/well) to a final volume of 249.6 μL. This mix was distributed by 96 wells in a PCR plate (2 μL/well) and 18 μL of each buffer from the JBS Solubility kit was added to each well in the plate. As a control 0.1 M NaOAc buffer + 0.1 M NaCl was used. In the second mix, 2.496 μL of 1M $CuSO_4$ (for a final 1 mM/well) were added. The low-profile 96-well unskirted PCR plates were sealed, incubated in the dark for 5 min and then placed in an iQ5 Real Time PCR. The experiment was run for excitation at 465 nm and emission at 590 nm and from 20ºC to 90ºC with 10 seconds cycles.

2.2.2.2.2. Dynamic light scattering (DLS)

After analysis of the results and the best buffer conditions in thermal stability assay were found, a dynamic light scattering assay was performed to determine which buffer confers more stability and solubility to hCp (Jancarik et al., 2004). The screening was performed at 20ºC by adding 500 μL of each selected buffer solution into each reservoir. Every buffer was centrifuged to eliminated any dust, Every drop was prepared at protein:precipitant proportion 1:1 by adding 1 μL of reservoir solution to 1 μL of hCp at 50 mg/mL. All drops were sealed with siliconized glass cover slips and the plate was placed at 293 K for 24 hours. During this period, vapor diffusion takes place and, depending on the stability of the protein in a given buffer, clear drops or drops with different degrees of

precipitation can be observed under a light microscope. After that time the plate was observed using a Leica microscope searching for the drops that are still clear. Those conditions that apparently keep the protein in solution were chosen for a DLS assay. The clear drops were then diluted into the same reservoir solution at a ratio of 1:2 and a DLS assay was performed using 2 μl of sample in a Zetasizer Nano Series to determine the homogeneity/monodispersity of the sample. If the protein sample appeared to be monodisperse in a particular buffer, then the protein was exchanged into that buffer at a final concentration of 100 mM and crystallization screens were performed.

Table 2.4 | Optimum solubility screen buffer (JBS solubility kit).

No	Buffer (0.1 M)	pH
1	Glycine	3
2	Citric acid	3.2
3	PIPPS	3.7
4	Citric acid	4
5	Sodium acetate	4.5
6	Sodium/potassium phosphate	5
7	Sodium citrate	5.5
8	Sodium/potassium phosphate	6
9	Bis-tris	6
10	MES	6.2
11	ADA	6.5
12	Bis-tris propane	6.5
13	Ammonium acetate	7
14	MOPS	7
15	Sodium/potassium phosphate	7
16	HEPES	7.5
17	Tris	7.5
18	EPPS	8
19	Imidazole	8
20	Bicine	8.5
21	Tris	8.5
22	CHES	9
23	CHES	9.5
24	CAPS	10

2.2.3. Human ceruloplasmin crystallization

2.2.3.1. Crystallization screens

Several crystallization screens were performed trying to obtain a new crystalline form of hCp using MRC 2-well crystallization plates (96 wells) and a Nanorobot Cartesian Microsys to perform drops of 0.2 μL in a protein:precipitant proportion of 1:1 (Table 2.5). The plates were sealed with a transparent adherent cover slip and placed at 293 K. The plates were observed after several days

and weeks of incubation using a Leica MZ16 microscope including a 10.4 Megapixel digital camera for photographs. Although blue protein crystals are expect, due to the type 1 copper centers present on hCp, a Desktop Minstrel HT UV imaging system was used to distinguish salt crystals from protein crystals since protein fluoresces in the presence of UV because of tyrosine and tryptophan. In some cases Izit from Hampton Research was also used to confirm the presence of protein crystals.

An in house crystallization screen was also performed. The Optiscreen is composed by crescent concentrations of NaCl, PEG3350, AmSO4 or MPD as reservoir solutions. The crystallization drop was composed by 0.2 μL of a mix solution of hCp at 50 mg/mL and 8% PEG 20 K, 6% PEG MME 550, 0.1 M NaOAc, 0.4 M Na formate pH 5.7 and 1 mM $CuSO_4$ at 2:1 proportion. For this case in each reservoir was added NaOAc and Na formate pH 5.7 to a final 0.1 and 0.2 M, respectively. These reservoir solutions were not added to the drops.

Table 2.5 | Crystallization screens and respective conditions used for hCP crystallization.

Crystallization screen	*hCp concentration (mg/mL)*	*Protein: precipitant drop proportion*	*Temperature (K)*
AmSO4 Suite	30	1:1	293
Index HT	50	1:1	293
MIDAS HT-96	30	1:1	293
Natrix HT	30	1:1	293
Nextal MPD Suite	30 and 40	1:1	277
Pact Premier HT-96	30	1:1	293
PEGs Suite	50 and 25	1:1	293
SaltRx HT	50	1:1	293
Structure I+II HT-96	40, 50 and 25	1:1	293
Structure I+II HT-96	30	1:1	277
Stura Footprint	40, 50 and 25	1:1	293

2.2.3.2. Scale up conditions

The scaled up drops from hits on crystallization screens were performed using the hanging-drop or the sitting-drop vapour-diffusion techniques using Cryschem plates (24 well sitting drop plate) or VDX plates (24 well hanging drop plate). Usually the protein:precipitant drop proportion is made accordingly to the crystallization screen. It can be changed along with the condition modification/ improvement. For the crystallization condition construction 500 μL of reservoir solution is added to the well. For the drop the protein at the desired concentration is first added and then is mixed with the reservoir solution at the desired proportion. All drops are sealed using silicone and round glass cover slips. All the pates are then placed at desire temperature and observed after days and weeks of incubation as described in 2.2.3.1. Some modifications for some conditions were performed in a search for better crystals.

2.2.3.3. Crystallization assess

In a first attempt, hCp in 0.1 M NaOAc buffer and 0.1 M NaCl, was also crystallized after purification as previously described to verify the purity of the protein (Bento et al., 2007). Using the hanging-drop vapour-diffusion technique 2 μL of protein at 50 mg/mL was mixed with 2 μL of a precipitant solution containing 8% PEG 20K, 8% PEG MME 550, 0.1M sodium acetate, 0.2 M sodium formate pH 5.6 in the drop. All drops were sealed with siliconized glass cover slips and placed at 293 K. Small blue crystals were obtained after about 3 days. In order to improve the aspect and size of the crystals several attempts of changing some variants in this condition were made (table 2.6). Also CuSO4 was added to the condition in an attempt to stabilize the protein and so the crystals.

Table 2.6 | Crystallization condition improvement (Bento et al., 2007).
The hanging-drop vapour-diffusion technique was used and the hCp at concentration of 50 mg/mL.

Protein:precipitant drop	PEG20K (%)	PEG MME 550 (%)	NaOAc (M)	Na Formate (M)	$CuSO_4$ (mM)	Temperature (K)
2:2	8	8	0.1	0.2	-	293
1:1	8	8	0.1	0.2	-	293
2:1	8	8	0.1	0.2	-	293
2:2	8	8	0.1	0.2	10	293
2:2	8	8	0.1	0.2	10	293
2:1	8	8	0.1	0.4	5	293
2:1	8	8	0.1	0.4	1	293
2:1	6	12	0.1	0.4	1	293
2:1	6	16	0.1	0.4	1	293
2:1	6	20	0.1	0.4	1	293
2:1	8	12	0.1	0.4	1	293
2:1	8	16	0.1	0.4	1	293
2:1	8	20	0.1	0.4	1	293
2:1	10	12	0.1	0.4	1	293
2:1	10	16	0.1	0.4	1	293
2:1	10	20	0.1	0.4	1	293
2:1	6	16	0.05	0.4	1	293
2:1	6	16	0.15	0.4	1	293
2:1	8	16	0.05	0.4	1	293
2:1	8	16	0.15	0.4	1	293
2:1	10	16	0.05	0.4	1	293
2:1	10	16	0.15	0.4	1	293
2:1	8	12	0.1	0.3	1	293
2:1	8	16	0.1	0.3	1	293
2:1	8	20	0.1	0.3	1	293
2:1	8	16	0.05	0.3	1	293
2:1	8	16	0.1	0.3	1	293
2:1	8	16	0.15	0.3	1	293
2:1	8	8	0.1	0.5	1	293

Table 2.6 | Crystallization condition improvement (Bento et al., 2007) (Continued)**.**
The hanging-drop vapour-diffusion technique was used and the hCp at concentration of 50 mg/mL

Protein:precipitant drop	PEG20K (%)	PEG MME 550 (%)	NaOAc (M)	Na Formate (M)	$CuSO_4$ (mM)	Temperature (K)
2:1	8	8	0.1	0.4	1	277
2:1	8	8	0.1	0.5	1	277
2:1	8	12	0.15	0.4	1	293
2:1	8	20	0.15	0.4	1	293
2:1	6	16	0.1	0.3	1	293
2:1	6	16	0.1	0.5	1	293
2:1	10	16	0.1	0.3	1	293
2:1	10	16	0.1	0.5	1	293
2:1	8	16	0.1	0.5	1	293
2:1	8	16	0.15	0.5	1	293
2:1	6	12	0.1	0.3	1	293
2:1	6	6	0.1	0.3	1	293
2:1	4	6	0.1	0.3	1	293
2:1	6	6	0.1	0.4	1	303
2:1	6	12	0.1	0.4	1	303
2:1	6	16	0.1	0.4	1	303
2:1	8	8	0.1	0.4	1	303
2:1	8	12	0.1	0.4	1	303
2:1	8	12	0.15	0.4	1	303
2:1	6	6	0.1	0.4	1	277
2:1	6	12	0.1	0.4	1	277
2:1	6	16	0.1	0.4	1	277
2:1	8	8	0.1	0.4	1	277
2:1	8	12	0.1	0.4	1	277
2:1	8	12	0.15	0.4	1	277
2:1	8	8	0.15	0.4	1	303
2:1	8	6	0.1	0.4	1	303
2:1	8	8	0.15	0.4	1	303
2:1	8	8	0.1	0.3	1	303
2:1	8	16	0.1	0.5	1	303
2:1	8	16	0.1	0.4	1	303
2:1	8	16	0.15	0.5	1	303
2:1	8	14	0.1	0.4	1	293
2:1	8	8	0.1	0.3	1	293
2:1	4	4	0.1	0.4	1	277
2:1	4	6	0.1	0.4	1	277
2:1	4	8	0.1	0.4	1	277
2:1	6	4	0.1	0.4	1	277
2:1	6	8	0.1	0.4	1	277
2:1	6	4	0.1	0.4	1	293

Table 2.6 | Crystallization condition improvement (Bento et al., 2007) (Continued)**.**
The hanging-drop vapour-diffusion technique was used and the hCp at concentration of 50 mg/mL.

Protein:precipitant drop	PEG20K (%)	PEG MME 550 (%)	NaOAc (M)	Na Formate pH 5.7 (M)	$CuSO_4$ (mM)	Temperature (K)
2:1	6	8	0.1	0.4	1	293
2:2	8	6	0.1	0.4	1	293
2:0.5	8	6	0.1	0.5	1	293
2:1	6	10	0.1	0.4	1	293
2:1	6	14	0.1	0.4	1	293
2:1	8	10	0.1	0.4	1	293
2:1	8	14	0.1	0.4	1	293
2:1	10	6	0.1	0.4	1	293
2:1	10	8	0.1	0.4	1	293
2:1	10	10	0.1	0.4	1	293
2:1	10	14	0.1	0.4	1	293
2:1	8	10	0.1	0.5	1	293
2:1	8	12	0.1	0.5	1	293
2:1	8	14	0.1	0.5	1	293
2:1	8	16	0.1	0.5	1	293

A condition previously described (Zaitseva et al., 1996) was also investigated and several modifications were performed in a search for bigger and better crystals (table 2.7).

Another hCp structure available in the PDB (http://www.rcsb.org/pdb/home/home.do) with the code 4ENZ was achieved using crystal grown in a precipitant solution 40% MPD, 0.1 M NaCl, 0.1 M NaOAc pH 4.6 and 0.01 M $CaCl_2$ at 280 K using the sitting drop vapor diffusion method. This condition was reproduced and some alterations were made in an attempt to have better crystals (table 2.8).

Table 2.7 | Crystallization condition modification and improvement (Zaitseva et al., 1996).
The hanging-drop vapour-diffusion technique was used and the hCp at concentration of 50 mg/mL.

Protein:precipitant	PEG20K (%)	NaOAc pH 5.5 (M)	NaCl (M)	$CuSO_4$ (mM)	Temperature (K)
0.5:0.5	3	0.1	0.1	-	293
0.5:0.5	3	0.1	0.25	-	293
0.5:0.5	3	0.1	0.4	-	293
0.5:0.5	5	0.1	0.1	-	293
0.5:0.5	5	0.1	0.25	-	293
0.5:0.5	5	0.1	0.4	-	293
0.5:0.5	7	0.1	0.4	-	293
0.5:0.5	7	0.1	0.4	-	293
0.5:0.5	7	0.1	0.4	-	293
0.5:0.5	10	0.1	0.4	-	293
0.5:0.5	10	0.1	0.5	1	293
0.5:0.5	10	0.1	0.4	1	293
0.5:0.5	10	0.15	0.4	1	293

Table 2.7 | Crystallization condition modification and improvement (Zaitseva et al., 1996) (Continued)**.**
The hanging-drop vapour-diffusion technique was used and the hCp at concentration of 50 mg/mL.

Protein:precipitant	PEG20K (%)	NaOAc pH 5.5 (M)	NaCl (M)	$CuSO_4$ (mM)	Temperature (K)
0.5:0.5	10	0.2	0.4	1	293
0.5:0.5	12	0.1	0.5	1	293
0.5:0.5	12	0.1	0.4	1	293
0.5:0.5	12	0.1	0.5	1	293
0.5:0.5	12	0.1	0.4	1	293
0.5:0.5	12	0.15	0.4	1	293
0.5:0.5	12	0.2	0.4	1	293
0.5:0.5	15	0.1	0.5	1	293
0.5:0.5	15	0.1	0.4	1	293
0.5:0.5	15	0.15	0.4	1	293
0.5:0.5	15	0.2	0.4	1	293
1:0.5	3	0.1	0.3	1	277
1:0.5	5	0.1	0.3	1	277
1:0.5	8	0.1	0.3	1	277
1:0.5	10	0.1	0.5	1	293
1:0.5	10	0.1	0.4	1	293
1:0.5	10	0.15	0.4	1	293
1:05	10	0.2	0.4	1	293

Table 2.8 | Crystallization condition modification and improvement.
The hanging-drop vapour-diffusion technique was used and the hCp at concentration of 50 mg/mL.

Protein:precipitant	MPD (%)	NaOAc pH 5.5 (M)	NaCl (M)	$CaCl_2$ (mM)	Temperature (K)
0.5:0.5	30	0.1	0.05	0.01	277
0.5:0.5	30	0.1	0.1	0.01	277
0.5:0.5	30	0.1	0.15	0.01	277
0.5:0.5	30	0.05	0.1	0.01	277
0.5:0.5	30	0.15	0.1	0.01	277
0.5:0.5	30	0.2	0.1	0.01	277
0.5:0.5	35	0.1	0.05	0.01	277
0.5:0.5	35	0.1	0.1	0.01	277
0.5:0.5	35	0.1	0.15	0.01	277
0.5:0.5	35	0.05	0.1	0.01	277
0.5:0.5	35	0.15	0.1	0.01	277
0.5:0.5	35	0.2	0.1	0.01	277
0.5:0.5	40	0.1	0.05	0.01	277
0.5:0.5	40	0.1	0.1	0.01	277
0.5:0.5	40	0.1	0.15	0.01	277
0.5:0.5	40	0.05	0.1	0.01	277
0.5:0.5	40	0.15	0.1	0.01	277
0.5:0.5	40	0.2	0.1	0.01	277

2.2.3.4. Additive screen

The hanging-drop vapour-diffusion method was applied to the additive screen (see 7.Anex, table 7.1). The drop was made using as precipitant a previous optimized condition and protein:precipitant:additive drop proportion was of 1:0.4:0.1 for a final drop of 1.5 μL and 500 μL of reservoir solution. All the different 96 additives were tested. The plates were treated and all the drops observed as described in 2.2.3.1. Those conditions which gave rise to good crystals were confirmed as being protein crystals and repeated.

2.2.3.5. Seed Screen

Crystals obtained using the previous optimized conditions were placed in 50 μL of their respective reservoir solution and mechanically homogenized on a standard laboratory vortex for 2 min at full speed for microseeds. Vapour-diffusion crystallization experiments and automated seeding were performed using an Oryx-8 crystallization robot. A 'matrix-seeding script' for the Oryx-8 robot allowed the simultaneous dispensing of protein, reservoir solutions and seeding stocks (D'Arcy et al., 2007). In control experiments (no seeds added), 0.3 ml screening solution was added to 0.3 ml protein solution in 96-well MRC 2-well crystallization plate; the reservoir wells contained 50 μL of the screen solution (structure I+II). For screens with seeding, 0.2 μL screening solution and 0.1 μL microseeds were added to 0.3 μLl protein solution using the same system as described above. The plates were sealed with clear plastic tape and incubated at 293 K. All drops were observed after a few days to several weeks and crystals confirmed as being protein crystals as described in 2.2.3.2.

2.2.3.6. Crosslinking experiments

To crosslink hCp crystals for a chance at improved handling using hanging drops the cover slip was transferred to a sitting drop plate with 4 μL of 25% glutaraldehyde into the sitting drop sit and 500 μL of crystallization solution into the surrounding reservoir. The drop was sealed with silicone and incubated from 30 min to 2 hours, allowing the glutaraldehyde to vapor diffuse into the sample drop containing the crystals. Crystals were then transferred for stabilizing/cryosolution drops.

2.2.3.7. Co-crystallizations

2.2.3.7.1. hCp with $CuSO_4$, $FeCl_2$ and $CoCl_2$

Ceruloplasmin was incubated with metals for posterior co-crystallization. Incubation of hCp at 55 mg/mL with 10 mM of CuSO4, FeCl3 or CoCl2 were made and placed at 277 K for 20 hours. This incubation was used to construct hanging-drop vapour-diffusion plates using a selected reservoir condition of 500 μL in the reservoir and a protein:precipitant proportion of 2:1 in the drop for a final volume of 3 μL. The plates were incubated at 293 K and observed as described in 2.2.3.1.

2.2.3.7.2. hCp with serotonin, epinephrine, dopamine and L-dopa

Several incubations were made regarding different concentrations of hCp and neurotransmitters (table 2.9). Some crystallization screens at 1:1 protein:precipitant drop proportion (table 2.10)

and scaled up drops were performed as previously described in a search for co-crystals. Some co-crystallization drops were performed using the incubations performed and a previous established reservoir solution / precipitant with some modifications (Bento et al., 2007). Then the crystals were transferred to equilibrated cryoprotectant drops before being freeze to 100 K in liquid nitrogen for further analysis by X-ray diffraction.

Table 2.9 | Ceruloplasmin and neurotransmitters incubations.
All incubations were performed at 277 K for about 24 hours.

Neurotransmitter	[Neurotr.] (mM)	[hCp] (mg/mL)
Dopamine	10	50
	10	25
	5	25
	2	25
	1	50
Epinephrine	10	50
	10	25
	5	25
	2	25
	1	50
L-Dopa	0.5	50
Serotonin	1	50

2.2.3.8. Soaking experiments

For hCp crystals soaking with neurotransmitters assay, the previously selected cryoprotectant condition was made and using the sitting-drop vapour-diffusion technique 500 μL of reservoir solution was used in the well and 5 μL in the drop. The drops were sealed and incubated for 30 min at desired temperature. Blue hCp crystals previously grown at optimum conditions were transferred to the cryoprotectant drops and then were soaked with the neurotransmitters at different concentration and incubated for several hours (table 2.10) before being freeze to 100 K in liquid nitrogen for further analysis by X-ray diffraction.

Table 2.10 | Crystallization screens for hCp and neurotransmitters co-crystallization.
All screens were incubated at 293 K.

Neurotransmitter	[Neurotr.] (mM)	[hCp] (mg/mL)	Crystal. screen
Dopamine	10	50	Structure I&II Stura footprint
	5	25	Stura footprint
	2	25	Optiscreen
Epinephrine	10	50	Structure I&II Stura footprint
	5	25	Stura footprint
	2	25	Optiscreen

Table 2.11 | hCp soaking experiments with neurotransmitters.
All incubations were made at 293 K.

Neurotransmitter	Neurotransmitter (mM)	Soaking time (hours)
Dopamine	1	20
	3	20
	5	3
	5	20
	10	20
Epinephrine	1	5
	1	20
	3	20
	5	3
	5	20
	10	20
L-dopa	2	20
	5	3
	5	20
Serotonin	2	20
	5	20
	5	3

2.2.4. Crystals cryoprotection

Prior to freeze crystals for X-ray analysis it is necessary to protect them against the cold temperatures. To do so crystals need to be transferred to an optimum cryoprotectant solution capable of preserve the crystals in their form and diffraction. Several cryoprotectants were added to the crystallization condition in order to found the best one in preserving the crystals: 25% PEG MME 550, 25% ethyleneglycol, 20% glycose, 25% MPD. The drops were set using the sitting-drop vapour-diffusion method in 24 well plates. The reservoir solution was added to the reservoir (500 μl) and to the drop (5 μL). Drops and plates were closed and incubated for 30 min at the desired temperature (277 or 293 K). Then the crystals were transferred to the equilibrated cryoprotectant drops and were observed for several hours to check if they preserve their form of if they start dissolving. The crystals were then fished from the solution using different sizes cryoloops and placed on vials to be freeze to 100 K in liquid nitrogen for further analysis by X-ray diffraction.

2.2.5. Crystals X-ray analysis

Crystals were analyzed in the in house X8 Proteum diffractometer AXS system at Macromolecular Crystallography Unit at ITQB or at the European Synchrotron Radiation Facility at Grenoble, France, at beamline ID14-1, a fixed energy station dedicated to high-throughput macromolecular crystallography (ADSC Q210 CCD and XFlash fluorescence detectors), and ID23-1 (ADSC Q315R detector).

3. RESULTS

This work started with a final purification step to eliminate hCp aggregates or degradation, as the purified protein samples were kept frozen at - 80ºC for quite some time. The strategy of this work is described in figure 3.1. After the purification and the determination of the protein concentration a differential scanning fluorimetry assay was performed to the protein in its present buffer (0.1 M NaOAc pH 8.8 and 0.1 M NaCl). This technique can determine if a given protein is stable in a given buffer which is required for crystallization or if a given ligand is capable of stabilized a given protein under determined conditions. After performing the thermofluor assay the best ligand was found to stabilize hCp. Then a solubility screen was also used for thermofluor analysis in order to find a buffer capable of preventing the protein aggregation which can inhibit crystal nucleation or growth. After find the best buffer, hCp was ready for crystallization alone or in combination with neurotransmitters.

3.1. Ceruloplasmin purification

To eliminate the aggregates and degradation present in the previously purified hCp samples a final size exclusion purification step was performed using a superdex 200 10/300 GL of 24 mL column. The sample was loaded in the column using 0.1 M NaOAc and 0.1 M NaCl as buffer and run at a flux of 0.5 mL/min for about 50 min. The run was followed by UV detection at 280 nm and the resulting chromatogram is shown in Figure 3.2, *a)*. A first peak is seen about 16 min after sample injection. This corresponds to 8 mL which is the void volume of this column and corresponds to high molecular weight proteins coming first out of the column. Around 24 min after the injection another peak is observed. This peak corresponds to the 132 kDa hCp coming out of the column after 12 mL column volume with some smaller molecular weight peptides. These smaller peptides are hCp subunits. hCp is known to originate polypeptides of 67 kDa, 50 kDa and 19 kDa spontaneously when is not fully stable (Kingston et al., 1977). hCp has an isoelectric point of 5.5 and is easily degraded in several subunits when in the presence of SDS or β-mercaptoehanol as this protein has 5 disulphide bridges connecting the 6 domains. Thus, a native basic polyacrylamide electrophoresis gel on samples from size exclusion purification was performed to avoid protein degradation. As observed in figure 3.2, *b)* there is a higher molecular weight protein corresponding to the full hCp and some small peptides. The gel filtration fractions 4, 6, 8, 9, 10, 11, 12 and 13 were analyzed on gel jointly with hCp sample before size exclusion purification. At “hCp” lane in figure 3.12 *b)* high molecular weight aggregates are observed along with the hCp and also some degraded subunits. In lanes “4” and “6” only the high molecular weight aggregates are present. Purification sample fractions 8 to 12 were pooled together and concentrated up to 50 mg/mL. Protein concentration was performed using Amicon Ultra-15 Centrifugal Filter Units MWCO 100 kDa. The cut-off of 100 kDa was chosen in an attempt to eliminate the ~60 kDa degraded peptides present in the samples, in order to have a more pure hCp final sample. Protein concentration was determined by Bradford method and confirmed by UV using a NanoDrop 1000 Spectrophotometer. In figure 3.2, *c)* is the native basic gel analysis of the final hCp sample. As observed the smaller peptides were not completly eliminated. To confirm if the final sample is stable and ready to crystallize a DSF followed by a solubility screen were performed prior to crystallization asses.

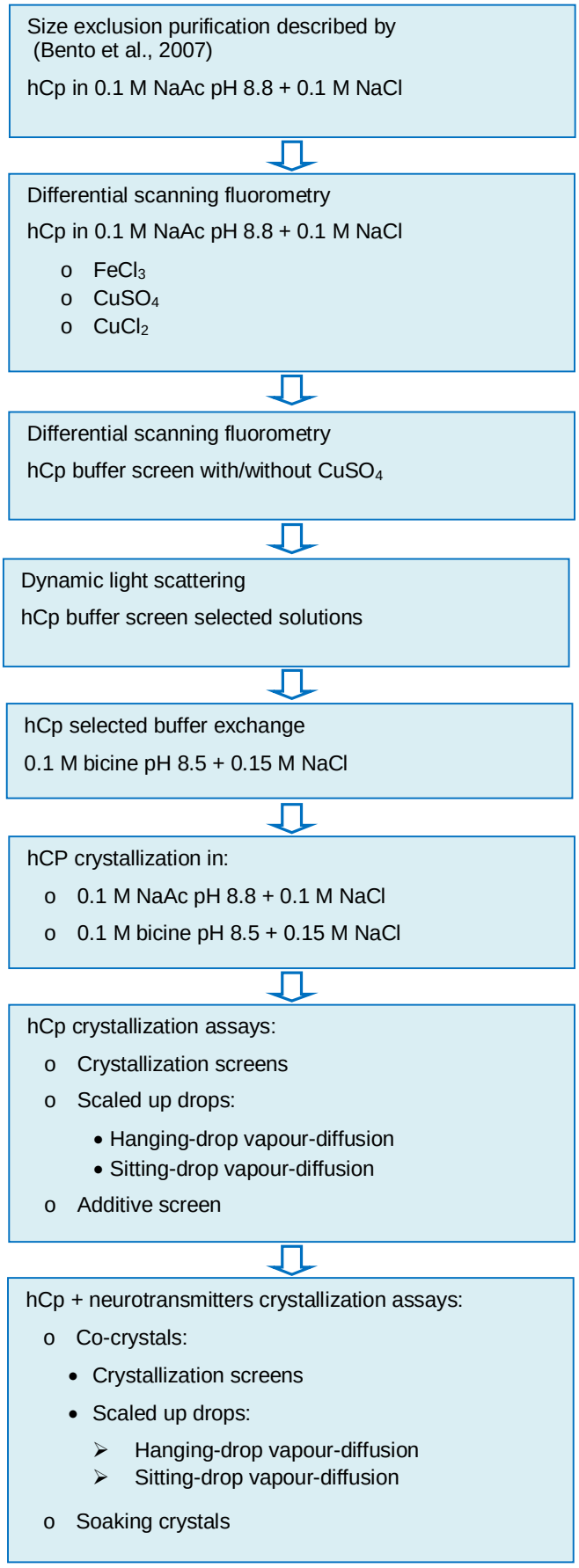

Figure 3.1 | Work strategy diagram.

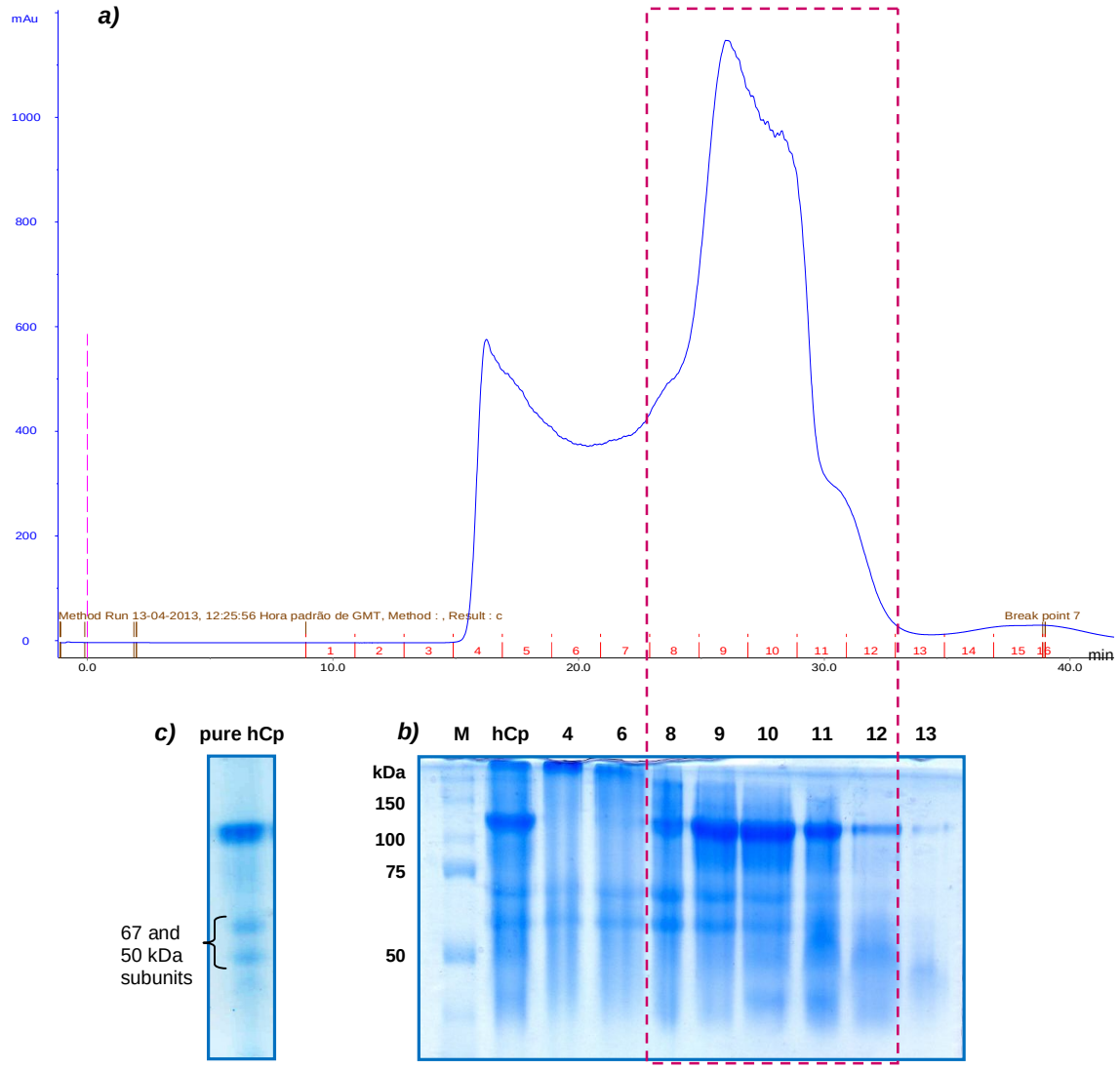

Figure 3.2 | Ceruloplasmin final size exclusion purification step. *a)* Resultant chromatogram at 280 nm. *b)* Native basic PAGE of the purification samples: M, marker; hCp, ceruloplasmin prior purification at ~100mg/mL with high molecular weight aggregates; 4-13; corresponding collected samples in the chromatogram in *a)*. *c)* Final native basic gel after concentration of pure hCp up to 50 mg/mL using a 100kDa cut off filter, some smaller subunits are still present at a minor concentration.

3.2. Ceruloplasmin stability and solubility evaluation

Purified ceruloplasmin is stable in 0.1 M NaOAc pH 8.8 with 0.1 M NaCl as previously described (Bento et al., 2007). However, conditions that stabilize proteins can improve protein purification and crystallization. Protein thermal stability was analyzed and evaluated by differential scanning fluorimetry and dynamic light scattering. The first technique can determine if a given protein is stable in a given buffer which is required for crystallization. The tendency of proteins to aggregate decreases under stabilizing conditions. Also some ligands can help stabilizing a protein by the protein-ligand interaction. The stability of most proteins decreases with the increase of the temperature. When the concentrations of folded and unfolded protein are equal the temperature is considered as melting temperature (Tm). When a compound binds to a protein, the protein-ligand complex is usually more stable and in most cases results in an increase in the Tm (Niesen et al., 2007).

3.2.1. Differential Scanning Fluorimetry

Protein stabilization by ligands may significantly improve the quality of purified proteins and also aid the crystallization process. The more favorable conditions will lead to a higher Tm. As hCp is a copper protein capable of oxidizing iron, both $CuSO_4$ and $FeCl_2$ were investigated about their capacity to stabilize hCp (figure 3.3). An assay using $CoCl_2$ was also performed as cobalt has been described as being capable of binding to copper centers (Lindley et al., 1997). Also different buffers were analyzed as potential better stabilizers for hCp crystallization than the present buffer used for its purification.

The fluorescent Sypro Orange was used in the thermofluor assays. When a protein starts to unfold this dye binds to the exposed hydrophobic parts of the protein resulting in an increase in the fluoresce emission along with the unfolding. The fluorescence intensity reaches a maximum as then decreases doe to precipitation and denatured protein. Plots of fluorescence intensity versus temperature were obtained showing a sigmoid shape expected for a two-state unfolding mechanism, and the temperature at which 50% of the protein is unfolded (Tm) can be estimated from the inflexion point of the curves (figure 3.3 and table 3.1). The melting curve for hCp alone showed two transition curves which indicate that this protein does not unfold globally. This biphasic melt curves shows a first peak with a Tm of 54ºC and a second higher peak of Tm 74ºC.This might indicate that the protein dissociates, which is expected since it is know that it originate polypeptides of 67 kDa, 50 kDa and 19 kDa spontaneously when is not perfectly stable. But when in the presence of $CuSO_4$ only one shift is observed and although the Tm is of 66ºC it seems that copper is capable of stabilizes this protein in a global way. Iron (III) seems not to cause any change in protein stabilization. The presence of cobalt seems to cause some destabilization and the protein dissociation is faster and higher. A higher concentration of Co originates a one phase curve with a lower Tm (47ºC). In all the cases a lower concentration of metal (10 mM) is better for the protein originating a higher Tm. High concentrations of metal might cause protein-metal precipitation. These results show that $CuSO_4$ seems to stabilize hCp and it could be useful for crystallization. However, as metal solutions and hCp samples are colorful this might also interfere with the results.

One application of the buffer screen is to find a suitable buffer for a particular protein, especially if the protein aggregates or precipitates from solution in the buffer of choice given that this might be correlated with protein stability. The buffer screen consisted of a set of 24 different buffers at a concentration of 0.1 M and with a pH from 3 to 10 alone or in combination with NaCl or KCl. This set of buffers were tested by differential scanning fluorimetry in order to obtain the most homogeneous and monodisperse protein conditions for hCp which tendency is to aggregate. Two different assays were performed, one with no CuSO4 and the other adding 10 mM of $CuSO_4$ (figures 3.4 and 3.5). For some reason precipitation was observed when adding 10 mM $CuSO_4$ to the protein and Sypro Orange mix. This was not verified in the previous assay. Nevertheless, 1 mM CuSO4 was then added to the mix and no precipitation was observed.

The hCp Tm values measured for each buffer were compared with the Tm values for the control experiments. A higher Tm can be coupled to an increase in structural order and a reduced conformational flexibility, whereas a decrease in stability, lower Tm, indicates that the buffer induces

Table 3.1 | Metal-dependent hCp stabilization and melting temperatures.

DSF assay	1st peak Tm (ºC)	2nd peak Tm (ºC)
hCp	54	74
hCp + 10 mM $CuSO_4$	69	-
hCp + 50 mM $CuSO_4$	58	-
hCp + 10 mM $CoCl_2$	52	79
hCp + 50 mM $CoCl_2$	47	-
hCp + 10 mM $FeCl_3$	54	74
hCp + 50 mM $FeCl_3$	53	73

protein structural changes toward a more disordered conformation or it can be a sign of misfolding. However, not only the Tm value is important, the shape of the melting curve is also a parameter to consider. A one transition melting curve is desirable as it indicates the global folding of the protein and a higher stability. In figure 3.4 the Tm for all buffers thermofluor assay are represented. As control ceruloplasmin in 0.1 M NaAc pH 8.8 plus 0.1 M NaCl was used and the biphasic melting curve exhibiting two Tm's (54/74ºC). In graphic A) no salt was added to any buffer and as observed for almost every buffer two Tm transitions are observed except for EPPS pH 8.0 (Tm = 57ºC), imidazole pH 8.5 (Tm = 52ºC), bicine pH 8.5 (Tm = 53ºC), tris pH 8.5 (Tm = 58ºC), CHES pH 9.0 (55ºC) and CAPS pH 10.0 (Tm = 55ºC). All this six buffers were chosen for a solubility test by hanging-drop vapour-difusion method. In figure 3.4, B) all hCp Tm for buffers in combination with 150 mM NaCl are shown. Only one buffer exhibited a one transition melting curve, 0.1M bicine pH 8.5 (Tm = 57ºC). This condition was also analyzed by the solubility test. In graphics C) and D) all buffers, in combination with 150 mM KCl and 500 mM KCl, respectively, showed to originate a hCp biphasic melting curve and therefore were not chosen for solubility test or dynamic light scattering. It seems that salts destabilize this protein.

As $CuSO_4$ was identified as being capable of stabilize ceruloplasmin in 0.1 M NaAc pH 8.8 plus 0.1 M NaCl, it was added to the buffer screen in an attempt to stabilize the protein and one transition melting curve was expected for more conditions than the ones obtained for the screen without copper. In figure 3.5 the melting temperatures for hCp in the presence of buffers in combination with 1 mM $CuSO_4$ are shown. As observed several conditions in presence of $CuSO_4$ are capable of stabilizing better ceruloplasmin, which exhibits one melting curve. The Tm values for those cases are between the two Tm points observed for the respective buffers in the absence of $CuSO_4$. This is observed for both cases with and without salt. However, there are several conditions that cause protein precipitation and no valid melting curves are exhibited. For higher pH with no salt this is observed, meaning that hCp at higher pH in the presence of $CuSO_4$ causes protein destabilization and consequent denaturation and precipitation (Figure 3.5, A). Ceruloplasmin seems also to be unstable at pH 7.0 – 8.0 in the presence of $CuSO_4$. The conditions, at 100mM in combination with 1 mM $CuSO_4$, NaAc pH 4.5 (Tm = 58/70ºC), ammonium acetate pH 7.0 (Tm = 56ºC), MOPS pH 7.0 (Tm = 57ºC), imidazole pH 8.0 plus 0.15 M NaCl (Tm = 60ºC), tris pH 8.5 plus 0.15M NaCl (Tm = 64ºC), MES pH 6.2 plus 0.15 M KCl (Tm = 63ºC), bicine pH 8.5 plus 0.15 M KCl (Tm = 66ºC) were chosen for a solubility test by hanging-drop vapour-difusion method.

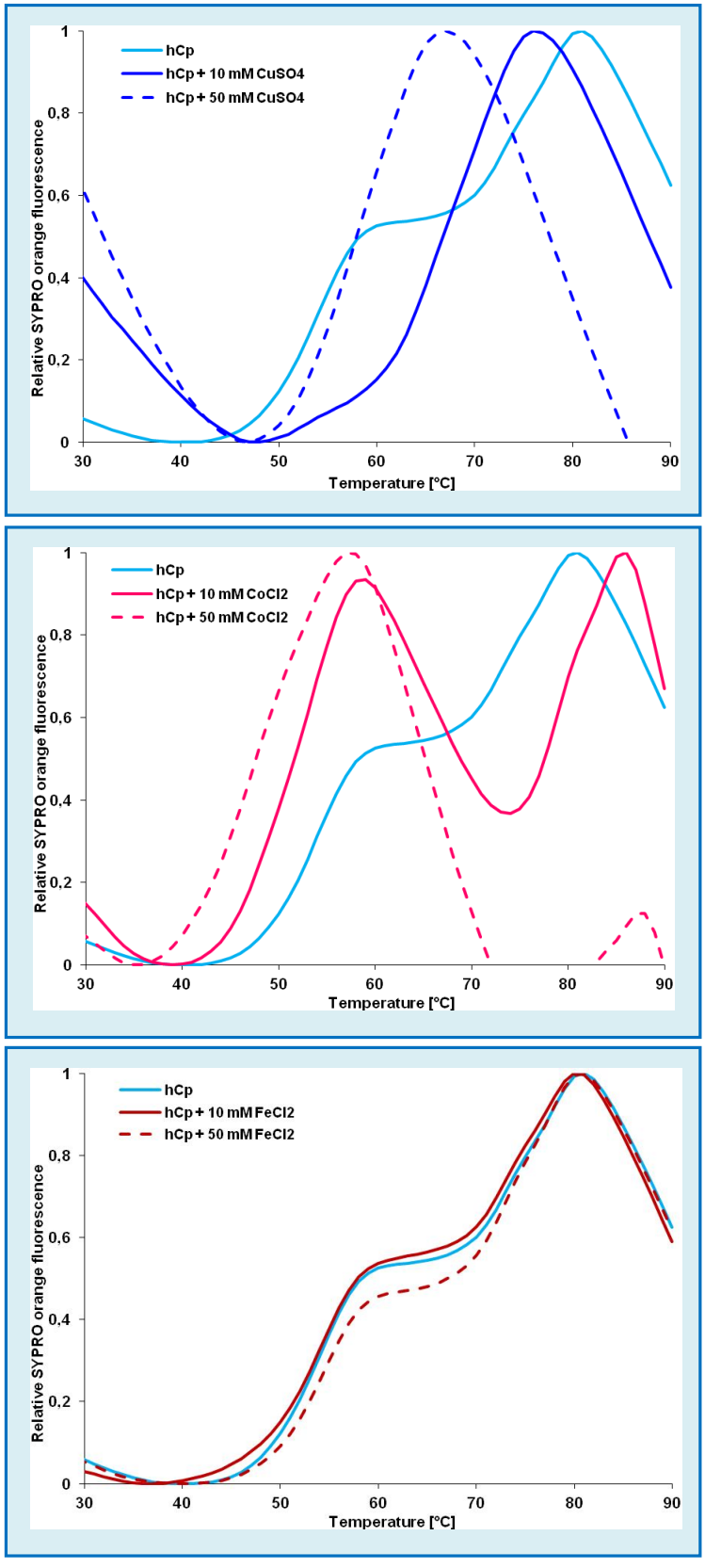

Figure 3.3 | Normalized graphics of ligand-dependent hCp stabilization measured by differential scanning fluorimetry. Metals $CuSO_4$, $FeCl_3$ or $CoCl_2$ were added to each assay at a final concentration of 10 mM or 50 mM. All the assays were performed in 0.1 M NaOAc pH 8.8 buffer with 0.1 M NaCl. The control assay was performed with hCp alone at same conditions.

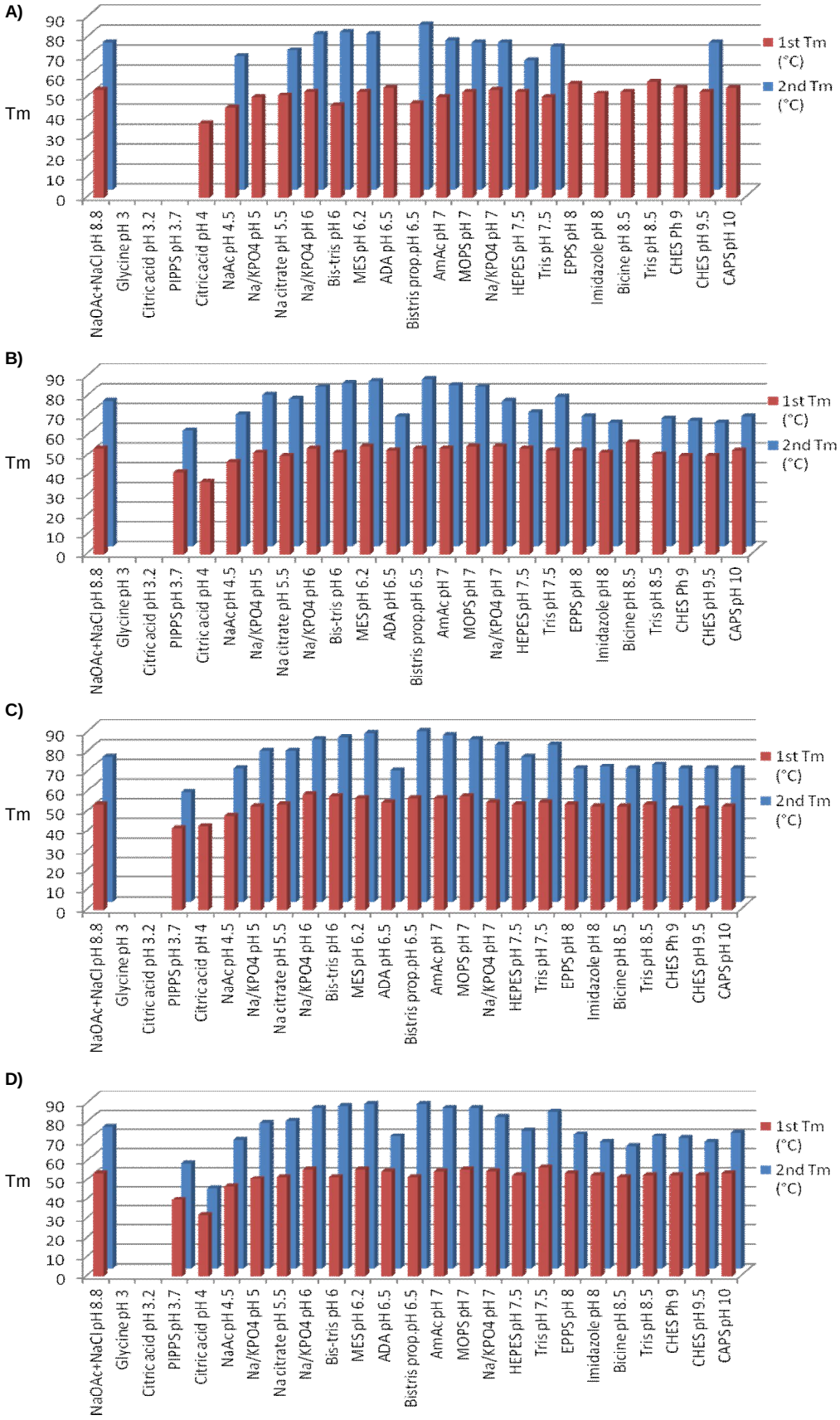

Figure 3.4 | Melting temperatures for hCp in the presence of buffers listed in table 2.4. All buffers are at 0.1 M. hCp purification buffer 0.1 M NaAc pH 8.8 with 0.1 M NaCl was used as control buffer. Salts were added to the assay: A) No salt; B) 150 mM NaCl; C) 150 mM KCl; D) 500 mM KCl.

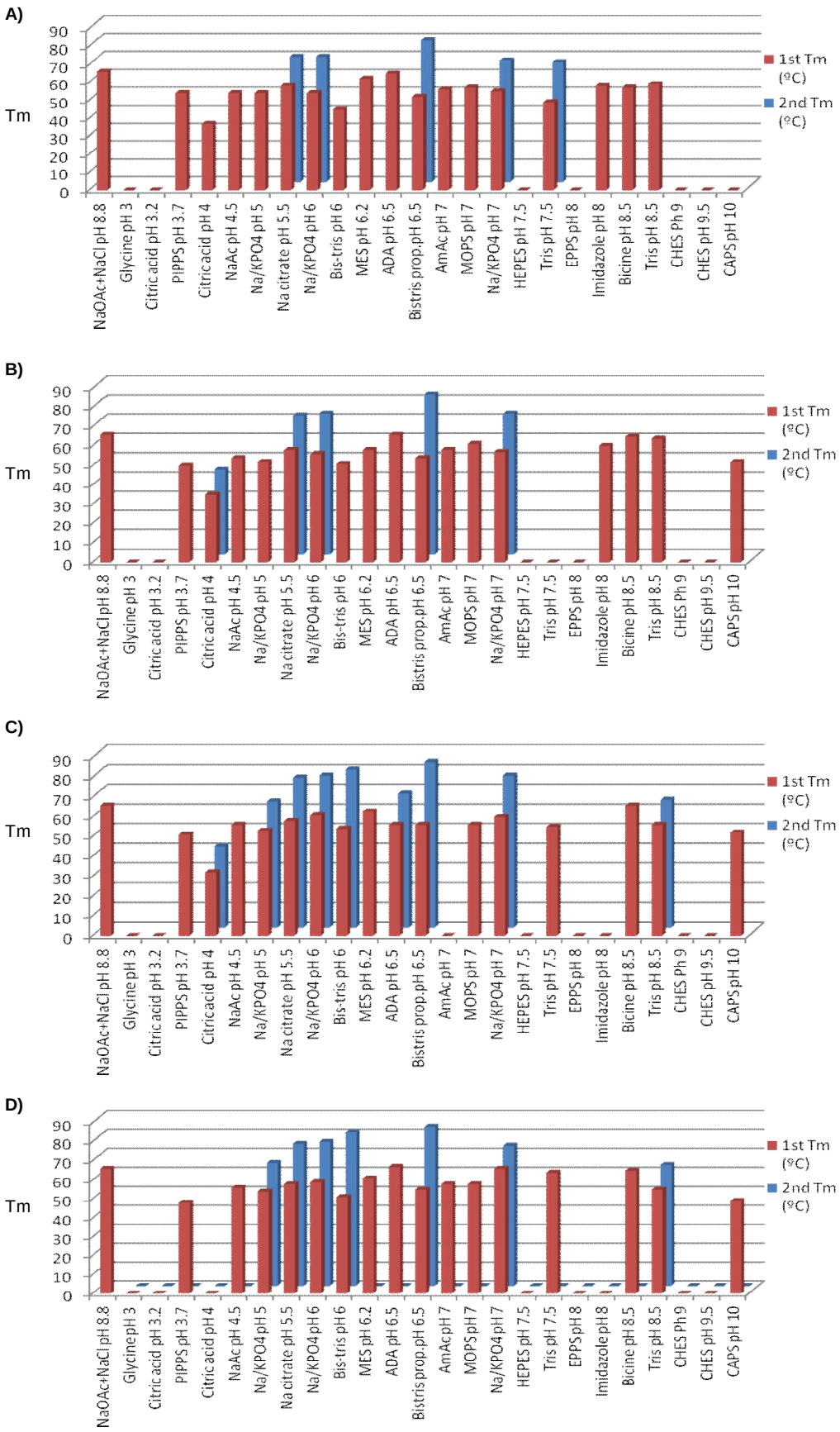

Figure 3.5 | Melting temperatures for hCp in the presence of buffers listed in table 2.4 and 1 mM $CuSO_4$. All buffers are at 0.1 M. As control hCp purification buffer 0.1 M NaAc pH 8.8 with 0.1 M NaCl was used. Salts were added to the assay: A) No salt; B) 150 mM NaCl; C) 150 mM KCl; D) 500 mM KCl.

In all cases, hCp at low pH between 3-3.5 always precipitate, it is known that at acidic pH copper centers disrupt and copper dissociates from the protein, causing in this case the denaturation and precipitation of hCp. As explained before not only the melting temperature values are important but also the shape of the curve. In figure 3.6 are shown the curves for selected buffers with (B) and without $CuSO_4$ (A). As control was used the hCp purification buffer 0.1 M NaAc pH 8.8 with 0.1 M NaCl with or without $CuSO_4$. A one transition midpoint curve is preferable to that biphasic but also a sharper curve is desirable. Sharper curves are observed in the presence of $CuSO_4$. However, in the presence of copper there are some precipitation maybe between the copper and the Sypro Orange dye and a medium high fluorescence is observed at the starting temperature of the assay (25ºC).

The best thermal shift curves for hCp buffer screen were tested using the hanging-drop vapor-diffusion method to monitor precipitation. All the conditions leaded to clear drops are were selected for DLS characterization to determine the best condition.

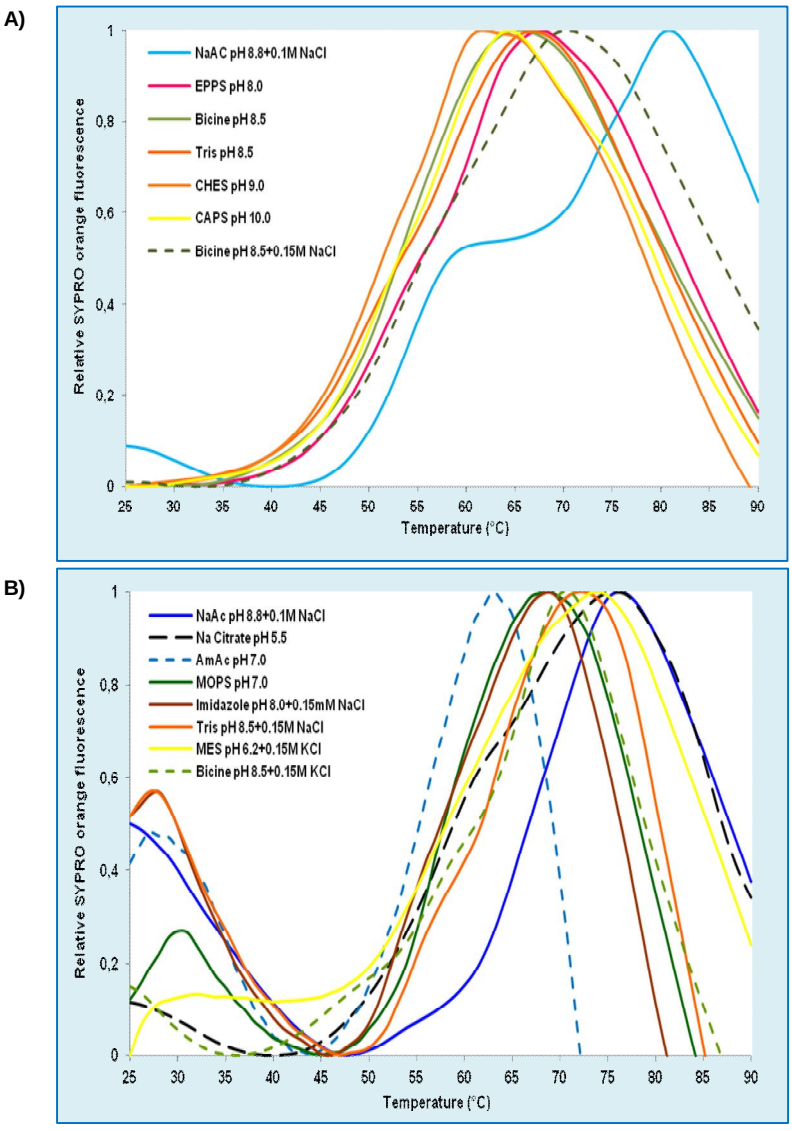

Figure 3.6 | Normalized graphics of best buffers for hCp stabilization measured by differential scanning fluorimetry. A) assay performed with no CuSO4; B) assay performed with 1 mM CuSO4. All buffers are at 0.1 M. As control hCp purification buffer 0.1 M NaAc pH 8.8 with 0.1 M NaCl was used.

3.2.2. Dynamic light scattering (DLS)

The DLS technique measures Brownian motion (random moving of particles suspended in a fluid (a liquid or a gas) resulting from their collision by the fast-moving atoms or molecules in the gas or liquid) and relates it to the size of the particles. It does this by illuminating the particles with a laser and analyzing the intensity fluctuations in the scattered light. The main purpose of using DLS in crystal screening is to help to understand the size distribution, stability, and aggregation state of proteins in solution.

Ceruloplasmin solubility in the buffer solutions listed in the table 3.2 was analyzed through DLS. The results show the radius in nm (for globular proteins) calculated by the DLS analysis. When the diameter and radius can be calculated the molecular weight can be inferred. In table 3.2 are describe the results for the DLS analysis. A molecular weight greater than the expected for hCP of about 132 kDa indicates aggregation and a lower one points to degradation of the protein. When a particle is alone and equal in a given solution only a peak should be detected and the intensity of the fluctuation should be 100%. When particles of different sizes are present in a solution more than one peak of intensity will be detected. In this experiment some results could not be obtained for some solutions maybe because of the presence of aggregates. For several buffers the indication of presence of a particle or protein with 145 kDa has been determined. This molecular size is very close to the one of hCp. However, only one buffer, 0.1M bicine pH 8.5 + 0.15M NaCl, showed 100% in one peak intensity and given this properties this buffer was chosen for hCp stabilization.

The hCp was in part exchanged for this buffer by dialysis at 40 mg/mL and the other part was kept in 0.1 M NaAc pH 8.8 + 0.1 M NaCl both for further crystallization.

Table 3.2 | Dymanic light scattering results for hCp-buffer assays at 20ºC.

Buffer (0.1M)	R.nm	MW.kDa	Int.%
EPPS pH 8	6.0	220	79
Bicine pH 8.5	5.0	145	83
Tris pH 8.5	5.0	145	81
CHES pH 9	3.75	75	91
CAPS pH 10	4.35	105	75
Bicine pH 8.5 + 0.15M NaCl	5.0	145	100
NaAc pH 8 + 1mM CuSO4	6.5	250	89
AmAc pH 7 + 1mM CuSO4	n/d	n/d	-
MOPS pH 7 + 1mM CuSO4	n/d	n/d	-
Imidazole pH 8 + 0.15M NaCl + 1mM CuSO4	5.0	145	94
Tris pH 8.5 + 0.15M NaCl + 1mM CuSO4	3.75	75	88
MES pH 6.2 + 0.15M KCl + 1mM CuSO4	n/d	n/d	-
Bicine pH 8.5 + 0.15M KCl + 1mM CuSO4	5.0	145	82

3.3. Human ceruloplasmin crystallization

Ceruloplasmin crystals that have been previously obtained have a high solvent content of about 70% (Bento et al., 2007; Zaitseva et al., 1996). This makes them poor diffracting crystals being difficult to solve the complete tridimensional structure of this protein. In order to improve these crystals or find a new crystal form that allows a reduction in the unit cell and so a different packing, several techniques of crystallization where performed.

3.3.1. Crystallization conditions improvement

After the dialysis of hCp in 0.1 M NaAc pH 8.8 and 0.1 M NaCl to 0.1 M bicine pH 8.5 and 0.15 M NaCl crystallization conditions were performed for hCp in both buffers As a first attempt of getting some hCp crystals some 4 μL drops were prepared as described in (Bento et al., 2007). hCp at 50 mg/mL in 0.1 M NaAc and 0.1 M NaCl was mixed in the drop in a ratio 2:2 with 8% PEG 20K, 8% PEG MME 550, 0.1 M NaAc and 0.2 M Na formate pH 5.7 as precipitant solution. The hanging-drop vapour-diffusion technique at 293 K gave rise to the 0.05x0.05x0.01 nm blue hexagonal crystals shown is figure 3.7, a).

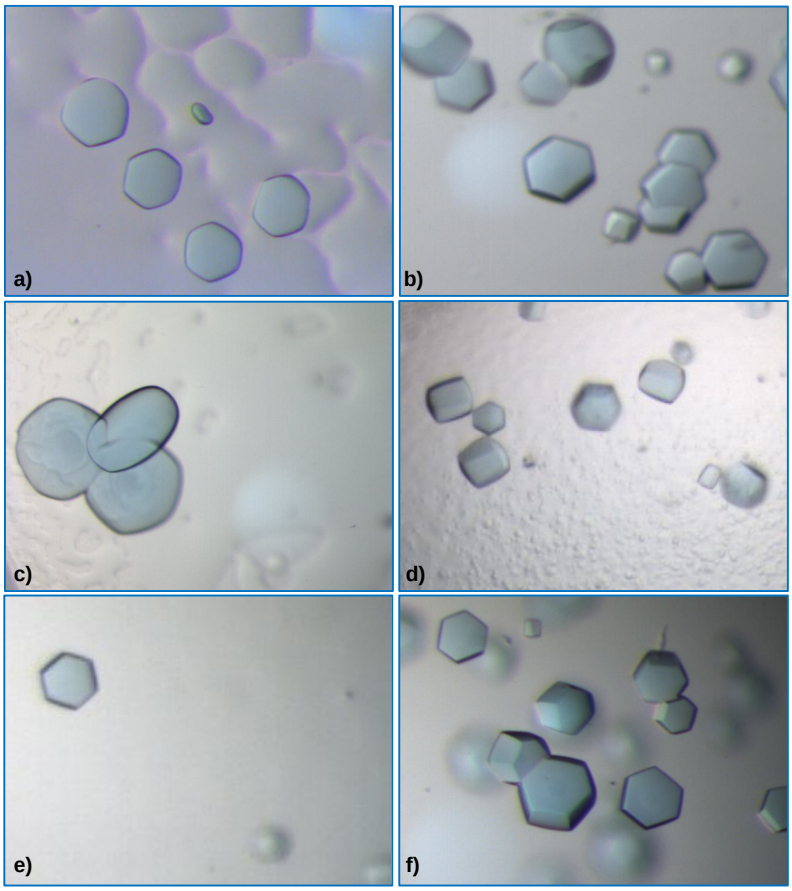

Figure 3.7 | hCp blue crystals using the hanging-drop vapour diffusion method at 293 K. a) 8% PEG 20K, 8% PEG MME 550, 0.1 M NaAc and 0.2 M Na formate pH 5.7; b) 8% PEG 20K, 8% PEG MME 550, 0.1 M NaAc, 0.2 M Na formate pH 5.7 and 1 mM $CuSO_4$; c) 6% PEG 20K, 12% PEG MME 550, 0.1 M NaAc, 0.4 M Na formate pH 5.7 and 1 mM $CuSO_4$; d) 6% PEG 20K,16% PEG MME 550, 0.1 M NaAc, 0.4 M Na formate pH 5.7 and 1 mM $CuSO_4$; e) 8% PEG 20K, 12% PEG MME 550, 0.1 M NaAc, 0.4 M Na formate pH 5.7 and 1 mM $CuSO_4$; f) 8% PEG 20K, 12% PEG MME 550, 0.15 M NaAc, 0.4 M Na formate pH 5.7 and 1 mM $CuSO_4$.

In an attempt to get bigger and better crystals 1, 5 and 10 mM $CuSO_4$ were added to the precipitant solution in the crystallization drops. In drops with 1 mM $CuSO_4$ blue crystals have grown in a few days (figure 3.7, b). These crystals are also small but thicker than the ones grown without $CuSO_4$. Several modifications were made to this condition in a search for bigger and better diffracting crystals: changing the drop proportion or the concentration of the compounds in the precipitant solution. The hexagonal crystals have sizes between 0.5 and 1.5 nm of diameter. However, these crystals are not always reproducible in these conditions, so some modifications were still made in search for reproducibility. After several attempts described in table 2.6 were made, a condition with more reproducibility was found: 8% PEG 20K, 6% PEG MME 550, 0.1 M NaAc, 0.4 M Na formate pH 5.7 and 1 mM $CuSO_4$ using the hanging drop method with a protein:precipitant proportion of 2:1. Blue thick crystals were obtained with 0.15 to 0.20 nm of diameter and are thicker than the ones observed before (figure 3.8). This condition were adapted and some drops were also performed at 277 K in an attempt to slower the evaporation in the drop creating a slower equilibration on the drop in order to allow the nucleation to occur and then the slow crystal growth and get bigger crystals. However, this low temperature and slow evaporation could originate more nucleation, originating more crystals and smaller, instead of less and bigger crystals. As observed in figure 3.9, that was what happened on this case, there were more, smaller and thinner crystals in the drop. The same drops were repeated and placed at 303 K trying to speed the evaporation and diminish the nucleation but no crystals have grown in the drops, maybe due to protein denaturation. hCp is more stable at lower temperatures.

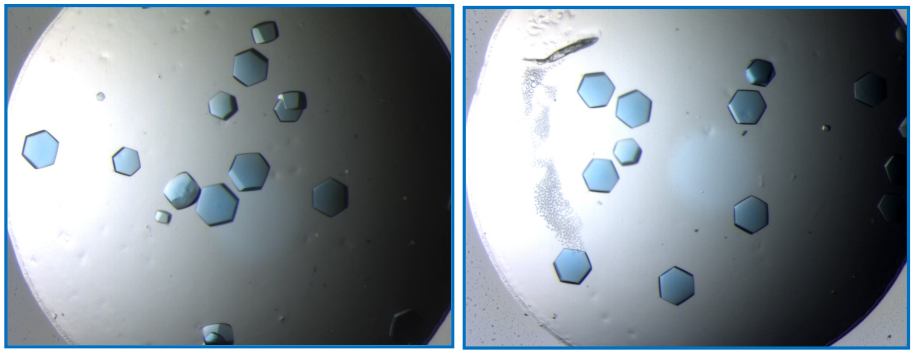

Figure 3.8 | hCp blue crystals using the hanging-drop vapour diffusion method at 293 K. Precipitant solution of 8% PEG 20K, 6% PEG MME 550, 0.1 M NaAc, 0.4 M Na formate pH 5.7 and 1 mM $CuSO_4$ using the hanging drop method at a protein:precipitant proportion of 2:1.

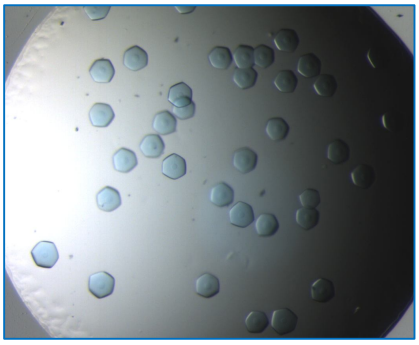

Figure 3.9 | **hCp blue crystals using the hanging-drop vapour diffusion method at 277 K.** Precipitant solution of 8% PEG 20K, 6% PEG MME 550, 0.1 M NaAc, 0.4 M Na formate pH 5.7 and 1 mM $CuSO_4$ using the hanging drop method at a protein:precipitant proportion of 2:1.

Some other modifications were made to this condition. Different concentrations of MPD, glycerol and isopropanol were added to the reservoir using the precipitant solution 8% PEG 20K, 6% PEG MME 550, 0.1 M NaAc, 0.4 M Na formate pH 5.7 and 1 mM $CuSO_4$ in an attempt to slow the evaporation and get fewer and bigger crystals but no improvements were achieved. Since no more improvements could be established to have better hCp crystals, the precipitant solution 8% PEG 20K, 6% PEG MME 550, 0.1 M NaAc, 0.4 M Na formate pH 5.7 and 1 mM $CuSO_4$ was used and crystals grown on this condition were transferred to a cryoprotectant solution and analyzed by X-ray diffraction. The use of additives and a cross linking assay were also performed. Another condition previously described (Zaitseva et al., 1996) was also investigated and several modifications were performed in a search for bigger and better crystals (table 2.7). These condition using the vapour-diffusion method and as precipitant solution 3% PEG 20K, 0.25 M KCl and 0.1 M NaAc pH 5.5 at 277 K. When trying to reproduce this condition some alterations where made and blue crystals have grown at 293 K using the hanging-drop technique and 10% PEG 20K, 0.4 M NaCl and 0.1 M NaAc pH 5.7 at 1:1 proportion. However, this condition was not reproducible. Also 1 mM $CuSO_4$ was added to the condition at 277 and 293 K in an attempt to stabilize the protein but again no crystals have grown. Searching on the PDB (http://www.rcsb.org/pdb/home/home.do) another hCp structure with the code 4ENZ was achieved using crystal grown in a precipitant solution of 40% MPD, 0.1 M NaCl, 0.1 M NaOAc pH 4.6 and 0.01 M $CaCl_2$ at 280 K using the sitting drop vapor diffusion method. This condition was reproduced and some alterations were made in an attempt to have better crystals (table 2.8). The hanging-drop method was also used and the pH of the solution was changed for 5.6 since an acidic pH causes some destabilization on copper centers. However, no crystals had grown under these conditions.

Also, hCp into 0.1 M bicine pH 8-5 and 0.15 M NaCl at 40 mg/mL was used in an attempt to get crystals. The precipitant solution 8% PEG 20K, 6% PEG MME 550, 0.1 M NaAc, 0.4 M Na formate pH 5.7 and 1 mM $CuSO_4$ was used at 293K and some blue hexagonal crystals have grown on the drops and were sent for X-ray diffraction analysis.

3.3.1.1. Co-crystallizations: $FeCl_3$, $CuSO_4$, $CoCl_2$

In an attempt to better stabilize the hCp crystals in order to obtain better diffracting ones, incubations with $FeCl_3$, $CuSO_4$ or $CoCl_2$ were performed and drops in the optimized crystallization condition were set. Also it was hoped that if proper diffracting crystals could be obtained some iron, copper or cobalt labile binding sites could be identified. Some crystal were obtained (figure 3.10) and sent for X-ray diffraction analysis.

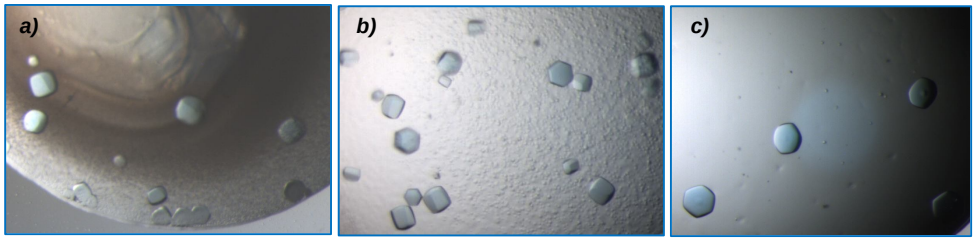

Figure 3.10 | hCp co-crystals using the hanging-drop vapour diffusion method at 293 K. Incubation with 5 mM of *a)* $FeCl_3$, *b)* $CuSO_4$ and *c)* $CoCl_2$.

3.3.1.2. Additive screen

The additive screen was performed as described in 2.2.3.3 using the hCp optimized crystallization condition 8% PEG 20K, 6% PEG MME 550, 0.1 M NaAc, 0.4 M Na formate pH 5.7 and 1 mM $CuSO_4$. The 96 additives were tested and the hanging-drop plates were incubated at 293 K. Crystals appeared after a couple of days. In table 3.3 are listed the additives that allowed the growth of hCp crystals. The best crystals seem to be the ones grown in the presence of $FeCl_3$ and $CoCl_2$ which was expected as ceruloplasmin is a multicopper ferroxidase and cobalt can occupy the binding places for copper stabilizing the protein. Surprisingly, the presence of $CuSO_4$ inhibited the growth of hCp crystals. This might be due to an excess of copper which causes protein precipitation. Also, the presence of NADH, TCEP and glycylglycylglycine seems to be very favorable to the growth of hCp crystals. These crystals were tested *in house* by X-ray diffraction but unfortunately they did not diffract. Some were sent for analysis at a synchrotron facility.

Table 3.3 | Additive screen results on optimized crystallization condition at 293K.

Code	Additive	Crystals description	Crystal Image
A4	$CoCl_2$	Blue hexagonal, 0.15x0.15nm	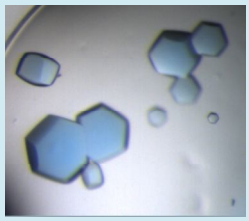
A11	$FeCl_3$	Blue/green hexagonal, 0.1x0.1nm	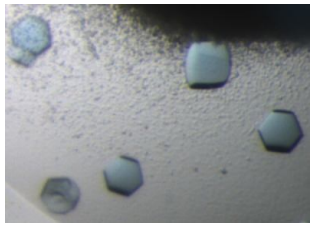
B7	Sodium fluoride	Small blue star shape	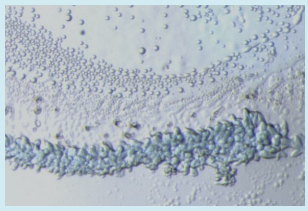
B8	Sodium Iodide	Colorless small neddles	Salt crystals
C11	Glycyl-glycyl-glycine	2 blue hexagonal crystals	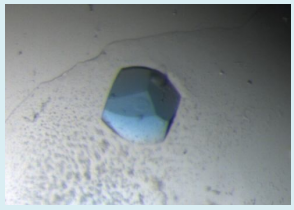

Table 3.3 | Additive screen results on optimized crystallization condition at 293K (continued)**.**

Code	Additive	Crystals description	Crystal Image
D4	$CoCl_2$ hexamine	Colorless deform crystals Colored blue with Izit	
D6	Trimethylamine HCL	Blue hexagonal, 01.x0.1nm	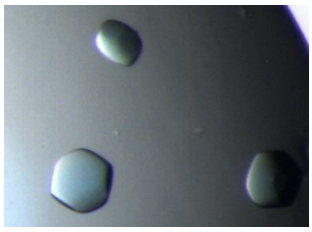
D9	NADH	Several blue hexagonal crystals	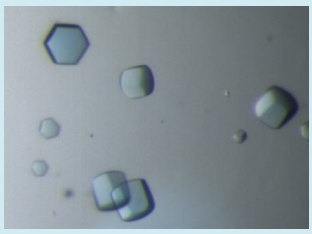
D11	TCEP	Some blue hexagonal crystals	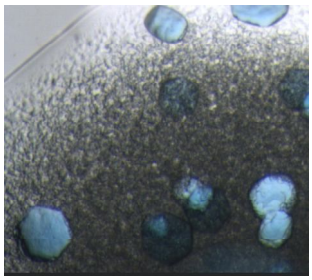
D12	Cystein	One blue hexagonal crystal	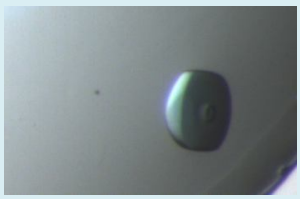
F4	NDSB-201	Small blue hexagonal crystals	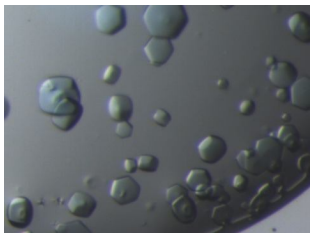
F11	Octyl β D glucoside	Several little blue cubic crystals	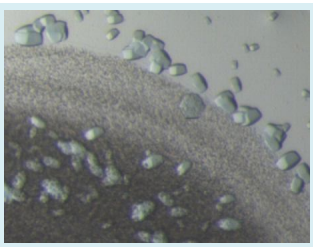

3.3.1.3. Seed Screen

It is known that if seeds are introduced into a crystallization drop, the level of supersaturation required for nucleation and subsequent crystal growth is lower and so seeding has become a well established strategy during the optimization of crystallization conditions. It could be macro seeding, transferring crystals from its mother drop to a fresh drop in order to allow the growth of the crystal; streak seeding, using a horse hair to touch a bad shape crystal and pass it trough new drops with crystallization solution or protein concentration modifications in a attempt to get better crystals; or a seed screen. The seed screen was performed in an attempt to find a new hCp crystal form. A previous study (Ireton and Stoddard, 2004) described a method where crystals with low diffraction are used to seed into other conditions and a crystal form with 10% reduction in the unit cell were obtained. To perform this screen hCp crystals grown in crystallization solution of 8% PEG 20K, 6% PEG MME 550, 0.1 M NaAc, 0.4 M Na formate pH 5.7 and 1 mM $CuSO_4$ at 293 K were used as microseeds and introduced into the Structure I+II crystallization screen with hCp at 50 mg/mL in a search for a new crystalline form. Unfortunately, almost every drop was precipitated what indicates an excesses of protein concentration. The assay should be repeated using hCp at a lower concentration.

3.3.2. Crystallization screenings

After the dialysis of hCp in 0.1 M NaAc pH 8.8 and 0.1 M NaCl to 0.1M bicine pH 8.5 + 0.15M NaCl crystallization screenings were performed for hCp in both buffers. When a hit condition in a crystallization screen is observed scaled up drops are made in order to reproduce the crystals and then improve their size and shape. Usually the sitting-drop vapour-diffusion method is used as the first attempt. Sometime both sitting-drop and hanging-drop techniques are used in a search for the best method. The drop proportion is usually the same as in the crystallization screen (1:1) and then some modifications are made when trying to get better crystals.

3.3.2.1. Commercial screens: the hCp challenge

All the commercial crystallization screens performed are described in table 2.5. In table 3.4 are described the hit conditions on crystallization screens performed with hCp in 0.1 M NaAc pH 8.8 and 0.1 M NaCl. The conditions where any crystalline form was observed are described.

In figure 3.11 there are some images as examples of some crystalline forms found using the commercial crystallization screens. There are some irregular shape crystals that have to be improved in shape and size and scaled up drops were performed.

Some crystallization screens were also performed using hCp at 40 mg/mL in 0.1M bicine pH 8.5 and 0.15 M NaCl. Screens Stura Footprint HT, Structure I+II and Nextal MPD were performed and hit conditions are listed in table 3.5. Best condition was found at Stura footprint screen, D5, 0.1M NaAc pH 5.5, 12% PEG 5K (figure 3.12). This same condition was a hit when using hCp in 0.1 M NaAc pH 8.8 and 0.1 M NaCl. The scale up of these conditions was not performed.

Table 3.4 | Crystallization screen hit conditions. Using hCp in 0.1 M NaAc pH 8.8 and 0.1 M NaCl.

Screen HT	hCp (mg/mL)	Code	Condition	Description
Structure I+II	50	A9	20% isopropanol, 20% PEG 4K, 0.1 M Na citrate	Microcrystals
		G2	30% PEH 5K, 0.1M MES, 0.2M $AmSO_4$	Microcrystals
		H10	10% PEG 1K, 10% PEG 8K	Microcrystals
	25	A6	0.1M NaAc pH 4.6, 8% PEG 4K	Crystals
		B2	0.2M $AmSO_4$, 0.1M Na cacodylate pH 6.5, 30% PEG 8K	Microcrystals
		B3	0.2M MgAc, 0.1M Na cacodylate pH 6.5, 20% PEG 8K	Microcrystals
		B6	0.2M NaAc, 0.1M Na cacodylate pH 6.5, 30% PEG 8K	Microcrystals
		B8	0.2M CdAc, 0.1M Na cacodylate pH 6.5, 18% PEG 8K	Microcrystals
		C5	0.1M NaHepes pH 7.5, 1.4 M Na citrate	Microcrystals
		D7	0.2M $AmSO_4$, 30% PEG 4K	Microcrystals
		D8	2M $AmSO_4$	Microcrystals
		E8	0.2M $AmPO_4$, 0.1M Tris pH 8.5, 50% MPD	Microcrystals
		E10	0.01M NiCl2, 0.1M Tris pH 8.5, 20% PEG 2K	Microcrystals
		F11	1.6M AmSO4, 0.1M MES pH 6.5, 10% dioxane	Microcrystals
		G3	0.01M ZnSO4, 0.1M MES pH 6.5, 25% PEG550	Microcrystals
		H2	0.1 M $CdCl_2$, 0.1M NaAc pH 4.6, 30% PEG400	Microcrystals
		H5	0.01M CTA13, 0.5M NaCl, 0.1M $MgCl_2$	Microcrystals
Index	50	H1	25% PEG3350, 0.1M tris pH 8.5, 0.2M $MgCl_2$	Crystalline dust
PEGs suite	50	Microcrystals and precipitate in almost all conditions		
SaltRX	50		No hit condition	
Stura Footprint	50 & 25	C8	0.1M Na Hepes pH 7.5, 45% PEG 600	Microcrystals
		D2	0.2M imidazole malate, 15% PEG 4K	Blue crystals
		D3	0.2M imidazole malate pH 6, 20% PEG 4K	Small blue crystals
		D5	0.1M NaAc pH 5.5, 12% PEG 5K	Blue crystals
		D9	0.1M AmAc pH 4.5, 9% PEG 10K	Deformed crystals
		G5	12% PEG 8K, 0.2M $AmSO_4$	Microcrystals
		G6	18% PEG 8K, 0.2M $AmSO_4$	Microcrystals
		G7	24% PEG 8K, 0.2M $AmSO_4$	Microcrystals
		H7	20% PEG 4K, 15% isopropanol, 0.1M Na citrate ph 5.5	Crystals
		H9	9% PEG 8K, 0.005M ZnAc, 0.1M Na Cacodylate pH 6.5	Many microcrystals
Pact premier	50	C10	20% PEG 6K, 0.1M Hepes pH 7, 0.2M $MgCl_2$	Microcrystals
		C11	20% PEG 6K, 0.1M Hepes pH 7, 0.2M $CaCl_2$	Microcrystals
		D10	20% PEG 6K, 0.1M Tris H 8, 0.2M $MgCl_2$	Spherulites
$AmSO_4$ suite	50	E4	0.8M AmSO4, 0.1 M Hepes pH 7	Spherulites
		G4	0.1M NaHepes pH 7.5, 1M AmSO4	Colorless crystals
		H3	5% PEG 400, 2M $AmSO_4$, 0.1M MES pH 6.5	Blue thin plates
MIDAS	50	A1	50% PPG400, 5% DMSO, 0.1 Na Hepes pH 6	Blue quasi-crystals
		E4	0.8M AmSo4, 0.1M Hepes pH 7	Spherulites
		H6	30% poliacrilate5100, 10% ethanol, 0.1M MES pH 6	Thin plates
Natrix	50	Almost all conditions have colorless crystals; might be Mg crystals		
Nextal MPD	50	A9	40% MPD, 0.2 M Am iodide	Blue small crystals
		A12	40% MPD, 0.2 M $AmCl_2$	Blue small crystals
		F11	40% MPD, 0.1M NaAc pH 4.6, 0.2M $CaCl_2$	microcrystals

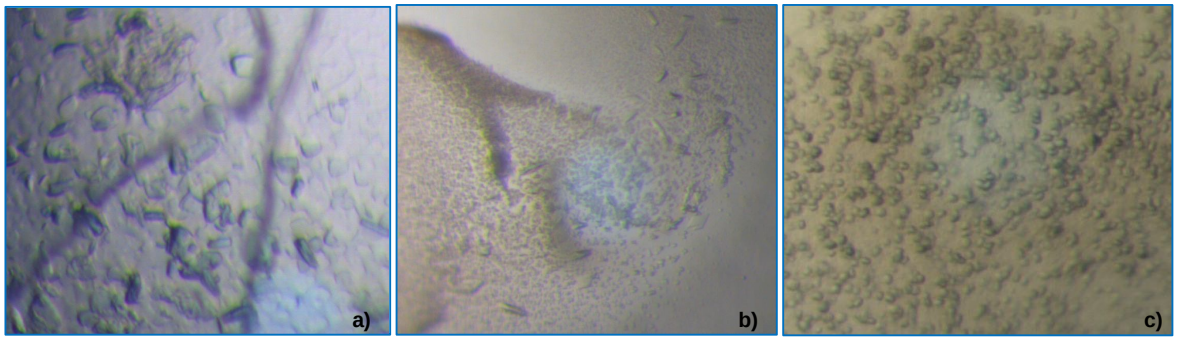

Figure 3.11 | hCp blue crystals grown in some screen conditions. a) Stura footprint, D5: 0.1M NaAc pH 5.5, 12% PEG 5K; b) Stura footprint, D9: 0.1M AmAc pH 4.5, 9% PEG 10K; c) Nextal MPD, A12: 40% MPD, 0.2 M $AmCl_2$.

Table 3.5 | Crystallization screen hit conditions.
Using hCp 40 mg/mL in 0.1 M bicine pH 8.5 and 0.15 M NaCl.

Screen HT	Code	Condition	Description
Structute I+II	B8	0.2M CaAc, 0.1M Na cacodylate pH 6.5, 18% PEG8K	Microcrystals
	B6	0.2M NaAc, 0.1M Na cacodylate pH 6.5, 30% PEG8K	Microcrystals
Stura Footprint	D5	0.1M NaAc pH 5.5, 12% PEG 5K	Crystal plates
MPD		No hits observed	

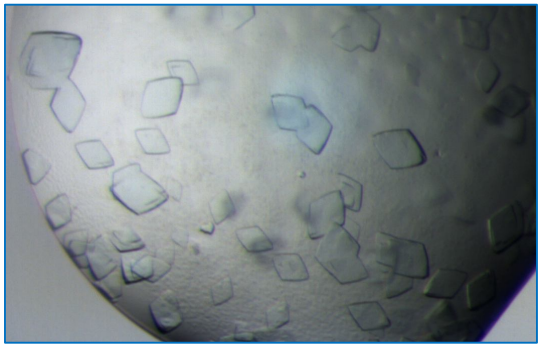

Figure 3.12 | hCp blue crystals grown in a screen condition. Stura Footprint, D5: 0.1M NaAc pH 5.5, 12% PEG 5K.

3.3.2.2. Scaled up drops

Some of the most promising hit conditions in the crystallization screens performed with hCp in 0.1 M NaAc pH 8.8 and 0.1 M NaCl were scaled up. Unfortunately, these assays were not very successful. A great part of the scaled up condition did not result in any crystals. An exception was observed and some crystals could be grown in a scaled up condition (figure 3.13, a). The A12 condition from Nextal MPD screen (40% MPD, 0.2 M $AmCl_2$) did successfully originate small blue crystals at 277 K in a few days that grew until 0.05x0.05nm. In an attempt to improve the size of the crystals $AmSO_4$ was used instead of $AmCl_2$ in the crystallization solution, since this protein seemed to be stabilized in the presence of this salt (table 3.4). Bigger blue crystals were obtained using this 45% MPD and 0.2 mM $AmSO_4$ with the hanging-drop method also at 277 K (figure 3.13, b). Those crystals were freeze and analyzed by X-ray diffraction at synchrotron facilities.

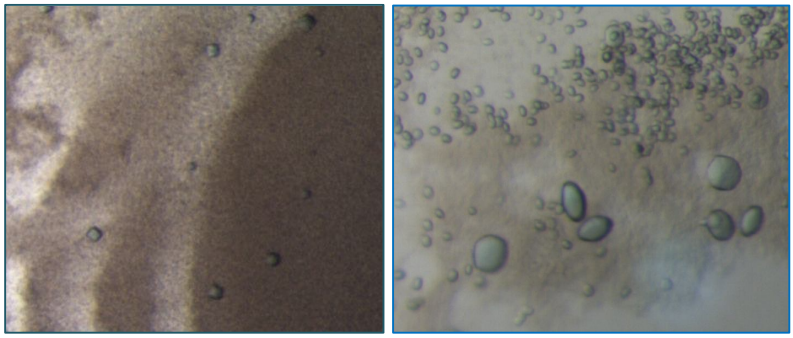

Figure 3.13 | Scaled up hit conditions and hCp blue crystals. Hanging-drop method at 277K with precipitant condition a) 40% MPD, 0.2M $AmCl_2$; b) 45% MPD, 0.2M $AmSO_4$.

3.3.2.3. Optiscreen

The Optiscreen is an *in house* screen created to improve some crystals that cannot be improved using other techniques. The idea behind this screening is to use the evaporation of some solutions placed in the reservoir to help the growth of protein crystals in a condition previously optimized in the drop. In this case crescent concentrations of NaCl, PEG3350, AmSO4 and MPD as reservoir solutions were used. The optimized crystallization solution 8% PEG 20 K, 6% PEG MME 550, 0.1 M NaOAc, 0.4 M Na formate pH 5.7 and 1 mM $CuSO_4$ was applied. First, no crystals were observed in any of the conditions and so it was added to each reservoir NaOAc and Na formate pH 5.7 to a final 0.1 and 0.2 M, respectively. These reservoir solutions were not added to the drops. This way the equilibrium in the drops moved in a way that allowed the growth of hCp crystals in some conditions using MPD at 35%, 40%, 45% and 50% in the reservoir. In the figure 3.14 there are showed some of the crystals obtained. They are light blue hexagonal crystals but are much thicker than the ones grown in the normal condition (figure 3.8). Several attempts to reproduce this crystals were made but with no success. Scaled up drops were also performed but it was not possible to grown this crystals in a scaled up condition. These crystals were cryopreserved and sent to X-ray diffraction analysis.

.

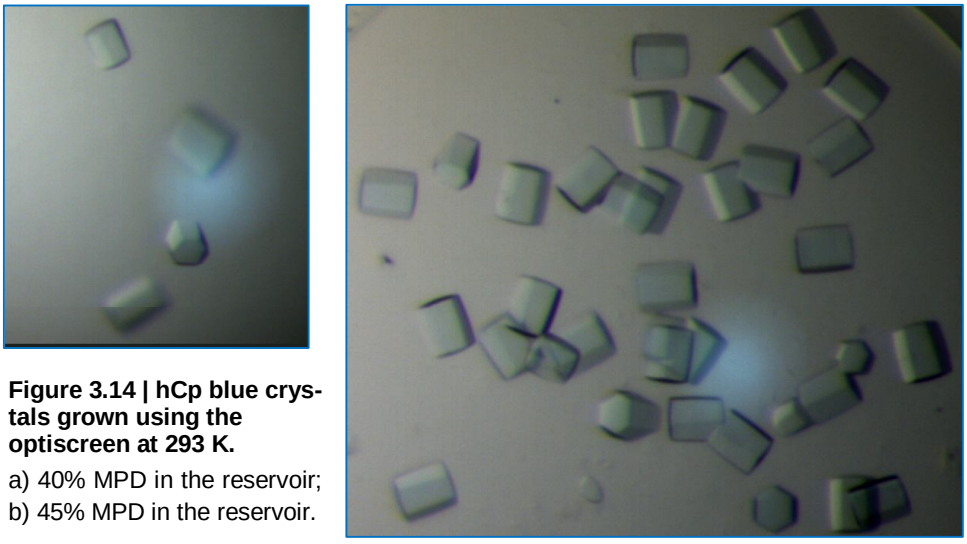

Figure 3.14 | hCp blue crystals grown using the optiscreen at 293 K.
a) 40% MPD in the reservoir;
b) 45% MPD in the reservoir.

3.4. Ceruloplasmin and neurotransmitters crystallization

One of the aims of this study is the determination of the tridimensional structure of ceruloplasmin in combination with neurotransmitters in order to identify its binding site and the residues involved in this stabilization. The neurotransmitters serotonin, epinephrine, dopamine and L-dopa were investigated mainly because of its role on brain homeostasis and functions. Thus, co-crystallization assays where performed using the previous optimized condition for hCp crystallization and also some commercial screens were performed.

3.4.1. Co-crystallization

Incubations of ceruloplasmin, in 0.1 M NaAc pH 8.8 and 0.1 M NaCl, with neurotransmitters were performed at 4ºC (table 2.9). Commercial screens were performed using different incubations with hCp at different concentrations combined with different concentrations of neurotransmitters. It is to notice that incubations with neurotransmitters turned from blue to red (epinephrine), brown (dopamine, green (serotonin) and grey (L-dopa) after a few hours. Unfortunately, no hit conditions were found. Almost all conditions in the different screen used (table 2.10) were precipitated. Also, some scaled up drops where set using these incubations and the optimized condition, 8% PEG 20K, 6% PEG MME 550, 0.1 M NaAc, 0.4 M Na formate pH 5.7 and 1 mM $CuSO_4$. No crystals could grown on the performed drops and only precipitate could be observed. However, when in the presence of a lower concentration of neurotransmitter (1mM) the drops seemed more clear and with some tendency to crystallize. No efforts were made on this and instead soaking experiments were performed.

3.4.2. Soaking experiments

Several soaking experiments were performed using hCp crystals grown mainly in the optimized condition 8% PEG 20K, 6% PEG MME 550, 0.1 M NaAc, 0.4 M Na formate pH 5.7 and 1 mM $CuSO_4$. These crystals of different sizes were transferred for a stabilizing/cryoprotective solution (section 3.5.) and then soaking with the neurotransmitters was performed (table 2.11). The resulting crystals changed color depending upon the neurotransmitter soaked (figure 3.15). The blue crystals turned brownish when soaked with dopamine and orange or red (depending on the concentration) with epinephrine. Crystals soaked with L-dopa turned grey and with serotonin light blue/greenish.

Because of the crystals handling from one solution to another they get sometimes injured. Also, the higher concentrations of neurotransmitters cause some cracks on the crystals. These damages will interfere and diminish the diffracting power of the crystals that have already poor diffraction. As previously described these crystals grown in the optimized described condition have a high solvent content which makes these crystals very fragile. A method to try to improve or diminish the fragility of the crystals is the use of crosslinking by gluteraldehyde. Glutaraldehyde is a linker that binds lysines and allows the stability of the protein molecules and its approach to each other. This can sometimes improve the diffracting power of a given crystal. However, an excess of glutaraldehyde or the time of exposion can cause deformed crystals that will lose diffraction. Thus, this technique relies primarily on lysine residues so the number of lysines as well as temperature can be two signif-

icant variables influencing crosslinking time. Ceruloplasmin as ~6% of lysine residues and crosslinking experiment was performed by 30 min, 1 hour and 2 hours. These crosslinked crystals are more resistant to manipulation and hopefully to the effect of the neurotransmitters soaking. Thus, these crystals were transferred to new stabilizing drops and soaked with the neurotransmitters. Although the crystals should be more resistant some bad shape crystals and even some cracked crystals resulted from the soaking experience. Those crystals were sent for analysis.

Other approach was to use crystals grown in the presence of $FeCl_3$ that seem more robust and oak it with the neurotransmitters. Again, some crystals cracked and are full of precipitate due, to the $FeCl_3$, that is very difficult to remove without damaging the crystals (figure 3.16). Nevertheless, all soaked crystals were freeze and sent for analysis to a synchrotron facility and for data collection.

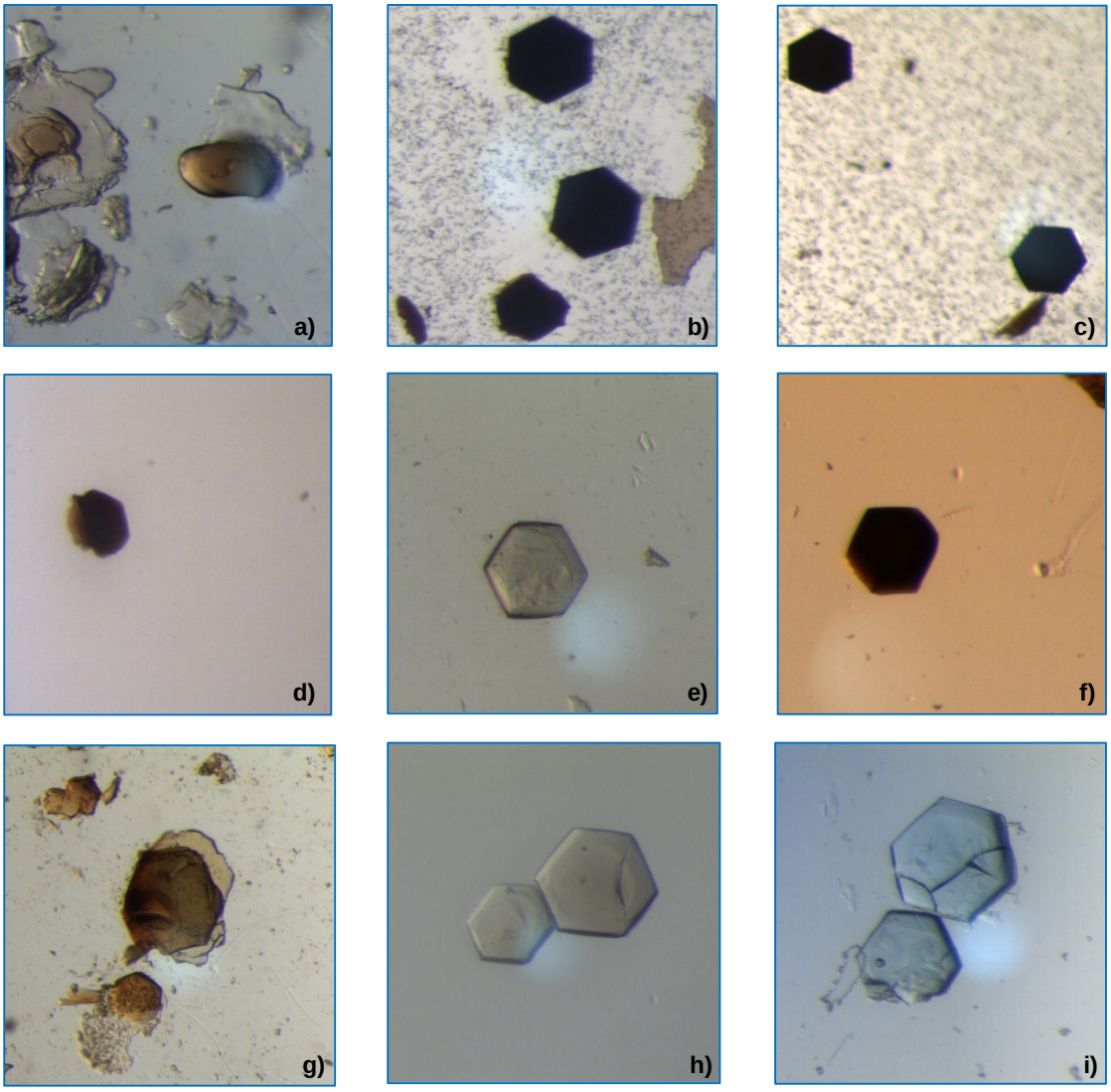

Figure 3.15 | hCp crystals soaked with neurotransmitters. Crystals of about 0.15 x 0.15 nm (but thin) were incubated with a) 5 mM dopamine for 5 H or b) for 20 H and c) 10 mM incubated for 20 H; crystals incubated with d) 3 mM epinephrine for 20 H, e) 5 mM for 5 H and f) 10 mM incubated for 20 H; crystals incubated with g) 2 mM L-dopa for 20 H and h) 5 mM for 5 H and i) 5 mM serotonin for 20 H.

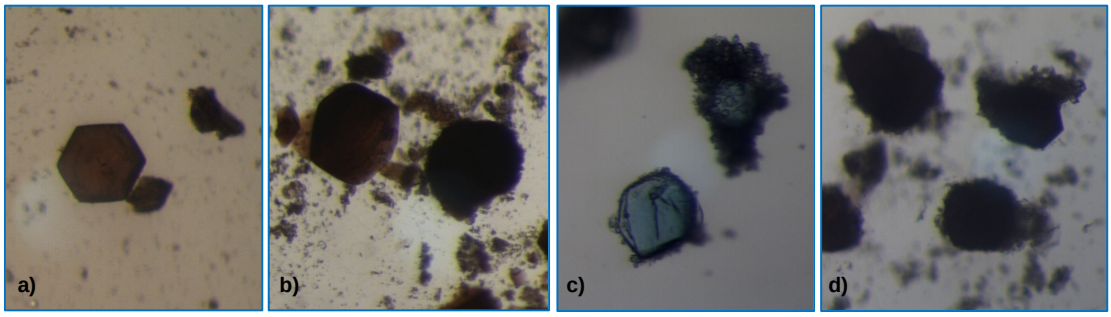

Figure 3.16 | hCp crystals grown in presence of $FeCl_3$ and soaked with neurotransmitters. Soaking was performed by 20H with 5 mM a) epinephrine, b) dopamine, c) serotonin and d) L-dopa.

3.5. Crystals cryoprotection

Prior to freeze crystals for X-ray analysis it is necessary to protect them against the cold temperatures. To do so crystals need to be transferred to an optimum cryoprotectant solution capable of preserve the crystals in their form and diffraction. Several cryoprotectants were added to the crystallization condition in order to found the best one in preserving the crystals: 25% PEG MME 550, 25% ethyleneglycol, 20% glycose, 25% MPD and drops were set as described in the section 2.2.4.

When the crystals were transferred into the cryoprotectant solutions but past 30 min the crystals started to dissolve into those drops with 25% glycerol. Those in ethyleneglycol and glucose also seemed to start dissolving. Crystals in MPD seemed fine and the ones in 35% PEG MME 550 were more stable for a longer time.

Crystals were sent for X-ray diffraction analysis to confirm which cryoprotectante would be better and 35% PEG MME550 was chosen. This PEG is already part of the crystallization condition and an increase in its concentration seems to stabilize the grown crystals and has also a cryoproctectant power, being used as a cryoprotectant solution on this study.

3.6. Crystals analysis

All crystals sent for X-ray diffraction analysis were kept at 100 K in liquid nitrogen in the cryoprotectant solution (8% PEG 20K, 35% PEG MME 550, 0.1 M NaAc, 0.4 M Na formate pH 5.7). Some crystals were tested using the in house X8 Proteum diffractometer AXS system at Macromolecular Crystallography Unit at Instituto de Tecnologia Química e Biológica (UNL), or at the European Synchrotron Radiation Facility at Grenoble, France, at beamline ID-14 and ID-23. The crystals analyzed at in house diffractomer did not exhibit a diffraction pattern. They were probably to small for the in house detector and so their diffraction could not been measured.

At ESRF several data was collected on crystals but structural analysis was not yet performed. Several hCp crystals diffracted at 3.5 Å. hCp crystals soaked with epinephrine diffracted at 3.5 Å and 3.8 Å. hCp crystals soaked with serotonin diffracted at 4.6 Å.

4. DISCUSSION

Normal iron and copper metabolism is essential to cell function and healthy body homeostasis as these elements are cofactors of several enzymes important for essential biological functions. The ability of these metals to participate in one-electron exchange reactions is the key for their essentiality but at the same time these elements are responsible for the generation of free radicals, trough Fenton reaction, that injure cells leading to death. A tight control of cellular copper and iron levels is crucial (Arredondo and Nunez, 2005).

Human ceruloplasmin is the molecular linker between the copper and iron metabolism and its importance in the homeostasis of human body has been implied in some neurological diseases. This plasma cuproenzyme has ferroxidase activity, oxidizing Fe^{2+} to Fe^{3+} and incorporating it into apotransferrin (Osaki et al., 1966). Also the role of hCp might be an efficient control of the level of ferrous iron oxidation without the production of hydrogen peroxide as an end product (Giurgea et al., 2005; Gutteridge, 1978). hCp has also aminoxidase activity being important in regulating the level of amine stress hormones in the bloodstream and brain.

In aceruloplasminemia there are low levels of iron in the plasma and its accumulation in the tissues, including brain (Harris et al., 1998). The increased levels of iron deposited in the brain, as well as the mental deterioration, suggest a connection as found in other neurodegenerative diseases (Gonzalez-Cuyar et al., 2008). A possible consequence of iron high levels in the brain is the formation of reactive species and lipid peroxidation which can lead to tissue damage and neuronal cell death (Yoshida et al., 2000). Thus, hCp is thought to have an important role in neurodegenerative diseases such as Alzheimer's or Parkinson's (Floris et al., 2000).

In Alzheimer's disease the neurons specifically have reduced levels of ceruloplasmin compared to control cases, possibly allowing the iron to accumulate unchecked, contributing to the neuronal degeneration (Castellani et al., 1999). Alzheimer's disease is the most common disease associated to degenerative dementia and the cause is not well understood. It is prevalent in people over 65 years of age affecting about 27 million people worldwide (0,4%) (Brookmeyer et al., 2007). There is no cure for this disease which is progressive and leads to death. The current treatments help with the symptoms but there are not available treatments that stop or reverse the symptoms or the progression of this disease. The cause for most Alzheimer's cases is still unknown. Only 1-5% of the cases have genetic causes. The deposition of β-amyloid plates as been described as the fundamental cause for these disease (Hardy and Allsop, 1991) but some other hypotheses include the reduced synthesis of acetylcholine (Francis et al., 1999), the formation of neurofribrillary tangles of tau protein (Goedert et al., 1991), the myelin breakdown with iron release causing neuronal damage, oxidative stress (Su et al., 2008) and the loss of norepinephrine (Heneka et al., 2010). As hCp is important for oxidative stress control and amine neurotransmitters oxidation the role of this protein in this neurodegenerative disease might be of importance but is not yet fully understood.

Parkinson's disease is the second most common neurodegenerative disorder associated to motor symptoms resulting from the death of dopamine-generating cells in the substantia *nigra*

caused by the accumulation of α-synuclein in neuronal Lewy-bodies. There is no cure for this disease affecting 7 million people worldwide (Elbaz and Moisan, 2008) and the treatment is mainly through the use of L-dopa and dopamine agonists. In PD the neuronal death causes iron release increasing the oxidative stress and again hCp can have a neuroprotective role but also cause the enhanced oxidation of dopamine.

To know more about the role of cerulopalsmin on the oxidation of neurotransmitters and its role on brain homeostasis it is essential to determinate the tri-dimensional structure of ceruloplasmin in complex with de neurotransmitters. This can be very useful to understand better this association and which protein residues are implied in the binding and stabilization of these complexes.

The primary source of structural information for protein-ligand complexes is X-ray crystallography. This is the most successful method to determine macromolecular 3D structures but has some limitations. The biggest one is to obtain good diffracting protein crystals. The high content of solvent (30-70%) makes the crystals very susceptible to damage in handling and by X-rays which can cause disordering of molecules within the crystal (Acharya and Lloyd, 2005). The radiation damage can be reduced by collecting data at liquid nitrogen temperatures and so crystals are kept at 100 K during X-ray analysis. Also some efforts can be performed during crystallization in order to diminish the solvent content in crystals or improve the crystal diffraction capability.

4.1. Ceruloplasmin purification, stability and solubility for crystallization

For protein crystallization a highly pure concentrated amount of the protein is needed is order to have good homogeneous crystals. If a protein sample is not >95% pure the chances of getting it to crystallize decrease considerably. In this present study the hCp sample was previously obtained from human sera using the Broman & Kjellin method (Moshkov et al., 1979) and a final gel filtration step was performed to eliminate some aggregates and smaller peptides resulting from protein degradation. Plasma ceruloplasmin has 132 kDa and it was possible to separate it from bigger aggregates but the smaller peptides were still present in the purified protein sample. Protein concentration was performed using a membrane filter with a cutoff of 100 kDa in an attempt to separate the degraded peptides. Although not all peptides could be removed from the protein sample it was present at a lower concentration and sample final achieved at a concentration of 60 mg/mL. Ceruloplasmin crystals could be obtained using a previously described crystallization condition (Bento et al., 2007).

When intending to crystallize a protein, besides being highly pure and concentrated, the sample needs to be stable at a buffer that confers solubility avoiding aggregation. Differential scanning fluorometry was used to evaluate the stability of hCp combined with iron, copper and also cobalt by reading the melting temperature of the protein. The presence of iron did not change much the Tm for hCp in its purification buffer which is expected as iron is implied in a transition reaction with a high V_m for this protein. Copper stabilized globally the hCp exhibiting only a one-transition melting curve. It is know from some mutants found *in vivo* in aceruloplasminemia patients that mutations affecting the binding or stabilization of copper in copper centers can lead to unstable protein that undergoes degradation. Although cobalt is thought to bind to copper sites its presence seems to destabilize

hCp globally and stabilize a specific domain of the protein. As copper seems to stabilize this protein the buffer screen using DSF was performed with and without $CuSO_4$.

As copper gets unstable at acidic pH the protein is unstable at low pH. Ceruloplasmin seems to be more sable between pH 8 to 10, although its isoelectric point is 5.5 (figure 3.4). Nevertheless, in the presence of $CuSO_4$ the protein seems to be stable at pH between 6 and 8.5 (figure 3.5). At more basic pH hCp seems to precipitate maybe due to the excess of copper. Several conditions were chosen as being good stabilizing buffer solutions for hCp (figure 3.6) and were tested for solubility ability by DLS and the best one was chosen to keep hCp stable for further crystallization (table 3.2). The 0.1 M bicine pH 8.5 and 0.15 M NaCl buffer solution showed one intensity peak for a protein with a molecular weight close to hCp's molecular weight. This indicates the presence of only one protein state in solution confirming hCp solubility in this buffer.

4.2. Ceruloplasmin crystallization

To have good diffracting crystals is important to have highly pure stable protein. A crystallization condition described previously (Bento et al., 2007) was used to perform hanging-drop vapour-diffusion technique with hCp in 0.1 M NaAc pH 8.8 with 0.1 M NaCl, the purification buffer, and in 0.1 M bicine pH 8.5 with 0.15 M NaCl. The protein crystallized using both buffers into 0.05x0.05 nm blue hexagonal crystals. These crystals were improved by the addition of 1 mM CuSO4 into the crystallization condition and some condition parameters alteration. Thicker crystals were sent to X-ray analysis and were further use for soaking with neurotransmitters.

Crystals were obtained when performing the additive screen using the improved crystallization condition. The presence of $CoCl_2$, $FeCl_3$, glycylglycylglycine, NADH and TCEP was favorable to the growth of bigger and thicker crystals. As previously described iron and cobalt bind to hCp and although DSF results seemed to indicate that those metals do not cause a great impact in protein stabilization, for crystallization the presence of these elements seemed to be favorable. Glycylglycylglycine is the tri peptide of glycine and has been reported has capable of increase protein solubility (Ghosh et al., 2004) and that can act as linker facilitating protein crystallization. It has been described that the presence of NADH enhances the ceruloplasmin catalyzed oxidation of catecholamines (Lovstad, 2006). It seems that the presence of NADH also stabilizes hCp better for crystallization. TCEP is a sulfhydryl protective reducing agent. Reducing agents are typically used to prevent the oxidation of free sulfhydryl residues in cysteines in the proteins and can help crystallization. This oxidation can lead to non-specific aggregation of the sample, sample heterogeneity, inactivity, or denaturation of the sample. However, none of those crystals did diffract when tested in the *in house* diffractometer. This might be due to the fact that crystals are too small for the capacity of the beam. Nevertheless, crystals were sent for analysis at synchrotron facilities.

Also co-crystals of hCp in combination with $FeCl_3$, $CuSO_4$ or $CoCl_2$ have grown in the optimized crystallization condition, in order to stabilize the ceruloplasmin crystals improving its diffraction and to identify the binding sites for these elements. Unfortunately, those crystals only diffract at 3.5 - 3.8 Å and no electronic density map could be detected for any of these three metals.

To produce crystals with a higher diffraction power from crystals grown at the optimized condition described, the seed screen was performed. Although if seeds are introduced into a crystallization drop, the level of supersaturation required for nucleation and subsequent crystal growth is lower, the conditions for this to occur need to be optimized. No crystals could grow in the present seed screen and almost all drops were precipitated. This indicates a too high concentrated protein which causes it to come out from solution and precipitate. Another seed screen could be repeated using lower protein concentration and also other crystallization screens can be used in a search for new crystals. Nextal MPD or Stura Footprint could be the first ones to try since several conditions were hit conditions when these screens were performed.

Although several crystallization screens were performed at different temperatures and using different protein concentrations not many promising hit conditions were observed. There were several conditions where microcrystals and spherulites were observed. It seems that hCp has some tendency to crystallize but the crystals are too small or have irregular shape. The only condition scaled up and optimized that gave rise to blue crystals was from Nextal MPD screen. It seems that ceruloplasmin crystallizes best in the presence of MPD at lower temperatures. It has been already described and deposited on the PDB a hCp structure using crystals grown in a precipitant solution of 40% MPD, 0.1 M NaCl, 0.1 M NaOAc pH 4.6 and 0.01 M $CaCl_2$. These crystals could not be reproduced on this study, but blue hexagonal crystals of 0.1x0.1 nm have grown in presence of 45% MPD and 0.2M $AmSO_4$ and were sent for analysis. Also, at Optiscreen crystals appeared when using MPD as reservoir solution. These crystals were again hexagonal shaped but very thick (figure 3.13) which could be good for a good diffraction power, however they were too small and did not diffract.

4.3. Ceruloplasmin and neurotransmitters crystallization

As one of the objectives of this work is to determine the tri-dimensional structure of ceruloplasmin in complex with neurotransmitters efforts were made to have co-crystals of these complexes. However, co-crystallization is not always well succeeding. Complexes of protein-ligand are usually more stable which makes co-crystallization easier but sometimes crystallization conditions cannot be established. Although different incubations with different concentrations of hCp combined with different concentrations of neurotransmitters were performed no co-crystals could be obtained and the drops were mainly precipitated. No crystals could be obtained neither in the crystallization screens or scaled up drops using the optimized conditions for hCp crystals. However, when using these conditions with lower concentrations of neurotransmitter the drops seemed to become more clear which might indicate that maybe co-crystals are possible to obtain if the concentration of neurotransmitter could be lowered. The problem can be that at lower concentrations of neurotransmitter might be then difficult to see it in the crystallographic data, more precisely, in the density map. Thus, soaking experiments were performed on hCp crystals.

hCp crystals were used for soaking with the neurotransmitters. Also crystals in combination with $FeCl_3$ were further used for soaking with neurotransmitters. Crystals soaked with neurotransmitters changes color after some hours, which proves that neurotramitters react with ceruloplasmin and

are much probably bound. However, these crystals are very fragile and difficult to handle. Some crystals cracked after being exposed to neurotransmitters soaking. Thus, some crystals were crosslinked before being soaked with neurotransmitters in an attempt to make them more resistant to manipulation and soaking. The times of explosion to gluteraldehyde were between 30 min and 2 hours. As hCp crystals are already poor diffracting crystals the time of crosslinking has to be short, once it can worsen its diffraction. On the other hand too less crosslinking time, and once these crystals have a high solvent content, may not be enough to protect crystals from handling damage. hCp crystals grown in presence of $FeCl_3$ were also crosslinked before soaking.

4.4. Crystallography data analysis

Protein crystals suffer at room temperature from serious X-ray radiation damage. Cryo-cooling the crystals to 100 K is a way to dramatically reduce the radiation damage. The cooling process needs to avoid the formation of ice crystals in the protein crystal since these destroy the order of the protein molecules in the protein crystal (Hope, 1988). It is extremely import to found a good cryoprotectant condition. In the case of crystals grown at 45% MDP and 0.2 M $AmSO_4$ no cryoprotectant was added once MPD has cryoprotectant properties. For hCp crystal the best cryoprotectant found using the optimized condition was 35% PEGMME 550 combined with the optimized crystallization condition, as no diffraction was obtained when analyzing crystals kept on other cryoprotectants.

Crystals analyzed in house did not diffract but that might be due to the small size of the crystals. Some of the crystals sent to ESRF diffracted between 3 Å and 4 Å. Data from hCp crystals and hCp combined with neurotransmitters was collected and analyzed for structure analysis. As the structure of ceruloplasmin crystallized at identical crystallization conditions was already solved, it will be easier to work on the collected data from ESRF. However, due to the crystals low resolution but no electronic density could be determined for any neurotransmitter analyzed.

5. CONCLUSIONS & FUTURE PERSPECTIVES

In this study several attempts were made to obtain human ceruloplasmin good diffracting crystals. Although ceruloplasmin is a protein not very difficult to crystallize, because of its higher solvent content the diffraction improvement is not very easy to achieve. One of the aims of this study was the establishment of a crystal form with reduction in the unit cell in order to obtain a better diffraction pattern and thus, a higher resolution structure. It was also very important to have good diffracting and resistant ceruloplasmin crystals for further soaking with the neurotransmitters, as the co-crystals could not be established.

To obtain good diffracting crystals stable and soluble protein samples are required. By DSF analysis it was determined that copper sulfate is capable of stabilize hCp, since this is a cuproenzyme. Not so god results were obtained for iron although hp is a ferroxidase. However, when incubating the hCp protein with $FeCl_3$ or even $CoCl_2$ the resulting crystals have a good looking aspect. Unfortunately, no diffraction data was collected from these crystals. Also by DSF, and in combination with DLS analysis, a new buffer was selected for hCp stabilization and further crystallization (01 M bicine pH 8.5 with 0.15 M NaCl). However, it was observed that hCp have better crystallization results when using the previously described purification solution buffer (0.1 M NaAc pH 8.8 and 0.1 M NaCl). Some improvements were made as using additives, performing some seeding and crosslinking. That was not here described but also dehydration technique was performed at PETRA facilities at Hamburg, Germany. However, when the hCp crystals are subjected to the dehydration technique all the structure collapses and the crystals are destroyed. Another form of dehydration is the successive transference of grown crystals from drops with optimized crystallization condition for new drops with crescent higher concentration of precipitant. This was also tried but the hCp crystals are so fragile that the repeated handling damages the crystals and diffraction is lost.

The combination of ceruloplasmin with copper, iron or cobalt in an attempt to achieve better diffracting crystals was not well succeeded as only 3.5A diffracting crystals could be obtained and not electronic density for any metal could be determined.

Another crystallization condition was obtained using the 96 conditions commercial crystallization screen Nextal MPD suite from Qiagen. Crystals have grown on hanging-drop vapour-diffusion drops with 45% MPD and 0.2 M $AmSO_4$ at 277 K. These small blue crystals were sent to analysis at ESFR and there is some untreated collected data.

Although these crystals grew in a different crystallization solution, so far it is thought that no new crystal form could be determined, but some improvements were made on the previously described crystallization condition (Bento et al., 2007).

Thus, some soaking experiments with neurotransmitters could take place. The best diffracting crystals were soaked with epinephrine and serotonin and we look forward to work on the data sets analysis from ESRF and solve the structural data. It is expected that at least one data set could be solved and at least one combined structure of ceruloplasmin with a neurotransmitter could be determined.

Even if no structure could be solved from this present study some major conclusions can be drawn that can help in achieving an improved ceruloplasmin structure in combination with neurotransmitters:

a) the crystallization condition described (Bento et al., 2007) was optimized and better looking crystals could be obtained. Some work can be further improved on the cryoprotectant solution;

b) ceruloplasmin seems rather crystallize in MPD. Some more efforts should be made in this direction. Also the *Optiscreen* with MPD should be repeated and investigated;

c) although no crystallization conditions could be established for co-crystallization of hCp with any of the neurotransmitters, it seems that it might co-crystallized in the described crystallization condition (Bento et al., 2007). Lower neurotransmitter concentration, lower protein concentration, lower precipitant concentration or lower temperature are all variants that should be investigated;

d) crystals soaking with neurotransmitters is a way of overcome the problem of having no co-crystals, but is a more aggressive treatment to the crystals. Also maybe a different stabilization condition different from cryoprotectant condition could be determined and introduced.

The determination of the structures of these hCp-neurotransmitter complexes can be of extreme importance to identify the residues involved in the binding and complex stabilization. This might be crucial to better understand the role of human ceruloplasmin in hormones and brain homeostasis and its importance in several neuronal diseases.

6. REFERENCES

Acharya, K.R., and Lloyd, M.D. (2005). The advantages and limitations of protein crystal structures. Trends Pharmacol Sci *26*, 10-14.

Agarwal, K.N. (2001). Iron and the brain: neurotransmitter receptors and magnetic resonance spectroscopy. Br J Nutr *85 Suppl 2*, S147-150.

Aisen, P., Enns, C., and Wessling-Resnick, M. (2001). Chemistry and biology of eukaryotic iron metabolism. Int J Biochem Cell Biol *33*, 940-959.

Aisen, P., and Listowsky, I. (1980). Iron transport and storage proteins. Annu Rev Biochem *49*, 357-393.

Aldred, A.R., Grimes, A., Schreiber, G., and Mercer, J.F. (1987). Rat ceruloplasmin. Molecular cloning and gene expression in liver, choroid plexus, yolk sac, placenta, and testis. J Biol Chem *262*, 2875-2878.

Altamura, S., and Muckenthaler, M.U. (2009). Iron toxicity in diseases of aging: Alzheimer's disease, Parkinson's disease and atherosclerosis. J Alzheimers Dis *16*, 879-895.

Arredondo, M., Munoz, P., Mura, C.V., and Nunez, M.T. (2003). DMT1, a physiologically relevant apical Cu1+ transporter of intestinal cells. Am J Physiol Cell Physiol *284*, C1525-1530.

Arredondo, M., and Nunez, M.T. (2005). Iron and copper metabolism. Mol Aspects Med *26*, 313-327.

Attieh, Z.K., Mukhopadhyay, C.K., Seshadri, V., Tripoulas, N.A., and Fox, P.L. (1999). Ceruloplasmin ferroxidase activity stimulates cellular iron uptake by a trivalent cation-specific transport mechanism. J Biol Chem *274*, 1116-1123.

Attri, S., Sharma, N., Jahagirdar, S., Thapa, B.R., and Prasad, R. (2006). Erythrocyte metabolism and antioxidant status of patients with Wilson disease with hemolytic anemia. Pediatr Res *59*, 593-597.

Barrass, B.C., and Coult, D.B. (1972). Interaction of some centrally active drugs with caeruloplasmin. Biochem Pharmacol *21*, 677-685.

Barrass, B.C., Coult, D.B., and Pinder, R.M. (1972). 3-Hydroxy-4-methoxyphenethylamine: the endogenous toxin of parkinsonism? J Pharm Pharmacol *24*, 499-501.

Barrass, B.C., Coult, D.B., Pinder, R.M., and Skeels, M. (1973). Substrate specificity of caeruloplasmin indoles and indole isosteres. Biochem Pharmacol *22*, 2891-2895.

Barrass, B.C., Coult, D.B., Rich, P., and Tutt, K.J. (1974). Substrate specificity of caeruloplasmin. Phenylalkylamine substrates. Biochem Pharmacol *23*, 47-56.

Beard, J.L. (2001). Iron biology in immune function, muscle metabolism and neuronal functioning. J Nutr *131*, 568S-579S; discussion 580S.

Beard, J.L., Wiesinger, J.A., and Connor, J.R. (2003). Pre- and postweaning iron deficiency alters myelination in Sprague-Dawley rats. Dev Neurosci *25*, 308-315.

Beinert, H., Holm, R.H., and Munck, E. (1997). Iron-sulfur clusters: nature's modular, multipurpose structures. Science *277*, 653-659.

Bento, I., Peixoto, C., Zaitsev, V.N., and Lindley, P.F. (2007). Ceruloplasmin revisited: structural and functional roles of various metal cation-binding sites. Acta Crystallogr D Biol Crystallogr *63*, 240-248.

Bradford, M.M. (1976). A rapid and sensitive method for the quantitation of microgram quantities of protein utilizing the principle of protein-dye binding. Anal Biochem *72*, 248-254.

Brookmeyer, R., Johnson, E., Ziegler-Graham, K., and Arrighi, H.M. (2007). Forecasting the global burden of Alzheimer's disease. Alzheimers Dement *3*, 186-191.

Bull, P.C., Thomas, G.R., Rommens, J.M., Forbes, J.R., and Cox, D.W. (1993). The Wilson disease gene is a putative copper transporting P-type ATPase similar to the Menkes gene. Nat Genet *5*, 327-337.

Carroll, M.C., Girouard, J.B., Ulloa, J.L., Subramaniam, J.R., Wong, P.C., Valentine, J.S., and Culotta, V.C. (2004). Mechanisms for activating Cu- and Zn-containing superoxide dismutase in the absence of the CCS Cu chaperone. Proc Natl Acad Sci U S A *101*, 5964-5969.

Castellani, R.J., Smith, M.A., Nunomura, A., Harris, P.L., and Perry, G. (1999). Is increased redox-active iron in Alzheimer disease a failure of the copper-binding protein ceruloplasmin? Free Radic Biol Med *26*, 1508-1512.

Chapman, R.F., Percival, A., and Swan, G.A. (1970). Studies related to the chemistry of melanins. XII. Some spectroscopic experiments regarding intermediates in melanogenesis. J Chem Soc Perkin 1 *12*, 1664-1667.

Connor, J.R. (2003). Iron transport proteins in the diseased brain. J Neurol Sci *207*, 112-113.

Connor, J.R., Tucker, P., Johnson, M., and Snyder, B. (1993). Ceruloplasmin levels in the human superior temporal gyrus in aging and Alzheimer's disease. Neurosci Lett *159*, 88-90.

D'Andrea, G., Maccarrone, M., Oratore, A., Avigliano, L., and Messerschmidt, A. (1989). Kinetic features of ascorbic acid oxidase after partial deglycation. Biochem J *264*, 601-604.

D'Arcy, A., Villard, F., and Marsh, M. (2007). An automated microseed matrix-screening method for protein crystallization. Acta Crystallogr D Biol Crystallogr *63*, 550-554.

Daimon, M., Kato, T., Kawanami, T., Tominaga, M., Igarashi, M., Yamatani, K., and Sasaki, H. (1995a). A nonsense mutation of the ceruloplasmin gene in hereditary ceruloplasmin deficiency with diabetes mellitus. Biochem Biophys Res Commun *217*, 89-95.

Daimon, M., Yamatani, K., Igarashi, M., Fukase, N., Kawanami, T., Kato, T., Tominaga, M., and Sasaki, H. (1995b). Fine structure of the human ceruloplasmin gene. Biochem Biophys Res Commun *208*, 1028-1035.

Danks, D.M. (1988). Copper deficiency in humans. Annu Rev Nutr *8*, 235-257.

Das, S.K., and Ray, K. (2006). Wilson's disease: an update. Nat Clin Pract Neurol *2*, 482-493.

de Bie, P., Muller, P., Wijmenga, C., and Klomp, L.W. (2007). Molecular pathogenesis of Wilson and Menkes disease: correlation of mutations with molecular defects and disease phenotypes. J Med Genet *44*, 673-688.

Dekker, M.C., Giesbergen, P.C., Njajou, O.T., van Swieten, J.C., Hofman, A., Breteler, M.M., and van Duijn, C.M. (2003). Mutations in the hemochromatosis gene (HFE), Parkinson's disease and parkinsonism. Neurosci Lett *348*, 117-119.

Desai, V., and Kaler, S.G. (2008). Role of copper in human neurological disorders. Am J Clin Nutr *88*, 855S-858S.

Dingwall, C. (2007). A copper-binding site in the cytoplasmic domain of BACE1 identifies a possible link to metal homoeostasis and oxidative stress in Alzheimer's disease. Biochem Soc Trans *35*, 571-573.

Donovan, A., Brownlie, A., Zhou, Y., Shepard, J., Pratt, S.J., Moynihan, J., Paw, B.H., Drejer, A., Barut, B., Zapata, A.*, et al.* (2000). Positional cloning of zebrafish ferroportin1 identifies a conserved vertebrate iron exporter. Nature *403*, 776-781.

Eagon, P.K., Teepe, A.G., Elm, M.S., Tadic, S.D., Epley, M.J., Beiler, B.E., Shinozuka, H., and Rao, K.N. (1999). Hepatic hyperplasia and cancer in rats: alterations in copper metabolism. Carcinogenesis *20*, 1091-1096.

Eckert, M. (2012). Disputed discovery: the beginnings of X-ray diffraction in crystals in 1912 and its repercussions. Acta Crystallogr A *68*, 30-39.

Elbaz, A., and Moisan, F. (2008). Update in the epidemiology of Parkinson's disease. Curr Opin Neurol *21*, 454-460.

Endo, M., Suzuki, K., Schmid, K., Fournet, B., Karamanos, Y., Montreuil, J., Dorland, L., van Halbeek, H., and Vliegenthart, J.F. (1982). The structures and microheterogeneity of the carbohydrate chains of human plasma ceruloplasmin. A study employing 500-MHz 1H-NMR spectroscopy. J Biol Chem *257*, 8755-8760.

Feder, J.N., Penny, D.M., Irrinki, A., Lee, V.K., Lebron, J.A., Watson, N., Tsuchihashi, Z., Sigal, E., Bjorkman, P.J., and Schatzman, R.C. (1998). The hemochromatosis gene product complexes with the transferrin receptor and lowers its affinity for ligand binding. Proc Natl Acad Sci U S A *95*, 1472-1477.

Feder, J.N., Tsuchihashi, Z., Irrinki, A., Lee, V.K., Mapa, F.A., Morikang, E., Prass, C.E., Starnes, S.M., Wolff, R.K., Parkkila, S.*, et al.* (1997). The hemochromatosis founder mutation in HLA-H disrupts beta2-microglobulin interaction and cell surface expression. J Biol Chem *272*, 14025-14028.

Fleming, M.D., Trenor, C.C., 3rd, Su, M.A., Foernzler, D., Beier, D.R., Dietrich, W.F., and Andrews, N.C. (1997). Microcytic anaemia mice have a mutation in Nramp2, a candidate iron transporter gene. Nature genetics *16*, 383-386.

Fleming, R.E., and Gitlin, J.D. (1990). Primary structure of rat ceruloplasmin and analysis of tissue-specific gene expression during development. J Biol Chem *265*, 7701-7707.

Floris, G., Medda, R., Padiglia, A., and Musci, G. (2000). The physiopathological significance of ceruloplasmin. A possible therapeutic approach. Biochem Pharmacol *60*, 1735-1741.

Fortna, R.R., Watson, H.A., and Nyquist, S.E. (1999). Glycosyl phosphatidylinositol-anchored ceruloplasmin is expressed by rat Sertoli cells and is concentrated in detergent-insoluble membrane fractions. Biol Reprod *61*, 1042-1049.

Fox, P.L. (2003). The copper-iron chronicles: the story of an intimate relationship. Biometals *16*, 9-40.

Francis, P.T., Palmer, A.M., Snape, M., and Wilcock, G.K. (1999). The cholinergic hypothesis of Alzheimer's disease: a review of progress. J Neurol Neurosurg Psychiatry *66*, 137-147.

Frieden, E., and Hsieh, H.S. (1976a). The biological role of ceruloplasmin and its oxidase activity. Adv Exp Med Biol *74*, 505-529.

Frieden, E., and Hsieh, H.S. (1976b). Iron and Copper Proteins (New York and London, Plenum Press).

Friedenberg, Z.B., and Brighton, C.T. (1966). Bioelectric potentials in bone. J Bone Joint Surg Am *48*, 915-923.

Gaggelli, E., Kozlowski, H., Valensin, D., and Valensin, G. (2006). Copper homeostasis and neurodegenerative disorders (Alzheimer's, prion, and Parkinson's diseases and amyotrophic lateral sclerosis). Chem Rev *106*, 1995-2044.

Galhardi, C.M., Diniz, Y.S., Faine, L.A., Rodrigues, H.G., Burneiko, R.C., Ribas, B.O., and Novelli, E.L. (2004). Toxicity of copper intake: lipid profile, oxidative stress and susceptibility to renal dysfunction. Food Chem Toxicol *42*, 2053-2060.

Gernert, K.M., Smith, R., and Carter, D.C. (1988). A simple apparatus for controlling nucleation and size in protein crystal growth. Anal Biochem *168*, 141-147.

Ghosh, S., Rasheedi, S., Rahim, S.S., Banerjee, S., Choudhary, R.K., Chakhaiyar, P., Ehtesham, N.Z., Mukhopadhyay, S., and Hasnain, S.E. (2004). Method for enhancing solubility of the expressed recombinant proteins in Escherichia coli. Biotechniques *37*, 418, 420, 422-413.

Gitlin, J.D. (1988). Transcriptional regulation of ceruloplasmin gene expression during inflammation. J Biol Chem *263*, 6281-6287.

Giurgea, N., Constantinescu, M.I., Stanciu, R., Suciu, S., and Muresan, A. (2005). Ceruloplasmin - acute-phase reactant or endogenous antioxidant? The case of cardiovascular disease. Med Sci Monit *11*, RA48-51.

Goedert, M., Spillantini, M.G., and Crowther, R.A. (1991). Tau proteins and neurofibrillary degeneration. Brain Pathol *1*, 279-286.

Gonzalez-Cuyar, L.F., Perry, G., Miyajima, H., Atwood, C.S., Riveros-Angel, M., Lyons, P.F., Siedlak, S.L., Smith, M.A., and Castellani, R.J. (2008). Redox active iron accumulation in aceruloplasminemia. Neuropathology *28*, 466-471.

Gutteridge, J.M. (1978). Caeruloplasmin: a plasma protein, enzyme, and antioxidant. Ann Clin Biochem *15*, 293-296.

Ha, C., Ryu, J., and Park, C.B. (2007). Metal ions differentially influence the aggregation and deposition of Alzheimer's beta-amyloid on a solid template. Biochemistry *46*, 6118-6125.

Halliwell, B. (1992). Reactive oxygen species and the central nervous system. J Neurochem *59*, 1609-1623.

Halliwell, B., and Gutteridge, J.M. (1985). The importance of free radicals and catalytic metal ions in human diseases. Mol Aspects Med *8*, 89-193.

Hallquist, N.A., McNeil, L.K., Lockwood, J.F., and Sherman, A.R. (1992). Maternal-iron-deficiency effects on peritoneal macrophage and peritoneal natural-killer-cell cytotoxicity in rat pups. Am J Clin Nutr *55*, 741-746.

Hamza, I., Schaefer, M., Klomp, L.W., and Gitlin, J.D. (1999). Interaction of the copper chaperone HAH1 with the Wilson disease protein is essential for copper homeostasis. Proc Natl Acad Sci U S A *96*, 13363-13368.

Hardy, J., and Allsop, D. (1991). Amyloid deposition as the central event in the aetiology of Alzheimer's disease. Trends Pharmacol Sci *12*, 383-388.

Harris, Z.L. (2002). Not all absent serum ceruloplasmin is Wilson disease: a review of aceruloplasminemia. J Investig Med *50*, 236S-238S.

Harris, Z.L. (2003). Aceruloplasminemia. J Neurol Sci *207*, 108-109.

Harris, Z.L., Klomp, L.W., and Gitlin, J.D. (1998). Aceruloplasminemia: an inherited neurodegenerative disease with impairment of iron homeostasis. Am J Clin Nutr *67*, 972S-977S.

Harris, Z.L., Takahashi, Y., Miyajima, H., Serizawa, M., MacGillivray, R.T., and Gitlin, J.D. (1995). Aceruloplasminemia: molecular characterization of this disorder of iron metabolism. Proc Natl Acad Sci U S A *92*, 2539-2543.

Hellman, N.E., and Gitlin, J.D. (2002). Ceruloplasmin metabolism and function. Annu Rev Nutr *22*, 439-458.

Hellman, N.E., Kono, S., Miyajima, H., and Gitlin, J.D. (2002). Biochemical analysis of a missense mutation in aceruloplasminemia. J Biol Chem *277*, 1375-1380.

Heneka, M.T., Nadrigny, F., Regen, T., Martinez-Hernandez, A., Dumitrescu-Ozimek, L., Terwel, D., Jardanhazi-Kurutz, D., Walter, J., Kirchhoff, F., Hanisch, U.K.*, et al.* (2010). Locus ceruleus controls Alzheimer's disease pathology by modulating microglial functions through norepinephrine. Proc Natl Acad Sci U S A *107*, 6058-6063.

Hentze, M.W., Muckenthaler, M.U., and Andrews, N.C. (2004). Balancing acts: molecular control of mammalian iron metabolism. Cell *117*, 285-297.

Holmberg, C.G. (1944). On the presence of a laccase-like enzyme in serum and its relation to the copper in serum. Acta Physiologica Scandinavica *8*, 227-229.

Holmberg, C.G., and Laurell, C.B. (1948). Investigations in serum copper II, isolation of the copper-containing protein and a description of some of its properties. Acta Physiologica Scandinavica *2*, 550-556.

Holwerda, R.A., Wherland, S., and Gray, H.B. (1976). Electron transfer reactions of copper proteins. Annu Rev Biophys Bioeng *5*, 363-396.

Hope, H. (1988). Cryocrystallography of biological macromolecules: a generally applicable method. Acta Crystallogr B *44 (Pt 1)*, 22-26.

Hope, H. (1990). Crystallography of biological macromolecules at ultra-low temperature. Annu Rev Biophys Biophys Chem *19*, 107-126.

Hung, I.H., Casareno, R.L., Labesse, G., Mathews, F.S., and Gitlin, J.D. (1998). HAH1 is a copper-binding protein with distinct amino acid residues mediating copper homeostasis and antioxidant defense. J Biol Chem *273*, 1749-1754.

Ireton, G.C., and Stoddard, B.L. (2004). Microseed matrix screening to improve crystals of yeast cytosine deaminase. Acta Crystallogr D Biol Crystallogr *60*, 601-605.

Jancarik, J., Pufan, R., Hong, C., Kim, S.H., and Kim, R. (2004). Optimum solubility (OS) screening: an efficient method to optimize buffer conditions for homogeneity and crystallization of proteins. Acta Crystallogr D Biol Crystallogr *60*, 1670-1673.

Jeong, S.Y., and David, S. (2003). Glycosylphosphatidylinositol-anchored ceruloplasmin is required for iron efflux from cells in the central nervous system. J Biol Chem *278*, 27144-27148.

Jin, L., Wang, J., Zhao, L., Jin, H., Fei, G., Zhang, Y., Zeng, M., and Zhong, C. (2011). Decreased serum ceruloplasmin levels characteristically aggravate nigral iron deposition in Parkinson's disease. Brain *134*, 50-58.

Johannesson, T., Kristinsson, J., Torsdottir, G., and Snaedal, J. (2012). [Ceruloplasmin (Cp) and iron in connection with Parkinson's disease (PD) and Alzheimer's disease (AD)]. Laeknabladid *98*, 531-537.

Kakhlon, O., and Cabantchik, Z.I. (2002). The labile iron pool: characterization, measurement, and participation in cellular processes(1). Free Radic Biol Med *33*, 1037-1046.

Kaneko, K., Nakamura, A., Yoshida, K., Kametani, F., Higuchi, K., and Ikeda, S. (2002a). Glial fibrillary acidic protein is greatly modified by oxidative stress in aceruloplasminemia brain. Free Radic Res *36*, 303-306.

Kaneko, K., Yoshida, K., Arima, K., Ohara, S., Miyajima, H., Kato, T., Ohta, M., and Ikeda, S.I. (2002b). Astrocytic deformity and globular structures are characteristic of the brains of patients with aceruloplasminemia. J Neuropathol Exp Neurol *61*, 1069-1077.

Kingston, I.B., Kingston, B.L., and Putnam, F.W. (1977). Chemical evidence that proteolytic cleavage causes the heterogeneity present in human ceruloplasmin preparations. Proc Natl Acad Sci U S A *74*, 5377-5381.

Klibanoff, E., Frieden, J., Spagnuolo, M., and Feinstein, A.R. (1966). "Rheumatic activity". A clinicopathologic correlation. JAMA *195*, 895-900.

Klomp, L.W., Farhangrazi, Z.S., Dugan, L.L., and Gitlin, J.D. (1996). Ceruloplasmin gene expression in the murine central nervous system. J Clin Invest *98*, 207-215.

Klomp, L.W., and Gitlin, J.D. (1996). Expression of the ceruloplasmin gene in the human retina and brain: implications for a pathogenic model in aceruloplasminemia. Hum Mol Genet *5*, 1989-1996.

Kohno, S., Miyajima, H., Takahashi, Y., Suzuki, H., and Hishida, A. (2000). Defective electron transfer in complexes I and IV in patients with aceruloplasminemia. J Neurol Sci *182*, 57-60.

Kono, S., and Miyajima, H. (2006). Molecular and pathological basis of aceruloplasminemia. Biol Res *39*, 15-23.

Koschinsky, M.L., Chow, B.K., Schwartz, J., Hamerton, J.L., and MacGillivray, R.T. (1987). Isolation and characterization of a processed gene for human ceruloplasmin. Biochemistry *26*, 7760-7767.

Koschinsky, M.L., Funk, W.D., van Oost, B.A., and MacGillivray, R.T. (1986). Complete cDNA sequence of human preceruloplasmin. Proc Natl Acad Sci U S A *83*, 5086-5090.

Kristinsson, J., Snaedal, J., Torsdottir, G., and Johannesson, T. (2012). Ceruloplasmin and iron in Alzheimer's disease and Parkinson's disease: a synopsis of recent studies. Neuropsychiatr Dis Treat *8*, 515-521.

Kuhlow, C.J., Krady, J.K., Basu, A., and Levison, S.W. (2003). Astrocytic ceruloplasmin expression, which is induced by IL-1beta and by traumatic brain injury, increases in the absence of the IL-1 type 1 receptor. Glia *44*, 76-84.

Lahey, M.E., Gubler, C.J., Chase, M.S., Cartwright, G.E., and Wintrobe, M.M. (1952). Studies on copper metabolism. II. Hematologic manifestations of copper deficiency in swine. Blood *7*, 1053-1074.

Linder, M.C., and Hazegh-Azam, M. (1996). Copper biochemistry and molecular biology. Am J Clin Nutr *63*, 797S-811S.

Linder, M.C., and Moor, J.R. (1977). Plasma ceruloplasmin. Evidence for its presence in and uptake by heart and other organs of the rat. Biochim Biophys Acta *499*, 329-336.

Lindley, P.C., G.

Zaitseva, I., Zaitev, V.R., B., and Selin-Lindgren, E.Y., K. (1997). A X-ray structural study of human ceruloplasmin in relation to ferroxidase activity. J Biol Inorg Chem *2*, 454-463.

Loeffler, D.A., LeWitt, P.A., Juneau, P.L., Sima, A.A., Nguyen, H.U., DeMaggio, A.J., Brickman, C.M., Brewer, G.J., Dick, R.D., Troyer, M.D*., et al.* (1996). Increased regional brain concentrations of ceruloplasmin in neurodegenerative disorders. Brain Res *738*, 265-274.

Loeffler, D.A., Sima, A.A., and LeWitt, P.A. (2001). Ceruloplasmin immunoreactivity in neurodegenerative disorders. Free Radic Res *35*, 111-118.

Logan, J.I., Harveyson, K.B., Wisdom, G.B., Hughes, A.E., and Archbold, G.P. (1994). Hereditary caeruloplasmin deficiency, dementia and diabetes mellitus. QJM *87*, 663-670.

Lonnerdal, B. (1996). Bioavailability of copper. Am J Clin Nutr *63*, 821S-829S.

Lovell, M.A., Robertson, J.D., Teesdale, W.J., Campbell, J.L., and Markesbery, W.R. (1998). Copper, iron and zinc in Alzheimer's disease senile plaques. J Neurol Sci *158*, 47-52.

Lovstad, R.A. (2006). A kinetic study on the phenothiazine dependent oxidation of NADH by bovine ceruloplasmin. Biometals *19*, 1-5.

Luft, J.R., Wolfley, J.R., and Snell, E.H. (2011). What's in a drop? Correlating observations and outcomes to guide macromolecular crystallization experiments. Cryst Growth Des *11*, 651-663.

Malmstrom, B.G. (1982). Enzymology of oxygen. Annu Rev Biochem *51*, 21-59.

Marques, L., Auriac, A., Willemetz, A., Banha, J., Silva, B., Canonne-Hergaux, F., and Costa, L. (2012). Immune cells and hepatocytes express glycosylphosphatidylinositol-anchored ceruloplasmin at their cell surface. Blood Cells Mol Dis *48*, 110-120.

McKie, A.T., Barrow, D., Latunde-Dada, G.O., Rolfs, A., Sager, G., Mudaly, E., Mudaly, M., Richardson, C., Barlow, D., Bomford, A*., et al.* (2001). An iron-regulated ferric reductase associated with the absorption of dietary iron. Science *291*, 1755-1759.

Medda, R., Calabrese, L., Musci, G., Padiglia, A., and Floris, G. (1996). Effect of ceruloplasmin on 6-hydroxydopamine oxidation. Biochem Mol Biol Int *38*, 721-728.

Menkes, J.H., Alter, M., Steigleder, G.K., Weakley, D.R., and Sung, J.H. (1962). A sex-linked recessive disorder with retardation of growth, peculiar hair, and focal cerebral and cerebellar degeneration. Pediatrics *29*, 764-779.

Mercer, J.F., Livingston, J., Hall, B., Paynter, J.A., Begy, C., Chandrasekharappa, S., Lockhart, P., Grimes, A., Bhave, M., Siemieniak, D*., et al.* (1993). Isolation of a partial candidate gene for Menkes disease by positional cloning. Nat Genet *3*, 20-25.

Messerschmidt, A., and Huber, R. (1990). The blue oxidases, ascorbate oxidase, laccase and ceruloplasmin. Modelling and structural relationships. Eur J Biochem *187*, 341-352.

Messerschmidt, A., Ladenstein, R., Huber, R., Bolognesi, M., Avigliano, L., Petruzzelli, R., Rossi, A., and Finazzi-Agro, A. (1992). Refined crystal structure of ascorbate oxidase at 1.9 A resolution. J Mol Biol *224*, 179-205.

Messerschmidt, A., Rossi, A., Ladenstein, R., Huber, R., Bolognesi, M., Gatti, G., Marchesini, A., Petruzzelli, R., and Finazzi-Agro, A. (1989). X-ray crystal structure of the blue oxidase ascorbate oxidase from zucchini. Analysis of the polypeptide fold and a model of the copper sites and ligands. J Mol Biol *206*, 513-529.

Messerschmidt, O. (1989). Combined effects of radiation and trauma. Adv Space Res *9*, 197-201.

Mittal, B., Doroudchi, M.M., Jeong, S.Y., Patel, B.N., and David, S. (2003). Expression of a membrane-bound form of the ferroxidase ceruloplasmin by leptomeningeal cells. Glia *41*, 337-346.

Miyajima, H. (2000a). [Aceruloplasminemia]. Rinsho Shinkeigaku *40*, 1290-1292.

Miyajima, H. (2000b). [Neuronal cell damage in aceruloplasminemia]. Nihon Shinkei Seishin Yakurigaku Zasshi *20*, 161-167.

Miyajima, H. (2003). Aceruloplasminemia, an iron metabolic disorder. Neuropathology *23*, 345-350.

Miyajima, H., Fujimoto, M., Kohno, S., Kaneko, E., and Gitlin, J.D. (1998). CSF abnormalities in patients with aceruloplasminemia. Neurology *51*, 1188-1190.

Miyajima, H., Kono, S., Takahashi, Y., and Sugimoto, M. (2002a). Increased lipid peroxidation and mitochondrial dysfunction in aceruloplasminemia brains. Blood Cells Mol Dis *29*, 433-438.

Miyajima, H., Nishimura, Y., Mizoguchi, K., Sakamoto, M., Shimizu, T., and Honda, N. (1987). Familial apoceruloplasmin deficiency associated with blepharospasm and retinal degeneration. Neurology *37*, 761-767.

Miyajima, H., Takahashi, Y., and Kono, S. (2003). Aceruloplasminemia, an inherited disorder of iron metabolism. Biometals *16*, 205-213.

Miyajima, H., Takahashi, Y., Kono, S., Sugimoto, M., Suzuki, Y., Hishida, A., Sakamoto, M., and Ouchi, Y. (2002b). Glucose and oxygen hypometabolism in aceruloplasminemia brains. Intern Med *41*, 186-190.

Moalem, S., Percy, M.E., Andrews, D.F., Kruck, T.P., Wong, S., Dalton, A.J., Mehta, P., Fedor, B., and Warren, A.C. (2000). Are hereditary hemochromatosis mutations involved in Alzheimer disease? Am J Med Genet *93*, 58-66.

Moller, L.B., Petersen, C., Lund, C., and Horn, N. (2000). Characterization of the hCTR1 gene: genomic organization, functional expression, and identification of a highly homologous processed gene. Gene *257*, 13-22.

Mollgard, K., Dziegielewska, K.M., Saunders, N.R., Zakut, H., and Soreq, H. (1988). Synthesis and localization of plasma proteins in the developing human brain. Integrity of the fetal blood-brain barrier to endogenous proteins of hepatic origin. Dev Biol *128*, 207-221.

Morita, H., Inoue, A., and Yanagisawa, N. (1992). [A case of ceruloplasmin deficiency which showed dementia, ataxia and iron deposition in the brain]. Rinsho Shinkeigaku *32*, 483-487.

Moshkov, K.A., Lakatos, S., Hajdu, J., Zavodsky, P., and Neifakh, S.A. (1979). Proteolysis of human ceruloplasmin. Some peptide bonds are particularly susceptible to proteolytic attack. Eur J Biochem *94*, 127-134.

Mukhopadhyay, C.K., Ehrenwald, E., and Fox, P.L. (1996). Ceruloplasmin enhances smooth muscle cell- and endothelial cell-mediated low density lipoprotein oxidation by a superoxide-dependent mechanism. J Biol Chem *271*, 14773-14778.

Mukhopadhyay, C.K., Mazumder, B., Lindley, P.F., and Fox, P.L. (1997). Identification of the prooxidant site of human ceruloplasmin: a model for oxidative damage by copper bound to protein surfaces. Proc Natl Acad Sci U S A *94*, 11546-11551.

Musci, G., Bellenchi, G.C., and Calabrese, L. (1999). The multifunctional oxidase activity of ceruloplasmin as revealed by anion binding studies. Eur J Biochem *265*, 589-597.

Musci, G., Bonaccorsi di Patti, M.C., and Calabrese, L. (1995). Modulation of the redox state of the copper sites of human ceruloplasmin by chloride. J Protein Chem *14*, 611-619.

Niesen, F.H., Berglund, H., and Vedadi, M. (2007). The use of differential scanning fluorimetry to detect ligand interactions that promote protein stability. Nat Protoc *2*, 2212-2221.

Nittis, T., and Gitlin, J.D. (2002). The copper-iron connection: hereditary aceruloplasminemia. Semin Hematol *39*, 282-289.

Osaki, S., Johnson, D.A., and Frieden, E. (1966). The possible significance of the ferrous oxidase activity of ceruloplasmin in normal human serum. J Biol Chem *241*, 2746-2751.

Osaki, S., Johnson, D.A., and Frieden, E. (1971). The mobilization of iron from the perfused mammalian liver by a serum copper enzyme, ferroxidase I. J Biol Chem *246*, 3018-3023.

Pantopoulos, K. (2004). Iron metabolism and the IRE/IRP regulatory system: an update. Ann N Y Acad Sci *1012*, 1-13.

Papanikolaou, G., and Pantopoulos, K. (2005). Iron metabolism and toxicity. Toxicol Appl Pharmacol *202*, 199-211.

Patel, B.N., and David, S. (1997). A novel glycosylphosphatidylinositol-anchored form of ceruloplasmin is expressed by mammalian astrocytes. J Biol Chem *272*, 20185-20190.

Patel, B.N., Dunn, R.J., and David, S. (2000). Alternative RNA splicing generates a glycosylphosphatidylinositol-anchored form of ceruloplasmin in mammalian brain. J Biol Chem *275*, 4305-4310.

Patel, B.N., Dunn, R.J., Jeong, S.Y., Zhu, Q., Julien, J.P., and David, S. (2002). Ceruloplasmin regulates iron levels in the CNS and prevents free radical injury. J Neurosci *22*, 6578-6586.

Percival, S.S. (1998). Copper and immunity. Am J Clin Nutr *67*, 1064S-1068S.

Perez-Aguilar, F. (2002). [Ceruloplasmine and iron metabolism: their implications in hemochromatosis, Wilson's disease and aceruloplasminemia]. Rev Clin Esp *202*, 649-651.

Petrat, F., de Groot, H., Sustmann, R., and Rauen, U. (2002). The chelatable iron pool in living cells: a methodically defined quantity. Biol Chem *383*, 489-502.

Ponka, P., Beaumont, C., and Richardson, D.R. (1998). Function and regulation of transferrin and ferritin. Semin Hematol *35*, 35-54.

Prohaska, J.R. (2011). Impact of copper limitation on expression and function of multicopper oxidases (ferroxidases). Adv Nutr *2*, 89-95.

Qian, Z.M., and Wang, Q. (1998). Expression of iron transport proteins and excessive iron accumulation in the brain in neurodegenerative disorders. Brain Res Brain Res Rev *27*, 257-267.

Rasia, R.M., Bertoncini, C.W., Marsh, D., Hoyer, W., Cherny, D., Zweckstetter, M., Griesinger, C., Jovin, T.M., and Fernandez, C.O. (2005). Structural characterization of copper(II) binding to alpha-synuclein: Insights into the bioinorganic chemistry of Parkinson's disease. Proc Natl Acad Sci U S A *102*, 4294-4299.

Roberts, S.A., Weichsel, A., Grass, G., Thakali, K., Hazzard, J.T., Tollin, G., Rensing, C., and Montfort, W.R. (2002). Crystal structure and electron transfer kinetics of CueO, a multicopper oxidase required for copper homeostasis in Escherichia coli. Proc Natl Acad Sci U S A *99*, 2766-2771.

Roos, P.M., Vesterberg, O., and Nordberg, M. (2006). Metals in motor neuron diseases. Exp Biol Med (Maywood) *231*, 1481-1487.

Rossmann, M.G. (1990). The molecular replacement method. Acta Crystallogr A *46 (Pt 2)*, 73-82.

Ryter, S.W., and Tyrrell, R.M. (2000). The heme synthesis and degradation pathways: role in oxidant sensitivity. Heme oxygenase has both pro- and antioxidant properties. Free Radic Biol Med *28*, 289-309.

Sadrzadeh, S.M., and Saffari, Y. (2004). Iron and brain disorders. Am J Clin Pathol *121 Suppl*, S64-70.

Sakurai, T., and Kataoka, K. (2007). Structure and function of type I copper in multicopper oxidases. Cell Mol Life Sci *64*, 2642-2656.

Salzer, J.L., Lovejoy, L., Linder, M.C., and Rosen, C. (1998). Ran-2, a glial lineage marker, is a GPI-anchored form of ceruloplasmin. J Neurosci Res *54*, 147-157.

Schaefer, M., Hopkins, R.G., Failla, M.L., and Gitlin, J.D. (1999). Hepatocyte-specific localization and copper-dependent trafficking of the Wilson's disease protein in the liver. Am J Physiol *276*, G639-646.

Scheinberg, I.H., and Gitlin, D. (1952). Deficiency of ceruloplasmin in patients with hepatolenticular degeneration (Wilson's disease). Science *116*, 239-242.

Smyth, M.S., and Martin, J.H. (2000). x ray crystallography. Mol Pathol *53*, 8-14.

Snaedal, J., Kristinsson, J., Gunnarsdottir, S., Olafsdottir, Baldvinsson, M., and Johannesson, T. (1998). Copper, ceruloplasmin and superoxide dismutase in patients with Alzheimer's disease . a case-control study. Dement Geriatr Cogn Disord *9*, 239-242.

Su, B., Wang, X., Nunomura, A., Moreira, P.I., Lee, H.G., Perry, G., Smith, M.A., and Zhu, X. (2008). Oxidative stress signaling in Alzheimer's disease. Curr Alzheimer Res *5*, 525-532.

Takahashi, N., Bauman, R.A., Ortel, T.L., Dwulet, F.E., Wang, C.C., and Putnam, F.W. (1983). Internal triplication in the structure of human ceruloplasmin. Proc Natl Acad Sci U S A *80*, 115-119.

Takahashi, N., Ortel, T.L., and Putnam, F.W. (1984). Single-chain structure of human ceruloplasmin: the complete amino acid sequence of the whole molecule. Proc Natl Acad Sci U S A *81*, 390-394.

Takahashi, Y., Miyajima, H., Shirabe, S., Nagataki, S., Suenaga, A., and Gitlin, J.D. (1996). Characterization of a nonsense mutation in the ceruloplasmin gene resulting in diabetes and neurodegenerative disease. Hum Mol Genet *5*, 81-84.

Taly, A.B., Meenakshi-Sundaram, S., Sinha, S., Swamy, H.S., and Arunodaya, G.R. (2007). Wilson disease: description of 282 patients evaluated over 3 decades. Medicine (Baltimore) *86*, 112-121.

Tanzi, R.E., Petrukhin, K., Chernov, I., Pellequer, J.L., Wasco, W., Ross, B., Romano, D.M., Parano, E., Pavone, L., Brzustowicz, L.M*., et al.* (1993). The Wilson disease gene is a copper transporting ATPase with homology to the Menkes disease gene. Nat Genet *5*, 344-350.

Taylor, J.P., Hardy, J., and Fischbeck, K.H. (2002). Toxic proteins in neurodegenerative disease. Science *296*, 1991-1995.

Torsdottir, G., Kristinsson, J., Hreidarsson, S., Snaedal, J., and Johannesson, T. (2001). Copper, ceruloplasmin and superoxide dismutase (SOD1) in patients with Down's syndrome. Pharmacol Toxicol *89*, 320-325.

Torsdottir, G., Kristinsson, J., Sveinbjornsdottir, S., Snaedal, J., and Johannesson, T. (1999). Copper, ceruloplasmin, superoxide dismutase and iron parameters in Parkinson's disease. Pharmacol Toxicol *85*, 239-243.

Trader, C.D., and Frieden, E. (1966). Dimerization and other chemical changes in amphibian hemoglobins during metamorphosis. J Biol Chem *241*, 357-366.

Tumer, Z., and Moller, L.B. (2010). Menkes disease. Eur J Hum Genet *18*, 511-518.

Vashchenko, G., and Macgillivray, R.T. (2013). Multi-copper oxidases and human iron metabolism. Nutrients *5*, 2289-2313.

Vulpe, C.D., Kuo, Y.M., Murphy, T.L., Cowley, L., Askwith, C., Libina, N., Gitschier, J., and Anderson, G.J. (1999). Hephaestin, a ceruloplasmin homologue implicated in intestinal iron transport, is defective in the sla mouse. Nat Genet *21*, 195-199.

Waggoner, D.J., Bartnikas, T.B., and Gitlin, J.D. (1999). The role of copper in neurodegenerative disease. Neurobiol Dis *6*, 221-230.

Wang, J., and Pantopoulos, K. (2011). Regulation of cellular iron metabolism. Biochem J *434*, 365-381.

Watenpaugh, K.D. (1985). Overview of phasing by isomorphous replacement. Methods Enzymol *115*, 3-15.

Yang, F., Naylor, S.L., Lum, J.B., Cutshaw, S., McCombs, J.L., Naberhaus, K.H., McGill, J.R., Adrian, G.S., Moore, C.M., Barnett, D.R.*, et al.* (1986). Characterization, mapping, and expression of the human ceruloplasmin gene. Proc Natl Acad Sci U S A *83*, 3257-3261.

Yazaki, M., Yoshida, K., Nakamura, A., Furihata, K., Yonekawa, M., Okabe, T., Yamashita, N., Ohta, M., and Ikeda, S. (1998). A novel splicing mutation in the ceruloplasmin gene responsible for hereditary ceruloplasmin deficiency with hemosiderosis. J Neurol Sci *156*, 30-34.

Yoshida, K., Furihata, K., Takeda, S., Nakamura, A., Yamamoto, K., Morita, H., Hiyamuta, S., Ikeda, S., Shimizu, N., and Yanagisawa, N. (1995). A mutation in the ceruloplasmin gene is associated with systemic hemosiderosis in humans. Nat Genet *9*, 267-272.

Yoshida, K., Kaneko, K., Miyajima, H., Tokuda, T., Nakamura, A., Kato, M., and Ikeda, S. (2000). Increased lipid peroxidation in the brains of aceruloplasminemia patients. J Neurol Sci *175*, 91-95.

Zaitsev, V.N., Zaitseva, I., Papiz, M., and Lindley, P.F. (1999). An X-ray crystallographic study of the binding sites of the azide inhibitor and organic substrates to ceruloplasmin, a multi-copper oxidase in the plasma. J Biol Inorg Chem *4*, 579-587.

Zaitseva, I., Zaitsev, V., Card, G., Moshkov, K., Bax, B., Ralph, A., and Lindley, P. (1996). The X-ray structure of human serum ceruloplasmin at 3.1 Å: nature of the copper centres. Journ Biol Inorg Chem *1*, 15-23.

Zerbinatti, C.V., Wozniak, D.F., Cirrito, J., Cam, J.A., Osaka, H., Bales, K.R., Zhuo, M., Paul, S.M., Holtzman, D.M., and Bu, G. (2004). Increased soluble amyloid-beta peptide and memory deficits in amyloid model mice overexpressing the low-density lipoprotein receptor-related protein. Proc Natl Acad Sci U S A *101*, 1075-1080.

7. ANNEXES

Index HT™ — HR2-134 Reagent Formulation

Well #	Salt	Well #	Buffer ◊	Well #	Precipitant
1. (A1)	None	1. (A1)	0.1 M Citric acid pH 3.5	1. (A1)	2.0 M Ammonium sulfate
2. (A2)	None	2. (A2)	0.1 M Sodium acetate trihydrate pH 4.5	2. (A2)	2.0 M Ammonium sulfate
3. (A3)	None	3. (A3)	0.1 M BIS-TRIS pH 5.5	3. (A3)	2.0 M Ammonium sulfate
4. (A4)	None	4. (A4)	0.1 M BIS-TRIS pH 6.5	4. (A4)	2.0 M Ammonium sulfate
5. (A5)	None	5. (A5)	0.1 M HEPES pH 7.5	5. (A5)	2.0 M Ammonium sulfate
6. (A6)	None	6. (A6)	0.1 M Tris pH 8.5	6. (A6)	2.0 M Ammonium sulfate
7. (A7)	None	7. (A7)	0.1 M Citric acid pH 3.5	7. (A7)	3.0 M Sodium chloride
8. (A8)	None	8. (A8)	0.1 M Sodium acetate trihydrate pH 4.5	8. (A8)	3.0 M Sodium chloride
9. (A9)	None	9. (A9)	0.1 M BIS-TRIS pH 5.5	9. (A9)	3.0 M Sodium chloride
10. (A10)	None	10. (A10)	0.1 M BIS-TRIS pH 6.5	10. (A10)	3.0 M Sodium chloride
11. (A11)	None	11. (A11)	0.1 M HEPES pH 7.5	11. (A11)	3.0 M Sodium chloride
12. (A12)	None	12. (A12)	0.1 M Tris pH 8.5	12. (A12)	3.0 M Sodium chloride
13. (B1)	None	13. (B1)	0.1 M BIS-TRIS pH 5.5	13. (B1)	0.3 M Magnesium formate dihydrate
14. (B2)	None	14. (B2)	0.1 M BIS-TRIS pH 6.5	14. (B2)	0.5 M Magnesium formate dihydrate
15. (B3)	None	15. (B3)	0.1 M HEPES pH 7.5	15. (B3)	0.5 M Magnesium formate dihydrate
16. (B4)	None	16. (B4)	0.1 M Tris pH 8.5	16. (B4)	0.3 M Magnesium formate dihydrate
17. (B5)	None	17. (B5)	None - pH 5.6	17. (B5)	1.26 M Sodium phosphate monobasic monohydrate, 0.14 M Potassium phosphate dibasic
18. (B6)	None	18. (B6)	None - pH 6.9	18. (B6)	0.49 M Sodium phosphate monobasic monohydrate, 0.91 M Potassium phosphate dibasic
19. (B7)	None	19. (B7)	None - pH 8.2	19. (B7)	0.056 M Sodium phosphate monobasic monohydrate, 1.344 M Potassium phosphate dibasic
20. (B8)	None	20. (B8)	0.1 M HEPES pH 7.5	20. (B8)	1.4 M Sodium citrate tribasic dihydrate
21. (B9)	None	21. (B9)	None	21. (B9)	1.8 M Ammonium citrate tribasic pH 7.0
22. (B10)	None	22. (B10)	None	22. (B10)	0.8 M Succinic acid pH 7.0
23. (B11)	None	23. (B11)	None	23. (B11)	2.1 M DL-Malic acid pH 7.0
24. (B12)	None	24. (B12)	None	24. (B12)	2.8 M Sodium acetate trihydrate pH 7.0
25. (C1)	None	25. (C1)	None	25. (C1)	3.5 M Sodium formate pH 7.0
26. (C2)	None	26. (C2)	None	26. (C2)	1.1 M Ammonium tartrate dibasic pH 7.0
27. (C3)	None	27. (C3)	None	27. (C3)	2.4 M Sodium malonate pH 7.0
28. (C4)	None	28. (C4)	None	28. (C4)	35% v/v Tacsimate pH 7.0
29. (C5)	None	29. (C5)	None	29. (C5)	60% v/v Tacsimate pH 7.0
30. (C6)	0.1 M Sodium chloride	30. (C6)	0.1 M BIS-TRIS pH 6.5	30. (C6)	1.5 M Ammonium sulfate
31. (C7)	0.8 M Potassium sodium tartrate tetrahydrate	31. (C7)	0.1 M Tris pH 8.5	31. (C7)	0.5% w/v Polyethylene glycol monomethyl ether 5,000
32. (C8)	1.0 M Ammonium sulfate	32. (C8)	0.1 M BIS-TRIS pH 5.5	32. (C8)	1% w/v Polyethylene glycol 3,350
33. (C9)	1.1 M Sodium malonate pH 7.0	33. (C9)	0.1 M HEPES pH 7.0	33. (C9)	0.5% v/v Jeffamine® ED-2001 pH 7.0
34. (C10)	1.0 M Succinic acid pH 7.0	34. (C10)	0.1 M HEPES pH 7.0	34. (C10)	1% w/v Polyethylene glycol monomethyl ether 2,000
35. (C11)	1.0 M Ammonium sulfate	35. (C11)	0.1 M HEPES pH 7.0	35. (C11)	0.5% w/v Polyethylene glycol 8,000
36. (C12)	15% v/v Tacsimate pH 7.0	36. (C12)	0.1 M HEPES pH 7.0	36. (C12)	2% w/v Polyethylene glycol 3,350
37. (D1)	None	37. (D1)	None	37. (D1)	25% w/v Polyethylene glycol 1,500
38. (D2)	None	38. (D2)	0.1 M HEPES pH 7.0	38. (D2)	30% v/v Jeffamine® M-600® pH 7.0
39. (D3)	None	39. (D3)	0.1 M HEPES pH 7.0	39. (D3)	30% v/v Jeffamine® ED-2001 pH 7.0
40. (D4)	None	40. (D4)	0.1 M Citric acid pH 3.5	40. (D4)	25% w/v Polyethylene glycol 3,350
41. (D5)	None	41. (D5)	0.1 M Sodium acetate trihydrate pH 4.5	41. (D5)	25% w/v Polyethylene glycol 3,350
42. (D6)	None	42. (D6)	0.1 M BIS-TRIS pH 5.5	42. (D6)	25% w/v Polyethylene glycol 3,350
43. (D7)	None	43. (D7)	0.1 M BIS-TRIS pH 6.5	43. (D7)	25% w/v Polyethylene glycol 3,350
44. (D8)	None	44. (D8)	0.1 M HEPES pH 7.5	44. (D8)	25% w/v Polyethylene glycol 3,350
45. (D9)	None	45. (D9)	0.1 M Tris pH 8.5	45. (D9)	25% w/v Polyethylene glycol 3,350
46. (D10)	None	46. (D10)	0.1 M BIS-TRIS pH 6.5	46. (D10)	20% w/v Polyethylene glycol monomethyl ether 5,000
47. (D11)	None	47. (D11)	0.1 M BIS-TRIS pH 6.5	47. (D11)	28% w/v Polyethylene glycol monomethyl ether 2,000
48. (D12)	0.2 M Calcium chloride dihydrate	48. (D12)	0.1 M BIS-TRIS pH 5.5	48. (D12)	45% v/v (+/-)-2-Methyl-2,4-pentanediol

Index HT™ — HR2-134 Reagent Formulation

Well #	Salt	Well #	Buffer ◊	Well #	Precipitant
49. (E1)	0.2 M Calcium chloride dihydrate	49. (E1)	0.1 M BIS-TRIS pH 6.5	49. (E1)	45% v/v (+/-)-2-Methyl-2,4-pentanediol
50. (E2)	0.2 M Ammonium acetate	50. (E2)	0.1 M BIS-TRIS pH 5.5	50. (E2)	45% v/v (+/-)-2-Methyl-2,4-pentanediol
51. (E3)	0.2 M Ammonium acetate	51. (E3)	0.1 M BIS-TRIS pH 6.5	51. (E3)	45% v/v (+/-)-2-Methyl-2,4-pentanediol
52. (E4)	0.2 M Ammonium acetate	52. (E4)	0.1 M HEPES pH 7.5	52. (E4)	45% v/v (+/-)-2-Methyl-2,4-pentanediol
53. (E5)	0.2 M Ammonium acetate	53. (E5)	0.1 M Tris pH 8.5	53. (E5)	45% v/v (+/-)-2-Methyl-2,4-pentanediol
54. (E6)	0.05 M Calcium chloride dihydrate	54. (E6)	0.1 M BIS-TRIS pH 6.5	54. (E6)	30% v/v Polyethylene glycol monomethyl ether 550
55. (E7)	0.05 M Magnesium chloride hexahydrate	55. (E7)	0.1 M HEPES pH 7.5	55. (E7)	30% v/v Polyethylene glycol monomethyl ether 550
56. (E8)	0.2 M Potassium chloride	56. (E8)	0.05 M HEPES pH 7.5	56. (E8)	35% v/v Pentaerythritol propoxylate (5/4 PO/OH)
57. (E9)	0.05 M Ammonium sulfate	57. (E9)	0.05 M BIS-TRIS pH 6.5	57. (E9)	30% v/v Pentaerythritol ethoxylate (15/4 EO/OH)
58. (E10)	None	58. (E10)	0.1 M BIS-TRIS pH 6.5	58. (E10)	45% v/v Polypropylene glycol P 400
59. (E11)	0.02 M Magnesium chloride hexahydrate	59. (E11)	0.1 M HEPES pH 7.5	59. (E11)	22% w/v Poly(acrylic acid sodium salt) 5,100
60. (E12)	0.01 M Cobalt(II) chloride hexahydrate	60. (E12)	0.1 M Tris pH 8.5	60. (E12)	20% w/v Polyvinylpyrrolidone K 15
61. (F1)	0.2 M L-Proline	61. (F1)	0.1 M HEPES pH 7.5	61. (F1)	10% w/v Polyethylene glycol 3,350
62. (F2)	0.2 M Trimethylamine N-oxide dihydrate	62. (F2)	0.1 M Tris pH 8.5	62. (F2)	20% w/v Polyethylene glycol monomethyl ether 2,000
63. (F3)	5% v/v Tacsimate pH 7.0	63. (F3)	0.1 M HEPES pH 7.0	63. (F3)	10% w/v Polyethylene glycol monomethyl ether 5,000
64. (F4)	0.005 M Cobalt(II) chloride hexahydrate, 0.005 M Nickel(II) chloride hexahydrate, 0.005 M Cadmium chloride hydrate, 0.005 M Magnesium chloride hexahydrate	64. (F4)	0.1 M HEPES pH 7.5	64. (F4)	12% w/v Polyethylene glycol 3,350
65. (F5)	0.1 M Ammonium acetate	65. (F5)	0.1 M BIS-TRIS pH 5.5	65. (F5)	17% w/v Polyethylene glycol 10,000
66. (F6)	0.2 M Ammonium sulfate	66. (F6)	0.1 M BIS-TRIS pH 5.5	66. (F6)	25% w/v Polyethylene glycol 3,350
67. (F7)	0.2 M Ammonium sulfate	67. (F7)	0.1 M BIS-TRIS pH 6.5	67. (F7)	25% w/v Polyethylene glycol 3,350
68. (F8)	0.2 M Ammonium sulfate	68. (F8)	0.1 M HEPES pH 7.5	68. (F8)	25% w/v Polyethylene glycol 3,350
69. (F9)	0.2 M Ammonium sulfate	69. (F9)	0.1 M Tris pH 8.5	69. (F9)	25% w/v Polyethylene glycol 3,350
70. (F10)	0.2 M Sodium chloride	70. (F10)	0.1 M BIS-TRIS pH 5.5	70. (F10)	25% w/v Polyethylene glycol 3,350
71. (F11)	0.2 M Sodium chloride	71. (F11)	0.1 M BIS-TRIS pH 6.5	71. (F11)	25% w/v Polyethylene glycol 3,350
72. (F12)	0.2 M Sodium chloride	72. (F12)	0.1 M HEPES pH 7.5	72. (F12)	25% w/v Polyethylene glycol 3,350
73. (G1)	0.2 M Sodium chloride	73. (G1)	0.1 M Tris pH 8.5	73. (G1)	25% w/v Polyethylene glycol 3,350
74. (G2)	0.2 M Lithium sulfate monohydrate	74. (G2)	0.1 M BIS-TRIS pH 5.5	74. (G2)	25% w/v Polyethylene glycol 3,350
75. (G3)	0.2 M Lithium sulfate monohydrate	75. (G3)	0.1 M BIS-TRIS pH 6.5	75. (G3)	25% w/v Polyethylene glycol 3,350
76. (G4)	0.2 M Lithium sulfate monohydrate	76. (G4)	0.1 M HEPES pH 7.5	76. (G4)	25% w/v Polyethylene glycol 3,350
77. (G5)	0.2 M Lithium sulfate monohydrate	77. (G5)	0.1 M Tris pH 8.5	77. (G5)	25% w/v Polyethylene glycol 3,350
78. (G6)	0.2 M Ammonium acetate	78. (G6)	0.1 M BIS-TRIS pH 5.5	78. (G6)	25% w/v Polyethylene glycol 3,350
79. (G7)	0.2 M Ammonium acetate	79. (G7)	0.1 M BIS-TRIS pH 6.5	79. (G7)	25% w/v Polyethylene glycol 3,350
80. (G8)	0.2 M Ammonium acetate	80. (G8)	0.1 M HEPES pH 7.5	80. (G8)	25% w/v Polyethylene glycol 3,350
81. (G9)	0.2 M Ammonium acetate	81. (G9)	0.1 M Tris pH 8.5	81. (G9)	25% w/v Polyethylene glycol 3,350
82. (G10)	0.2 M Magnesium chloride hexahydrate	82. (G10)	0.1 M BIS-TRIS pH 5.5	82. (G10)	25% w/v Polyethylene glycol 3,350
83. (G11)	0.2 M Magnesium chloride hexahydrate	83. (G11)	0.1 M BIS-TRIS pH 6.5	83. (G11)	25% w/v Polyethylene glycol 3,350
84. (G12)	0.2 M Magnesium chloride hexahydrate	84. (G12)	0.1 M HEPES pH 7.5	84. (G12)	25% w/v Polyethylene glycol 3,350
85. (H1)	0.2 M Magnesium chloride hexahydrate	85. (H1)	0.1 M Tris pH 8.5	85. (H1)	25% w/v Polyethylene glycol 3,350
86. (H2)	0.2 M Potassium sodium tartrate tetrahydrate	86. (H2)	None	86. (H2)	20% w/v Polyethylene glycol 3,350
87. (H3)	0.2 M Sodium malonate pH 7.0	87. (H3)	None	87. (H3)	20% w/v Polyethylene glycol 3,350
88. (H4)	0.2 M Ammonium citrate tribasic pH 7.0	88. (H4)	None	88. (H4)	20% w/v Polyethylene glycol 3,350
89. (H5)	0.1 M Succinic acid pH 7.0	89. (H5)	None	89. (H5)	15% w/v Polyethylene glycol 3,350
90. (H6)	0.2 M Sodium formate	90. (H6)	None	90. (H6)	20% w/v Polyethylene glycol 3,350
91. (H7)	0.15 M DL-Malic acid pH 7.0	91. (H7)	None	91. (H7)	20% w/v Polyethylene glycol 3,350
92. (H8)	0.1 M Magnesium formate dihydrate	92. (H8)	None	92. (H8)	15% w/v Polyethylene glycol 3,350
93. (H9)	0.05 M Zinc acetate dihydrate	93. (H9)	None	93. (H9)	20% w/v Polyethylene glycol 3,350
94. (H10)	0.2 M Sodium citrate tribasic dihydrate	94. (H10)	None	94. (H10)	20% w/v Polyethylene glycol 3,350
95. (H11)	0.1 M Potassium thiocyanate	95. (H11)	None	95. (H11)	30% w/v Polyethylene glycol monomethyl ether 2,000
96. (H12)	0.15 M Potassium bromide	96. (H12)	None	96. (H12)	30% w/v Polyethylene glycol monomethyl ether 2,000

MPD Suite Refill-Hit Solutions (4 x 12.5 ml tubes)

Number	Salt	Buffer	Precipitant	Cat. no.
1	0.2 M Cadmium chloride		40 %(v/v) MPD	134501
2	0.2 M Potassium fluoride		40 %(v/v) MPD	134502
3	0.2 M Ammonium fluoride		40 %(v/v) MPD	134503
4	0.2 M Lithium chloride		40 %(v/v) MPD	134504
5	0.2 M Magnesium chloride		40 %(v/v) MPD	134505
6	0.2 M Sodium chloride		40 %(v/v) MPD	134506
7	0.2 M Calcium chloride		40 %(v/v) MPD	134507
8	0.2 M Potassium chloride		40 %(v/v) MPD	134508
9	0.2 M Ammonium chloride		40 %(v/v) MPD	134509
10	0.2 M Sodium iodide		40 %(v/v) MPD	134510
11	0.2 M Potassium iodide		40 %(v/v) MPD	134511
12	0.2 M Ammonium iodide		40 %(v/v) MPD	134512
13	0.2 M Sodium thiocyanate		40 %(v/v) MPD	134513
14	0.2 M Potassium thiocyanate		40 %(v/v) MPD	134514
15	0.2 M Lithium nitrate		40 %(v/v) MPD	134515
16	0.2 M Magnesium nitrate		40 %(v/v) MPD	134516
17	0.2 M Sodium nitrate		40 %(v/v) MPD	134517
18	0.2 M Potassium nitrate		40 %(v/v) MPD	134518
19	0.2 M Ammonium nitrate		40 %(v/v) MPD	134519
20	0.2 M Zinc sulfate		40 %(v/v) MPD	134520
21	0.2 M Sodium formate		40 %(v/v) MPD	134521
22	0.2 M Potassium formate		40 %(v/v) MPD	134522
23	0.2 M Ammonium formate		40 %(v/v) MPD	134523
24	0.2 M Lithium acetate		40 %(v/v) MPD	134524
25	0.2 M Magnesium acetate		40 %(v/v) MPD	134525
26	0.2 M Sodium malonate		40 %(v/v) MPD	134526
27	0.2 M Sodium acetate		40 %(v/v) MPD	134527
28	0.2 M Calcium acetate		40 %(v/v) MPD	134528
29	0.2 M Potassium acetate		40 %(v/v) MPD	134529
30	0.2 M Ammonium acetate		40 %(v/v) MPD	134530
31	0.2 M Lithium sulfate		40 %(v/v) MPD	134531
32	0.2 M Magnesium sulfate		40 %(v/v) MPD	134532
33	0.2 M Cesium chloride		40 %(v/v) MPD	134533
34	0.2 M Nickel chloride		40 %(v/v) MPD	134534
35	0.2 M Ammonium sulfate		40 %(v/v) MPD	134535
36	0.2 M di-Sodium tartate		40 %(v/v) MPD	134536
37	0.2 M K/Na tartrate		40 %(v/v) MPD	134537
38	0.2 M di-Ammonium tartrate		40 %(v/v) MPD	134538
39	0.2 M Sodium phosphate		40 %(v/v) MPD	134539
40	0.2 M Potassium bromide		40 %(v/v) MPD	134540
41	0.2 M Sodium bromide		40 %(v/v) MPD	134541
42	0.2 M di-Potassium phosphate		40 %(v/v) MPD	134542
43	0.2 M Ammonium phosphate		40 %(v/v) MPD	134543
44	0.2 M di-Ammonium phosphate		40 %(v/v) MPD	134544
45	0.2 M tri-Lithium citrate		40 %(v/v) MPD	134545
46	0.2 M tri-Sodium citrate		40 %(v/v) MPD	134546
47	0.2 M tri-Potassium citrate		40 %(v/v) MPD	134547
48	0.2 M di-Ammonium citrate		40 %(v/v) MPD	134548

MPD Suite Refill-Hit Solutions (4 x 12.5 ml tubes)

Number	Salt	Buffer	Precipitant	Cat. no.
49		0.1 M Citric acid pH 4.0	10 %(v/v) MPD	134549
50		0.1 M Sodium acetate pH 5.0	10 %(v/v) MPD	134550
51		0.1 M MES pH 6.0	10 %(v/v) MPD	134551
52		0.1 M HEPES pH 7.0	10 %(v/v) MPD	134552
53		0.1 M Tris pH 8.0	10 %(v/v) MPD	134553
54		0.1 M BICINE pH 9.0	10 %(v/v) MPD	134554
55		0.1 M Citric acid pH 4.0	20 %(v/v) MPD	134555
56		0.1 M Sodium acetate pH 5.0	20 %(v/v) MPD	134556
57		0.1 M MES pH 6.0	20 %(v/v) MPD	134557
58		0.1 M HEPES pH 7.0	20 %(v/v) MPD	134558
59		0.1 M Tris pH 8.0	20 %(v/v) MPD	134559
60		0.1 M BICINE pH 9.0	20 %(v/v) MPD	134560
61		0.1 M Citric acid pH 4.0	40 %(v/v) MPD	134561
62		0.1 M Sodium acetate pH 5.0	40 %(v/v) MPD	134562
63		0.1 M MES pH 6.0	40 %(v/v) MPD	134563
64		0.1 M HEPES pH 7.0	40 %(v/v) MPD	134564
65		0.1 M Tris pH 8.0	40 %(v/v) MPD	134565
66		0.1 M BICINE pH 9.0	40 %(v/v) MPD	134566
67		0.1 M Sodium acetate pH 4.0	65 %(v/v) MPD	134567
68		0.1 M Sodium acetate pH 5.0	65 %(v/v) MPD	134568
69		0.1 M MES pH 6.0	65 %(v/v) MPD	134569
70		0.1 M HEPES pH 7.0	65 %(v/v) MPD	134570
71		0.1 M Tris pH 8.0	65 %(v/v) MPD	134571
72		0.1 M BICINE pH 9.0	65 %(v/v) MPD	134572
73	0.1 M tri-Sodium citrate	0.1 M HEPES sodium salt pH 7.5	10 %(w/v) MPD	134573
74	0.05 M Magnesium chloride	0.1 M Tris.HCl pH 8.5	12 %(w/v) MPD	134574
75	0.02 M Calcium chloride	0.1 M Sodium acetate pH 4.6	15 %(w/v) MPD	134575
76		0.1 M Imidazole.HCl pH 8.0	15 %(w/v) MPD, 5 %(w/v) PEG 4000	134576
77	0.2 M Ammonium acetate	0.1 M tri-Sodium citrate pH 5.6	15 %(w/v) MPD	134577
78	0.2 M Magnesium acetate	0.1 M MES sodium salt pH 6.5	15 %(w/v) MPD	134578
79	0.2 M tri-Sodium citrate	0.1 M HEPES sodium salt pH 7.5	15 %(w/v) MPD	134579
80	0.1 M tri-Sodium citrate	0.1 M HEPES sodium salt pH 7.5	20 %(w/v) MPD	134580
81		0.1 M Imidazole.HCl pH 8.0	20 %(w/v) MPD	134581
82	0.2 M Sodium chloride		20 %(w/v) MPD, 4 %(w/v) Glyerol	134582
83	0.02 M Calcium chloride	0.1 M Sodium acetate pH 4.6	30 %(w/v) MPD	134583
84	0.2 M Ammonium acetate	0.1 M tri-Sodium citrate pH 5.6	30 %(w/v) MPD	134584
85	0.2 M Magnesium acetate	0.1 M MES sodium salt pH 6.5	30 %(w/v) MPD	134585
86	0.5 M Ammonium sulfate	0.1 M HEPES sodium salt pH 7.5	30 %(w/v) MPD	134586
87	0.2 M tri-Sodium citrate	0.1 M HEPES sodium salt pH 7.5	30 %(w/v) MPD	134587
88		0.1 M HEPES sodium salt pH 7.5	30 %(w/v) MPD, 5 %(w/v) PEG 4000	134588
89		0.1 M Imidazole.HCl pH 8.0	30 %(w/v) MPD, 10 %(w/v) PEG 4000	134589
90			30 %(w/v) MPD, 20 %(w/v) Ethanol	134590
91			35 %(w/v) MPD	134591
92		0.1 M Imidazole.HCl pH 8.0	35 %(w/v) MPD	134592
93		0.1 M Tris.HCl pH 8.5	40 %(w/v) MPD	134593
94		0.1 M HEPES sodium salt pH 7.5	47 %(w/v) MPD	134594
95			47 %(w/v) MPD, 2 %(w/v) tert-Butanol	134595
96			50 %(w/v) MPD	134596

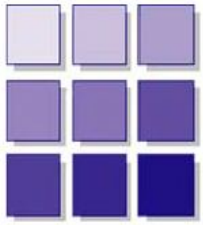

moleculardimensions.com

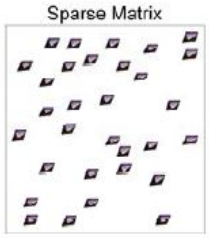

Structure Screen 1 & 2 HT-96 Rows A - D MD1-30

HT#	Salt	Buffer	pH	Precipitant
A1	0.02 M calcium chloride	0.1 M Na acetate	4.6	30 % v/v MPD
A2	0.2 M ammonium acetate	0.1 M Na acetate	4.6	30 % w/v PEG 4000
A3	0.2 M ammonium sulfate	0.1 M Na acetate	4.6	25 % w/v PEG 4000
A4	None	0.1 M Na acetate	4.6	2.0 M sodium formate
A5	None	0.1 M Na acetate	4.6	2.0 M ammonium sulfate
A6	None	0.1 M Na acetate	4.6	8 % w/v PEG 4000
A7	0.2 M ammonium acetate	0.1 M Na citrate	5.6	30 % w/v PEG 4000
A8	0.2 M ammonium acetate	0.1 M Na citrate	5.6	30 % v/v MPD
A9	None	0.1 M Na citrate	5.6	20 % v/v 2-propanol, 20 % w/v PEG 4000
A10	None	0.1 M Na citrate	5.6	1.0 M ammonium dihydrogen phosphate
A11	0.2 M calcium chloride	0.1 M Na acetate	4.6	20 % v/v 2-propanol
A12	None	0.1 M Na cacodylate	6.5	1.4 M sodium acetate
B1	0.2 M sodium citrate	0.1 M Na cacodylate	6.5	30 % v/v 2-propanol
B2	0.2 M ammonium sulfate	0.1 M Na cacodylate	6.5	30 % w/v PEG 8000
B3	0.2 M magnesium acetate	0.1 M Na cacodylate	6.5	20 % w/v PEG 8000
B4	0.2 M magnesium acetate	0.1 M Na cacodylate	6.5	30 % v/v MPD
B5	None	0.1 M imidazole	6.5	1.0 M sodium acetate
B6	0.2 M sodium acetate	0.1 M Na cacodylate	6.5	30 % w/v PEG 8000
B7	0.2 M zinc acetate	0.1 M Na cacodylate	6.5	18 % w/v PEG 8000
B8	0.2 M calcium acetate	0.1 M Na cacodylate	6.5	18 % w/v PEG 8000
B9	0.2 M sodium citrate	0.1 M Na HEPES	7.5	30 % v/v MPD
B10	0.2 M magnesium chloride	0.1 M Na HEPES	7.5	30 % v/v 2-propanol
B11	0.2 M calcium chloride	0.1 M Na HEPES	7.5	28 % v/v PEG 400
B12	0.2 M magnesium chloride	0.1 M Na HEPES	7.5	30 % v/v PEG 400
C1	0.2 M sodium citrate	0.1 M Na HEPES	7.5	20 % v/v 2-propanol
C2	None	0.1 M Na HEPES	7.5	0.8 M K/Na tartrate
C3	None	0.1 M Na HEPES	7.5	1.5 M lithium sulfate
C4	None	0.1 M Na HEPES	7.5	0.8 M sodium dihydrogen phosphate 0.8 M potassium dihydrogen phosphate
C5	None	0.1 M Na HEPES	7.5	1.4 M tri-sodium citrate
C6	None	0.1 M Na HEPES	7.5	2 % v/v PEG 400,2.0 M ammonium sulfate
C7	None	0.1 M Na HEPES	7.5	10 % v/v 2-propanol, 20 % w/v PEG 4000
C8	None	0.1 M Tris	8.5	2.0 M ammonium sulfate
C9	0.2 M magnesium chloride	0.1 M Tris	8.5	30 % w/v PEG 4000
C10	0.2 M sodium citrate	0.1 M Tris	8.5	30 % v/v PEG 400
C11	0.2 M lithium sulfate	0.1 M Tris	8.5	30 % w/v PEG 4000
C12	0.2 M ammonium acetate	0.1 M Tris	8.5	30 % v/v 2-propanol
D1	0.2 M sodium acetate	0.1 M Tris	8.5	30 % w/v PEG 4000
D2	None	0.1 M Tris	8.5	8 % w/v PEG 8000
D3	None	0.1 M Tris	8.5	2.0 M ammonium dihydrogen phosphate
D4	None	None	None	0.4 M K/Na tartrate
D5	None	None	None	0.4 M ammonium dihydrogen phosphate
D6	0.2 M ammonium sulfate	None	None	30 % w/v PEG 8000
D7	0.2 M ammonium sulfate	None	None	30 % w/v PEG 4000
D8	None	None	None	2.0 M ammonium sulfate
D9	None	None	None	4.0 M sodium formate
D10	0.05 M potassium dihydrogen phosphate	None	None	20 % w/v PEG 8000
D11	None	None	None	30 % w/v PEG 1500
D12	None	None	None	0.2 M magnesium formate

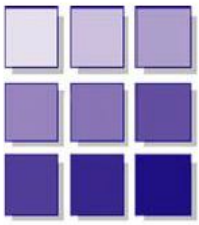

moleculardimensions.com

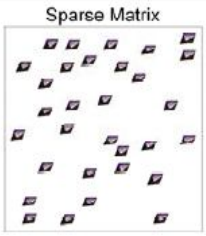

Structure Screen 1 & 2 HT-96 Rows E – H MD1-30

HT#	Salt	Buffer	pH	Precipitant
E1	0.1 M sodium chloride	0.1 M Bicine	9.0	30 % v/v PEG 550 MME
E2	None	0.1 M Bicine	9.0	2.0 M magnesium chloride
E3	2 % v/v dioxane	0.1 M Bicine	9.0	10 % w/v PEG 20,000
E4	0.2 M magnesium chloride	0.1 M Tris	8.5	3.4 M 1,6-hexanediol
E5	None	0.1 M Tris	8.5	25 % v/v *tert*-Butanol
E6	0.01 M nickel chloride	0.1 M Tris	8.5	1.0 M lithium sulfate
E7	1.5 M ammonium sulfate	0.1 M Tris	8.5	12 % v/v glycerol
E8	0.2 M ammonium phosphate monobasic	0.1 M Tris	8.5	50 % v/v MPD
E9	None	0.1 M Tris	8.5	20 % v/v ethanol
E10	0.01 M nickel chloride	0.1 M Tris	8.5	20 % w/v PEG 2000 MME
E11	0.5 M ammonium sulfate	0.1 M Na HEPES	7.5	30 % v/v MPD
E12	None	0.1 M Na HEPES	7.5	10 % w/v PEG 6000, 5% v/v MPD
F1	None	0.1 M Na HEPES	7.5	20 % v/v Jeffamine M-600
F2	0.1 M sodium chloride	0.1 M Na HEPES	7.5	1.6 M ammonium sulfate
F3	None	0.1 M Na HEPES	7.5	2.0 M ammonium formate
F4	0.05 M cadmium sulfate	0.1 M Na HEPES	7.5	1.0 M sodium acetate
F5	None	0.1 M Na HEPES	7.5	70 % v/v MPD
F6	None	0.1 M Na HEPES	7.5	4.3 M sodium chloride
F7	None	0.1 M Na HEPES	7.5	10 % w/v PEG 8000, 8 % v/v ethylene glycol
F8	None	0.1 M MES	6.5	1.6 M magnesium sulfate
F9	0.1 M sodium dihydrogen phosphate 0.1 M potassium dihydrogen phosphate	0.1 M MES	6.5	2.0 M sodium chloride
F10	None	0.1 M MES	6.5	12 % w/v PEG 20,000
F11	1.6 M ammonium sulfate	0.1 M MES	6.5	10 % v/v dioxane
F12	0.05 M caesium chloride	0.1 M MES	6.5	30 % v/v Jeffamine M-600
G1	0.01 M cobalt chloride	0.1 M MES	6.5	1.8 M ammonium sulfate
G2	0.2 M ammonium sulfate	0.1 M MES	6.5	30 % w/v PEG 5000 MME
G3	0.01 M zinc sulfate	0.1 M MES	6.5	25 % v/v PEG 550 MME
G4	None	0.1 M Na HEPES	7.5	20 % w/v PEG 10,000
G5	0.2 M K/Na Tartrate	0.1 M Na citrate	5.6	2.0 M ammonium sulfate
G6	0.5 M ammonium sulfate	0.1 M Na citrate	5.6	1.0 M lithium sulfate
G7	0.5 M sodium chloride	0.1 M Na citrate	5.6	4% v/v polyethyleneimine
G8	None	0.1 M Na citrate	5.6	35 % v/v *tert*-Butanol
G9	0.01 M ferric chloride	0.1 M Na citrate	5.6	10 % v/v Jeffamine M-600
G10	0.01 M manganese chloride	0.1 M Na citrate	5.6	2.5 M 1,6-hexanediol
G11	None	0.1 M Na acetate	4.6	2.0 M sodium chloride
G12	0.2 M sodium chloride	0.1 M Na acetate	4.6	30 % v/v MPD
H1	0.01 M cobalt chloride	0.1 M Na acetate	4.6	1.0 M 1,6-hexanediol
H2	0.1 M cadmium chloride	0.1 M Na acetate	4.6	30 % v/v PEG 400
H3	0.2 M ammonium sulfate	0.1 M Na acetate	4.6	30 % w/v PEG 2000 MME
H4	2.0 M sodium chloride	None	None	10 % w/v PEG 6000
H5	0.01 M CTAB	None	None	0.5 M sodium chloride 0.1 M magnesium chloride
H6	None	None	None	25 % v/v ethylene glycol
H7	None	None	None	35 % v/v dioxane
H8	2.0 M ammonium sulfate	None	None	5 % v/v 2-propanol
H9	None	None	7.0	1.0 M imidazole
H10	None	None	None	10 % w/v PEG 1000, 10% w/v PEG 8000
H11	1.5 M sodium chloride	None	None	10 % v/v ethanol
H12	None	None	6.5	1.6 M sodium citrate

Abbreviations:
Bicine; N,N-Bis(2-hydroxyethyl)glycine, **CTAB**; cetyltrimethylammonium bromide. **HEPES**; N-(2-hydroxyethyl)-piperazine-N'-2-ethanesulfonic acid, **MES**; 2-(N-morpholino)ethanesulfonic acid, **MME**; Monomethylether, **MPD;** 2,4-methyl pentanediol, **PEG**; Polyethylene glycol, **Tris**; 2-Amino-2-(hydroxymethyl)propane-1,3-diol.

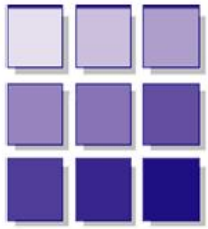

moleculardimensions.com

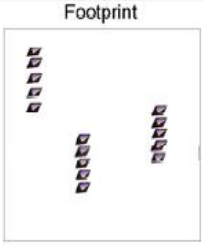

Stura Footprint Screen Rows A – D

MD1-43

HT#	Salt/Buffer	pH	Precipitant
A1	0.2 M imidazole malate	5.5	15% v/v PEG 600
A2	0.2 M imidazole malate	5.5	24 %v/v PEG 600
A3	0.2 M imidazole malate	5.5	33 % v/v PEG 600
A4	0.2 M imidazole malate	5.5	42 % v/v PEG 600
A5	0.2 M imidazole malate	7.0	10 % w/v PEG 4000
A6	0.2 M imidazole malate	7.0	15 % w/v PEG 4000
A7	0.2 M imidazole malate	7.0	20 % w/v PEG 4000
A8	0.2 M imidazole malate	7.0	25 % PEG w/v 4000
A9	0.2 M imidazole malate	8.5	7.5 % w/v PEG 10,000
A10	0.2 M imidazole malate	8.5	12.5 % w/v PEG 10,000
A11	0.2 M imidazole malate	8.5	17.5 % w/v PEG 10,000
A12	0.2 M imidazole malate	8.5	22.5 % w/v PEG 10,000
B1	0.15 M sodium citrate	5.5	0.75 M ammonium sulfate
B2	0.15 M sodium citrate	5.5	1.0 M ammonium sulfate
B3	0.15 M sodium citrate	5.5	1.5 M ammonium sulfate
B4	0.15 M sodium citrate	5.5	2.0 M ammonium sulfate
B5	0.8 M NaH_2PO_4/K_2HPO_4	7.0	-
B6	1.32 M NaH_2PO_4/K_2HPO_4	7.0	-
B7	1.6 M NaH_2PO_4/K_2HPO_4	7.0	-
B8	2.0 M NaH_2PO_4/K_2HPO_4	7.0	-
B9	0.01 M sodium borate	8.5	0.75 M sodium citrate
B10	0.01 M sodium borate	8.5	1.0 M sodium citrate
B11	0.01 M sodium borate	8.5	1.2 M sodium citrate
B12	0.01 M sodium borate	8.5	1.5 M sodium citrate
C1	0.1 M Na HEPES	8.2	30 % v/v PEG 550 MME
C2	0.1 M Na HEPES	8.2	40 % v/v PEG 550 MME
C3	0.1 M Na HEPES	8.2	50 % v/v PEG 550 MME
C4	0.1 M Na HEPES	8.2	60 % v/v PEG 550 MME
C5	0.1 M Na HEPES	7.5	18 % v/v PEG 600
C6	0.1 M Na HEPES	7.5	27 % v/v PEG 600
C7	0.1 M Na HEPES	7.5	36 % v/v PEG 600
C8	0.1 M Na HEPES	7.5	45 % v/v PEG 600
C9	0.1 M sodium cacodylate	6.5	18 % w/v PEG 2000 MME
C10	0.1 M sodium cacodylate	6.5	27 % w/v PEG 2000 MME
C11	0.1 M sodium cacodylate	6.5	36 % w/v PEG 2000 MME
C12	0.1 M sodium cacodylate	6.5	45 % w/v PEG 2000 MME
D1	0.2 M imidazole malate	6.0	8 % w/v PEG 4000
D2	0.2 M imidazole malate	6.0	15 % w/v PEG 4000
D3	0.2 M imidazole malate	6.0	20 % w/v PEG 4000
D4	0.2 M imidazole malate	6.0	30 % w/v PEG 4000
D5	0.1 M sodium acetate	5.5	12% PEG w/v 5000 MME
D6	0.1 M sodium acetate	5.5	18% PEG w/v 5000 MME
D7	0.1 M sodium acetate	5.5	24% PEG w/v 5000 MME
D8	0.1 M sodium acetate	5.5	36% PEG w/v 5000 MME
D9	0.1 M ammonium acetate	4.5	9 % w/v PEG 10,000
D10	0.1 M ammonium acetate	4.5	15 % w/v PEG 10,000
D11	0.1 M ammonium acetate	4.5	22.5 % w/v PEG 10,000
D12	0.1 M ammonium acetate	4.5	27 % w/v PEG 10,000

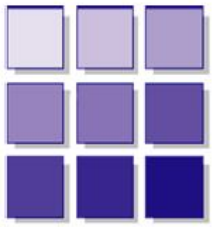

moleculardimensions.com

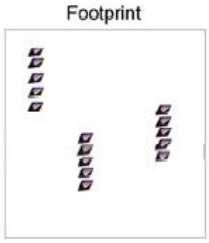

MacroSol Rows E – H

MD1-43

HT#	Reagent 1	Reagent 2	Buffer	pH
E1	10% v/v MPD	0.02 M calcium chloride	0.1 M sodium acetate	4.5
E2	20% v/v MPD	0.02 M calcium chloride	0.1 M sodium acetate	4.5
E3	30% v/v MPD	-	0.1 M sodium acetate	4.5
E4	30% v/v MPD	0.02 M calcium chloride	0.1 M sodium acetate	4.5
E5	1.0 M sodium acetate	0.1 M sodium dihydrogen phosphate	0.1 M sodium cacodylate	6.5
E6	1.4 M sodium acetate	0.1 M sodium dihydrogen phosphate	0.1 M sodium cacodylate	6.5
E7	1.7 M sodium acetate	0.1 M sodium dihydrogen phosphate	0.1 M sodium cacodylate	6.5
E8	1.7 M sodium acetate	-	0.1 M sodium cacodylate	6.5
E9	8% w/v PEG 3350	0.2 M ammonium acetate	0.1 M sodium acetate	4.5
E10	15% w/v PEG 3350	0.2 M ammonium acetate	0.1 M sodium acetate	4.5
E11	20% w/v PEG 3350	0.2 M ammonium acetate	0.1 M sodium acetate	4.5
E12	30% w/v PEG 3350	0.2 M ammonium acetate	0.1 M sodium acetate	4.5
F1	0.75 M ammonium dihydrogen phosphate	-	0.1 M sodium citrate	5.5
F2	1.0 M ammonium dihydrogen phosphate	-	0.1 M sodium citrate	5.5
F3	1.5 M ammonium dihydrogen phosphate	-	0.1 M sodium citrate	5.5
F4	2.0 M ammonium dihydrogen phosphate	-	0.1 M sodium citrate	5.5
F5	10% v/v 2-propanol	0.2 M magnesium chloride	0.1 M Na HEPES	7.5
F6	15% v/v 2-propanol	0.2 M magnesium chloride	0.1 M Na HEPES	7.5
F7	20% v/v 2-propanol	0.2 M magnesium chloride	0.1 M Na HEPES	7.5
F8	30% v/v 2-propanol	0.2 M magnesium chloride	0.1 M Na HEPES	7.5
F9	16% w/v PEG 3350	0.2 M lithium sulfate	0.1 M Tris	8.5
F10	25% w/v PEG 3350	0.2 M lithium sulfate	0.1 M Tris	8.5
F11	30% w/v PEG 3350	0.2 M lithium sulfate	0.1 M Tris	8.5
F12	25% w/v PEG 3350	0.5 M lithium sulfate	0.1 M Tris	8.5
G1	2% w/v PEG 8000	1.0 M lithium sulfate	-	
G2	2% w/v PEG 8000	1.0 M lithium sulfate	0.1 M imidazole malate	5.5
G3	2% w/v PEG 8000	1.0 M lithium sulfate	0.1 M imidazole malate	6.5
G4	2% w/v PEG 8000	1.0 M lithium sulfate	0.1 M imidazole malate	7.5
G5	12% w/v PEG 8000	0.2 M ammonium sulfate	-	-
G6	18% w/v PEG 8000	0.2 M ammonium sulfate	-	-
G7	24% w/v PEG 8000	0.2 M ammonium sulfate	-	-
G8	30% w/v PEG 8000	0.2 M ammonium sulfate	-	-
G9	10% w/v PEG 4000	0.5 M ammonium sulfate	-	-
G10	20% w/v PEG 4000	0.3 M ammonium sulfate	-	-
G11	30% w/v PEG 4000	0.2 M ammonium sulfate	-	-
G12	36% w/v PEG 4000	0.2 M ammonium sulfate	-	-
H1	1.0 M ammonium sulfate	2% v/v PEG 400	0.1 M Na HEPES	7.5
H2	1.5 M ammonium sulfate	2% v/v PEG 400	0.1 M Na HEPES	7.5
H3	2.0 M ammonium sulfate	2% v/v PEG 400	0.1 M Na HEPES	7.5
H4	2.0 M ammonium sulfate	5% v/v PEG 400	0.1 M Na HEPES	7.5
H5	12% w/v PEG 4000	5% v/v 2-propanol	0.1 M sodium citrate	5.5
H6	16% w/v PEG 4000	10% v/v 2-propanol	0.1 M sodium citrate	5.5
H7	20% w/v PEG 4000	15% v/v 2-propanol	0.1 M sodium citrate	5.5
H8	20% w/v PEG 4000	20% v/v 2-propanol	0.1 M sodium citrate	5.5
H9	9% w/v PEG 8000	0.005 M zinc acetate	0.1 M sodium cacodylate	6.5
H10	12% w/v PEG 8000	0.005 M zinc acetate	0.1 M sodium cacodylate	6.5
H11	18% w/v PEG 8000	0.005 M zinc acetate	0.1 M sodium cacodylate	6.5
H12	24% w/v PEG 8000	0.005 M zinc acetate	0.1 M sodium cacodylate	6.5

Abbreviations: Na HEPES; 2-(4-(2-Hydroxyethyl)-1-piperazinyl)ethanesulfonic Acid Sodium Salt, **PEG**; Polyethylene glycol, **Tris**; 2-Amino-2-(hydroxymethyl) propane-1,3-diol. Note: The pH of each final reagent is checked and adjusted back to the stated pH of the buffer (±0.2 pH units) as appropriate.

Additive Screen™ — HR2-428 Reagent Formulation

Tube #	Salt	Classification	Suggested Drop Concentration
1. (A1)	0.1 M Barium chloride dihydrate	Multivalent	0.01 M (10 mM)
2. (A2)	0.1 M Cadmium chloride hydrate	Multivalent	0.01 M (10 mM)
3. (A3)	0.1 M Calcium chloride dihydrate	Multivalent	0.01 M (10 mM)
4. (A4)	0.1 M Cobalt(II) chloride hexahydrate	Multivalent	0.01 M (10 mM)
5. (A5)	0.1 M Copper(II) chloride dihydrate	Multivalent	0.01 M (10 mM)
6. (A6)	0.1 M Magnesium chloride hexahydrate	Multivalent	0.01 M (10 mM)
7. (A7)	0.1 M Manganese(II) chloride tetrahydrate	Multivalent	0.01 M (10 mM)
8. (A8)	0.1 M Strontium chloride hexahydrate	Multivalent	0.01 M (10 mM)
9. (A9)	0.1 M Yttrium(III) chloride hexahydrate	Multivalent	0.01 M (10 mM)
10. (A10)	0.1 M Zinc chloride	Multivalent	0.01 M (10 mM)
11. (A11)	0.1 M Iron(III) chloride hexahydrate	Multivalent	0.01 M (10 mM)
12. (A12)	0.1 M Nickel(II) chloride hexahydrate	Multivalent	0.01 M (10 mM)
13. (B1)	0.1 M Chromium(III) chloride hexahydrate	Multivalent	0.01 M (10 mM)
14. (B2)	0.1 M Praseodymium(III) acetate hydrate	Multivalent	0.01 M (10 mM)
15. (B3)	1.0 M Ammonium sulfate	Salt	0.1 M (100 mM)
16. (B4)	1.0 M Potassium chloride	Salt	0.1 M (100 mM)
17. (B5)	1.0 M Lithium chloride	Salt	0.1 M (100 mM)
18. (B6)	2.0 M Sodium chloride	Salt	0.2 M (200 mM)
19. (B7)	0.5 M Sodium fluoride	Salt	0.05 M (50 mM)
20. (B8)	1.0 M Sodium iodide	Salt	0.1 M (100 mM)
21. (B9)	2.0 M Sodium thiocyanate	Salt	0.2 M (200 mM)
22. (B10)	1.0 M Potassium sodium tartrate tetrahydrate	Salt	0.1 M (100 mM)
23. (B11)	1.0 M Sodium citrate tribasic dihydrate	Salt	0.1 M (100 mM)
24. (B12)	1.0 M Cesium chloride	Salt	0.1 M (100 mM)
25. (C1)	1.0 M Sodium malonate pH 7.0	Salt	0.1 M (100 mM)
26. (C2)	0.1 M L-Proline	Amino Acid	0.01 M (10 mM)
27. (C3)	0.1 M Phenol	Dissociating Agent	0.01 M (10 mM)
28. (C4)	30% v/v Dimethyl sulfoxide	Dissociating Agent	3.0%
29. (C5)	0.1 M Sodium bromide	Dissociating Agent	0.01 M (10 mM)
30. (C6)	30% w/v 6-Aminohexanoic acid	Linker	3.0%
31. (C7)	30% w/v 1,5-Diaminopentane dihydrochloride	Linker	3.0%
32. (C8)	30% w/v 1,6-Diaminohexane	Linker	3.0%
33. (C9)	30% w/v 1,8-Diaminooctane	Linker	3.0%
34. (C10)	1.0 M Glycine	Linker	0.1 M (100 mM)
35. (C11)	0.3 M Glycyl-glycyl-glycine	Linker	0.03 M (30 mM)
36. (C12)	0.1 M Taurine	Linker	0.01 M (10 mM)
37. (D1)	0.1 M Betaine hydrochloride	Linker	0.01 M (10 mM)
38. (D2)	0.1 M Spermidine	Polyamine	0.01 M (10 mM)
39. (D3)	0.1 M Spermine tetrahydrochloride	Polyamine	0.01 M (10 mM)
40. (D4)	0.1 M Hexammine cobalt(III) chloride	Polyamine	0.01 M (10 mM)
41. (D5)	0.1 M Sarcosine	Polyamine / Osmolyte	0.01 M (10 mM)
42. (D6)	0.1 M Trimethylamine hydrochloride	Chaotrope	0.01 M (10 mM)
43. (D7)	1.0 M Guanidine hydrochloride	Chaotrope	0.1 M (100 mM)
44. (D8)	0.1 M Urea	Chaotrope	0.01 M (10 mM)
45. (D9)	0.1 M β-Nicotinamide adenine dinucleotide hydrate	Co-factor	0.01 M (10 mM)
46. (D10)	0.1 M Adenosine-5'-triphosphate disodium salt hydrate	Co-factor	0.01 M (10 mM)
47. (D11)	0.1 M TCEP hydrochloride	Reducing Agent	0.01 M (10 mM)
48. (D12)	0.01 M GSH (L-Glutathione reduced), 0.01 M GSSG (L-Glutathione oxidized)	Reducing Agent	0.001 M (1 mM)

Additive Screen contains ninety-six unique reagents beginning at position A1.
To determine the formulation of each reagent, simply read across the page.

Additive Screen™ — HR2-428 Reagent Formulation

Tube #	Salt	Tube #	Classification	Tube #	Suggested Drop Concentration
49. (E1)	0.1 M Ethylenediaminetetraacetic acid disodium salt dihydrate	49. (E1)	Chelating Agent	49. (E1)	0.01 M (10 mM)
50. (E2)	5% w/v Polyvinylpyrrolidone K15	50. (E2)	Polymer	50. (E2)	0.5%
51. (E3)	30% w/v Dextran sulfate sodium salt (M_r 5,000)	51. (E3)	Polymer	51. (E3)	3.0%
52. (E4)	40% v/v Pentaerythritol ethoxylate (3/4 EO/OH)	52. (E4)	Polymer	52. (E4)	4.0%
53. (E5)	10% w/v Polyethylene glycol 3,350	53. (E5)	Polymer	53. (E5)	1.0%
54. (E6)	30% w/v D-(+)-Glucose monohydrate	54. (E6)	Carbohydrate	54. (E6)	3.0%
55. (E7)	30% w/v Sucrose	55. (E7)	Carbohydrate	55. (E7)	3.0%
56. (E8)	30% w/v Xylitol	56. (E8)	Carbohydrate	56. (E8)	3.0%
57. (E9)	30% w/v D-Sorbitol	57. (E9)	Carbohydrate	57. (E9)	3.0%
58. (E10)	12% w/v myo-Inositol	58. (E10)	Carbohydrate	58. (E10)	1.2%
59. (E11)	30% w/v D-(+)-Trehalose dihydrate	59. (E11)	Carbohydrate	59. (E11)	3.0%
60. (E12)	30% w/v D-(+)-Galactose	60. (E12)	Carbohydrate	60. (E12)	3.0%
61. (F1)	30% v/v Ethylene glycol	61. (F1)	Polyol	61. (F1)	3.0%
62. (F2)	30% v/v Glycerol	62. (F2)	Polyol	62. (F2)	3.0%
63. (F3)	3.0 M NDSB-195	63. (F3)	Non-detergent	63. (F3)	0.3 M (300 mM)
64. (F4)	2.0 M NDSB-201	64. (F4)	Non-detergent	64. (F4)	0.2 M (200 mM)
65. (F5)	2.0 M NDSB-211	65. (F5)	Non-detergent	65. (F5)	0.2 M (200 mM)
66. (F6)	2.0 M NDSB-221	66. (F6)	Non-detergent	66. (F6)	0.2 M (200 mM)
67. (F7)	1.0 M NDSB-256	67. (F7)	Non-detergent	67. (F7)	0.1 M (200 mM)
68. (F8)	0.15 mM CYMAL®-7	68. (F8)	Amphiphile	68. (F8)	0.000015 M (0.015 mM)
69. (F9)	20% w/v Benzamidine hydrochloride	69. (F9)	Amphiphile	69. (F9)	2.0%
70. (F10)	5% w/v n-dodecyl-N,N-dimethylamine-N-oxide, (LDAO, DDAO)	70. (F10)	Detergent	70. (F10)	0.5%
71. (F11)	5% w/v n-Octyl-β-D-glucoside	71. (F11)	Detergent	71. (F11)	0.5%
72. (F12)	5% w/v n-Dodecyl-β-D-maltoside	72. (F12)	Detergent	72. (F12)	0.5%
73. (G1)	30% w/v Trimethylamine N-oxide dihydrate	73. (G1)	Osmolyte	73. (G1)	3.0%
74. (G2)	30% w/v 1,6-Hexanediol	74. (G2)	Organic, Non-volatile	74. (G2)	3.0%
75. (G3)	30% v/v (+/-)-2-Methyl-2,4-pentanediol	75. (G3)	Organic, Non-volatile	75. (G3)	3.0%
76. (G4)	50% v/v Polyethylene glycol 400	76. (G4)	Organic, Non-volatile	76. (G4)	5.0%
77. (G5)	50% v/v Jeffamine® M-600® pH 7.0	77. (G5)	Organic, Non-volatile	77. (G5)	5.0%
78. (G6)	40% v/v 2,5-Hexanediol (mixture of isomers)	78. (G6)	Organic, Non-volatile	78. (G6)	4.0%
79. (G7)	40% v/v (±)-1,3-Butanediol	79. (G7)	Organic, Non-volatile	79. (G7)	4.0%
80. (G8)	40% v/v Polypropylene glycol P 400	80. (G8)	Organic, Non-volatile	80. (G8)	4.0%
81. (G9)	30% v/v 1,4-Dioxane	81. (G9)	Organic, Volatile	81. (G9)	3.0%
82. (G10)	30% v/v Ethanol	82. (G10)	Organic, Volatile	82. (G10)	3.0%
83. (G11)	30% v/v 2-Propanol	83. (G11)	Organic, Volatile	83. (G11)	3.0%
84. (G12)	30% v/v Methanol	84. (G12)	Organic, Volatile	84. (G12)	3.0%
85. (H1)	10% v/v 1,2-Butanediol	85. (H1)	Organic, Volatile	85. (H1)	1.0%
86. (H2)	40% v/v tert-Butanol	86. (H2)	Organic, Volatile	86. (H2)	4.0%
87. (H3)	40% v/v 1,3-Propanediol	87. (H3)	Organic, Volatile	87. (H3)	4.0%
88. (H4)	40% v/v Acetonitrile	88. (H4)	Organic, Volatile	88. (H4)	4.0%
89. (H5)	40% v/v Formamide	89. (H5)	Organic, Volatile	89. (H5)	4.0%
90. (H6)	40% v/v 1-Propanol	90. (H6)	Organic, Volatile	90. (H6)	4.0%
91. (H7)	5% v/v Ethyl acetate	91. (H7)	Organic, Volatile	91. (H7)	0.5%
92. (H8)	40% v/v Acetone	92. (H8)	Organic, Volatile	92. (H8)	4.0%
93. (H9)	0.25% v/v Dichloromethane	93. (H9)	Organic, Volatile	93. (H9)	0.025%
94. (H10)	7% v/v 1-Butanol	94. (H10)	Organic, Volatile	94. (H10)	0.7%
95. (H11)	40% v/v 2,2,2-Trifluoroethanol	95. (H11)	Organic, Volatile	95. (H11)	4.0%
96. (H12)	40% v/v 1,1,1,3,3,3-Hexafluoro-2-propanol	96. (H12)	Organic, Volatile	96. (H12)	4.0%

Additive Screen contains ninety-six unique reagents beginning at position A1.
To determine the formulation of each reagent, simply read across the page.

34 Journey
Aliso Viejo, CA 92656-3317 U.S.A.

HAMPTON RESEARCH
Solutions for Crystal Growth